THE

LONDON, EDINBURGH, AND DUBLIN

PHILOSOPHICAL MAGAZINE

AND

JOURNAL OF SCIENCE.

[SEVENTH SERIES.]

JUNE 1937.

XCVIII. *The Hall Effect and some other Physical Constants of Alloys.*—Part VI. *The Silver-Tin Series of Alloys.*

By W. G. JOHN, *Ph.D.*, *and* Prof. E. J. EVANS, *D.Sc.*, *Physics Department, University College of Swansea* *.

THE present investigation deals with the Hall effect and other physical properties of the silver-tin system of alloys, and is a continuation of previous work [1] carried out by the authors on the silver-antimony system.

The variation of the electrical resistivity, temperature-coefficient of resistance, thermo-electric power, Hall coefficient, and density, with the composition of the alloys, has been determined, and the results have been examined in relation to the equilibrium diagrams, which have been given by various investigators.

The constitution of the silver-tin alloys has been examined by Gautier [2], Charpy [3], Heycock and Neville [4], Herschkowitsch [5], Campbell [6], van Laar [7], Petrenko [8], Joyner [9], and Murphy [10].

Heycock and Neville determined the freezing-points of the alloys, and later Petrenko investigated the equilibrium diagram of the system. The result of his investigations is given in Graph 1 A.

The system was again examined by Murphy, who obtained the equilibrium diagram shown in Graph 1 B.

* Communicated by Prof. E. J. Evans.

The melting-point curves obtained by Heycock and Neville, Petrenko, and Murphy are in good agreement.

According to Petrenko silver can hold in solution 23 per cent. of tin at 480° C., and this amount diminishes to about 19 per cent. at 100° C. The compound Ag_3Sn containing 26·87 per cent. of tin is formed as a result of a peritectic reaction. He found no evidence of a solid solution of silver in tin, and the region between the

Graph 1 A.

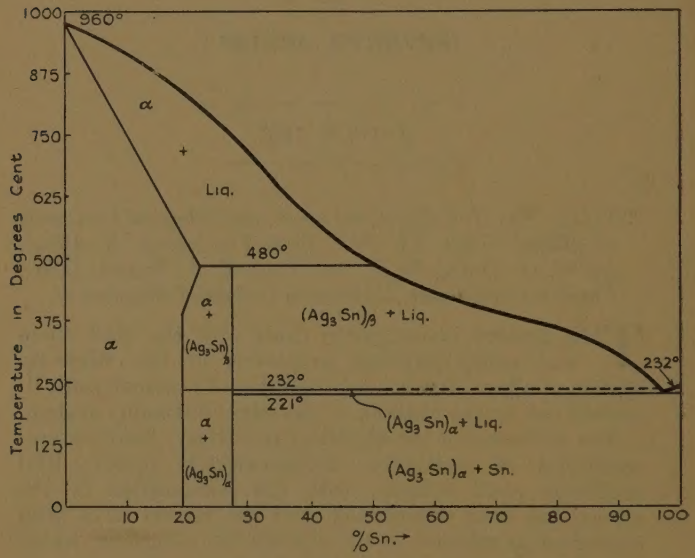

compound Ag_3Sn and the tin end of the series consisted of a mixture of this compound and pure tin. Petrenko also found that an allotropic change, associated with the presence of the compound, occurred at 232° C. He represents this change by a horizontal line dividing the α Ag_3Sn and the β Ag_3Sn states, the α state being stable at the lower temperature.

A diagram given by Guertler [11] agrees in the main with that given by Petrenko. Guertler's diagram shows two allotropic changes, one at 18° C. and the other at 161° C., neither of which are indicated by Petrenko.

Murphy observed that the solubility of tin in silver extended only to 13·3 per cent. tin at 724° C., and that it decreased to about 11 per cent. at 100° C. A new phase β is formed by the action of this solid solution with the liquid at a composition of 14·5 per cent. tin. At room-temperature the β phase extends from 12·5 to 19 per cent. tin, and at 26·85 per cent. tin the γ constituent (the compound Ag_3Sn) is produced by a

Graph 1 B.

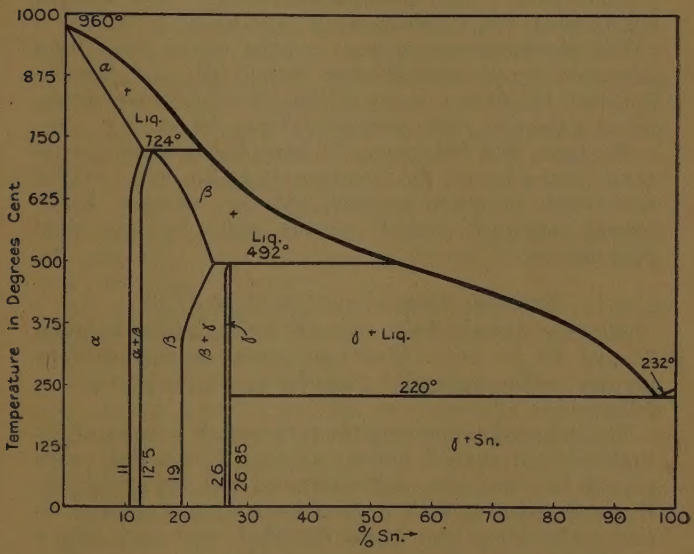

poritectic reaction between the β phase and the liquid. This γ phase has a small range of about 1 per cent. at room-temperature.

Alloys richer in tin than the compound were a mixture of Ag_3Sn and tin or of Ag_3Sn and a very dilute solution of silver in tin. He found that the solid solution of silver in tin did not exceed 0·1 per cent. by weight. This result is supported by the later investigations of Hanson, Sandford, and Stephens [12].

Murphy failed to detect the allotropic change in the γ phase which was observed by Petrenko, but as the

result of measurements of the resistivities of the alloys in this region he found an allotropic change at 60° C.

Matthiessen [13] measured the specific gravity of the alloys, and Maey [14] determined their specific volumes. The latter found that the specific volume curve had a singular point corresponding to the tritastannide Ag_3Sn.

Matthiessen [15] and his co-workers measured the electrical conductivities of the alloys, and A. W. Smith [16] studied the relation between the electrical and thermal conductivities. This relationship has also been studied by Bernoulli [17], Hardenbeck [18], and Schenck [19].

The thermoelectric powers of the alloys have been measured by Seebeck [20] and Batelli [21], and Herschkowitsch [22], from a study of their electrolytic potentials, found a singular point corresponding to Ag_4Sn.

Westgren and Phragmen [23] have discussed the structural analogies of the compound Ag_3Sn with similar compounds in other systems, but the complete X-ray crystal structure analysis of the series has not been undertaken.

Preparation and Annealing of the Alloys.

Alloys of silver and tin, except those containing between 70 and 80 per cent. silver, are comparatively easy to prepare. The general procedure adopted was as follows:—

The required amounts of the pure metals were carefully weighed and placed under carbon. The metals were melted in a coal-gas muffle furnace, and the melt, after thorough stirring with a graphite rod, was allowed to cool. The alloy was again remelted and cast into a graphite mould. For the tin end of the series the alloys were chill cast, but in the case of alloys containing between 80 and 100 per cent. silver it was necessary to heat the mould in a Bunsen flame before a good cast was obtained.

Alloys containing between 70 and 80 per cent. silver were usually cast *in vacuo*. In this way good plates, free from oxide and blowholes, were obtained. The density of the alloy of composition Ag_3Sn was in good agreement with that obtained by calculation from the known lattice constants. The density of a plate of this alloy, if prepared in the ordinary way, was usually 2 or 3 per cent. lower. After casting the plates were planed and trimmed, so that they were approximately

12 cm. long, 2 cm. broad, and 0·2 cm. thick. The final values of the breadth and thickness of each plate were the mean of a large number of measurements taken over the entire plate. The resistivity of each plate was then measured at the temperature of melting ice. The plates were then annealed at a suitable temperature in an evacuated annealing furnace. The annealing temperatures were obtained from the equilibrium diagram of the system given by Murphy.

Annealing of the Alloys.

Alloys of composition between 26·85 and 100 per cent. tin were initially kept at a temperature of 200° C. for about a fortnight. The furnace was allowed to cool slowly, and the resistivities were measured at 0° C. The alloys were again annealed at the same temperature for two days, and the resistivities at 0° C. were remeasured. The second annealing produced no change in the resistivities, and it was therefore assumed that the alloys had reached a state of equilibrium. The above process of annealing was repeated at temperatures of 150°, 100°, 80°, and 50° C.

Alloys containing from 19 to 26·85 per cent. tin were initially annealed at 450° C., and later at 350°, 300°, 250°, 150°, 100°, 80°, and 50° C.

The alloys in the β and $\alpha+\beta$ phases were initially annealed at 650° C., and the two alloys in the α phase containing 3 and 8·4 per cent. tin were annealed at 850° and 800° C. respectively for a period of two days. When the resistivities of the two specimens had reached a constant value they were annealed down to room-temperature by steps of about 100° C. Similarly the alloys in the β and $\alpha+\beta$ phases were also annealed down to room-temperature. The whole process of annealing in the case of these alloys occupied a period of about six weeks.

Analysis of the Alloys.

The percentage of silver contained in each alloy was determined, and then the percentage of tin was obtained by difference. A known weight of a particular alloy was dissolved in concentrated nitric acid, and the silver nitrate, formed was separated from the white stannic oxide by filtration. The filtrate, consisting of silver

nitrate, was titrated with potassium thiocyanate in the presence of ferric sulphate. The thiocyanate precipitated white silver thiocyanate from the solution, the end of the reaction being indicated by a red coloration. The potassium thiocyanate was of approximately decinormal strength, and had been previously standardized with silver nitrate solution of known strength. In this way the percentage of silver in the alloy could be determined. Samples of an alloy were taken from each end of a plate, and it was found that as far as could be detected by analysis the composition of each plate was uniform. On an average it is estimated that the error in the analysis was not greater than 0·2 per cent. The percentage compositions by weight of the various alloys are given in Table I.

TABLE I.

Percentage composition by weight of alloys.

Silver.	Tin.	Silver.	Tin.
0·00	100·00	74·07	25·93
1·57	98·43	76·10	23·90
5·62	94·38	81·00	19·00
9·72	90·28	84·47	15·53
30·43	69·57	87·35	12·65
41·30	58·70	88·02	11·98
72·40	27·60	88·90	11·10
73·17	26·83	91·60	8·40
73·65	26·35	97·00	3·00
		100·00	0·00

Measurement of the Physical Constants.

In a previous communication [24] the methods employed in the determination of the Hall coefficients and the other physical constants of alloys have been discussed in detail, and here it is only necessary to give a brief account of the measurements undertaken.

Resistivity.

The resistivity of each alloy was measured at 0° C., and the experimental results are given in Table II., and plotted in Graph 2. It is estimated that the error in the measurements is on the average not greater than 0·3 per cent.

TABLE II.

Composition by weight of silver.	Resistivities at 0° C. in microhms per cm.³.	
	Before annealing.	After annealing.
Per cent.		
0·00	10·36	10·49
1·57	10·56	10·47
5·62	10·42	10·42
9·72	10·58	10·07
30·43	10·57	9·87
41·30	10·75	10·00
72·40	20·04	9·45
73·17	19·40	9·38
73·65	17·12	18·59
74·07	27·74	27·22
76·10	45·50	25·55
81·00	76·42	74·98
84·47	48·17	51·81
87·35	41·92	34·68
88·02	34·08	31·91
88·90	33·85	30·46
91·60	24·26	25·03
97·00	9·86	9·68
100·00	1·51	1·51

Graph 2.

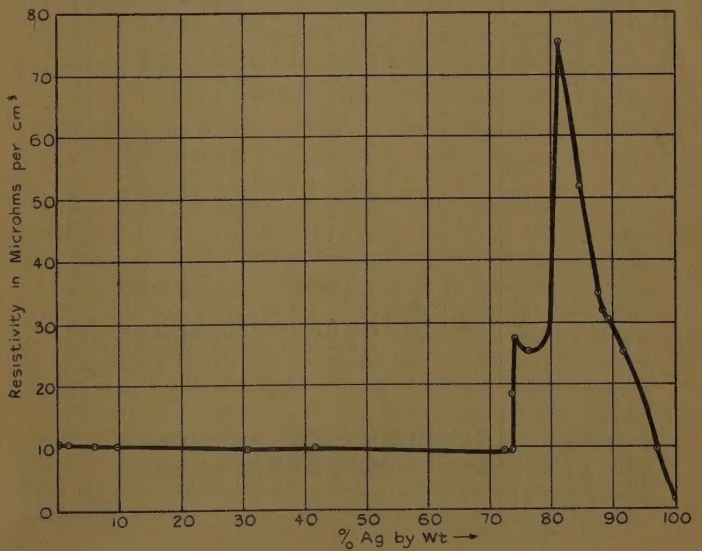

Table III.

Composition by weight of Ag.	Hall coefficients in absolute units; magnetic fields in gauss.						Mean value of coefficient.	Temp. in degrees Cent.
	3089.	4641.	5797.	6740.	7535.	8346.		
Per cent.								
*0·00	—	—	—	—	—	—	—	—
1·57	—	Too small to measure.			—	—	—	—
5·62	—	—	—	—	—	$+\cdot2\times10^{-4}$	$+\cdot2\times10^{-4}$	17
9·72	—	—	—	—	—	$+\cdot5\times10^{-4}$	$+\cdot5\times10^{-4}$	17
30·43	—	—	$+2\cdot73\times10^{-4}$	$+2\cdot80\times10^{-4}$	$+2\cdot78\times10^{-4}$	$+2\cdot83\times10^{-4}$	$+2\cdot78\times10^{-4}$	15·8
41·30	$+3\cdot30\times10^{-4}$	$+3\cdot26\times10^{-4}$	$+3\cdot26\times10^{-4}$	$+3\cdot21\times10^{-4}$	$+3\cdot21\times10^{-4}$	$+3\cdot22\times10^{-4}$	$+3\cdot24\times10^{-4}$	16·2
72·40	$+4\cdot24\times10^{-4}$	$+4\cdot09\times10^{-4}$	$+4\cdot16\times10^{-4}$	$+4\cdot33\times10^{-4}$	$+4\cdot18\times10^{-4}$	$+4\cdot14\times10^{-4}$	$+4\cdot19\times10^{-4}$	17
73·17	$+4\cdot28\times10^{-4}$	$+4\cdot30\times10^{-4}$	$+4\cdot25\times10^{-4}$	$+4\cdot34\times10^{-4}$	$+4\cdot23\times10^{-4}$	$+4\cdot21\times10^{-4}$	$+4\cdot27\times10^{-4}$	17·1
73·65	—	—	—	$+1\cdot53\times10^{-4}$	$+1\cdot54\times10^{-4}$	$+1\cdot57\times10^{-4}$	$+1\cdot55\times10^{-4}$	19
74·07	—	—	—	—	—	$+\cdot2\times10^{-4}$	$+\cdot2\times10^{-4}$	16·5
76·10	—	—	—	$+1\cdot05\times10^{-4}$	$+1\cdot09\times10^{-4}$	$+1\cdot11\times10^{-4}$	$+1\cdot08\times10^{-4}$	17·3
81·00	—	—	$-2\cdot75\times10^{-4}$	$-2\cdot73\times10^{-4}$	$-2\cdot72\times10^{-4}$	$-2\cdot79\times10^{-4}$	$-2\cdot75\times10^{-4}$	19
84·47	$-5\cdot95\times10^{-4}$	$-5\cdot90\times10^{-4}$	$-6\cdot11\times10^{-4}$	$-6\cdot20\times10^{-4}$	$-6\cdot19\times10^{-4}$	$-6\cdot09\times10^{-4}$	$-6\cdot07\times10^{-4}$	17
87·35	$-7\cdot67\times10^{-4}$	$-7\cdot62\times10^{-4}$	$-7\cdot72\times10^{-4}$	$-7\cdot77\times10^{-4}$	$-7\cdot79\times10^{-4}$	$-7\cdot60\times10^{-4}$	$-7\cdot69\times10^{-4}$	17·2
88·02	$-7\cdot42\times10^{-4}$	$-7\cdot47\times10^{-4}$	$-7\cdot51\times10^{-4}$	$-7\cdot60\times10^{-4}$	$-7\cdot55\times10^{-4}$	$-7\cdot61\times10^{-4}$	$-7\cdot53\times10^{-4}$	17
88·90	$-7\cdot28\times10^{-4}$	$-7\cdot30\times10^{-4}$	$-7\cdot38\times10^{-4}$	$-7\cdot41\times10^{-4}$	$-7\cdot42\times10^{-4}$	$-7\cdot45\times10^{-4}$	$-7\cdot37\times10^{-4}$	14
91·60	$-6\cdot40\times10^{-4}$	$-6\cdot42\times10^{-4}$	$-6\cdot43\times10^{-4}$	$-6\cdot46\times10^{-4}$	$-6\cdot45\times10^{-4}$	$-6\cdot40\times10^{-4}$	$-6\cdot43\times10^{-4}$	18
97·00	$-7\cdot81\times10^{-4}$	$-7\cdot82\times10^{-4}$	$-7\cdot80\times10^{-4}$	$-7\cdot81\times10^{-4}$	$-7\cdot67\times10^{-4}$	$-7\cdot68\times10^{-4}$	$-7\cdot76\times10^{-4}$	18·5
100·00	$-8\cdot97\times10^{-4}$	$-8\cdot98\times10^{-4}$	$-8\cdot93\times10^{-4}$	$-8\cdot91\times10^{-4}$	$-8\cdot85\times10^{-4}$	$-8\cdot89\times10^{-4}$	$-8\cdot92\times10^{-4}$	16

* Hall coefficient of pure tin $=-4\times10^{-5}$ (Campbell, 'Galvanomagnetic and Thermomagnetic Effects,' p. 124).

The Hall Effect.

Since there was a possibility of a complication due to an allotropic change in the γ phase at 60° C. the Hall coefficients of the alloys at room-temperature were determined before measurements of the temperature coefficients of resistance and thermoelectric powers were undertaken. The Hall coefficient of each alloy was measured for magnetic fields of 3089, 4641, 5797, 6740, 7535, and 8346 gauss. For silver the coefficient has a negative value of $8{\cdot}92 \times 10^{-4}$ absolute units, whilst for

Graph 3.

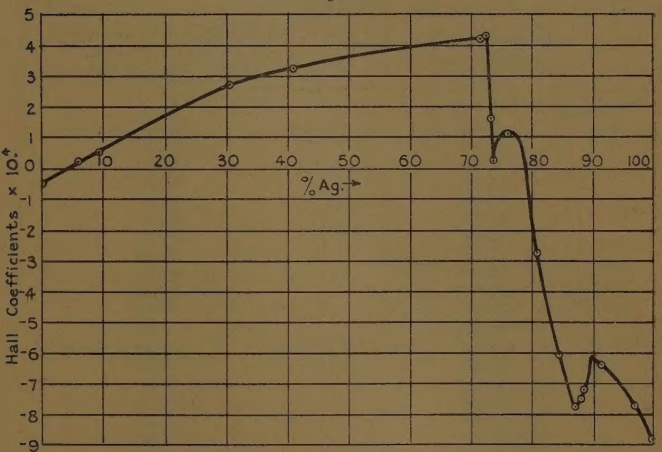

tin it is of the order of 4×10^{-5} absolute units. The smallness of the deflexions obtained with plates near the tin end of the series made accurate determinations of the Hall coefficients in that region impossible. It was found that no alloy had a coefficient greater than that of silver, and consequently each plate was planed down to make its thickness as small as possible, consistent with mechanical strength. Since the Hall electromotive force varies inversely as the thickness of the plate, greater accuracy was thus obtained. It is estimated that for alloys with Hall coefficients comparable with that of silver the error of measurement is on the average not greater than 2 per cent., but for alloys near the tin

end of the series the error is decidedly greater. The results are given in Table III., and plotted in Graph 3. For alloys whose coefficients are comparatively small only the values for the higher fields are tabulated.

Temperature Coefficient of Resistance and Thermoelectric Power.

In the first place the mean temperature coefficients of resistance of alloys in and near the γ phase were

TABLE IV.

Composition by weight of Ag.	Mean temperature coefficient of resistance between 0° and 100° C. $\times 10^4$.
Per cent.	
0·00	43·70
1·57	43·60
5·62	42·30
9·72	42·10
30·43	40·00
41·30	39·00
72·40	36·30
73·17	35·80
73·65	16·80
74·07	10·00
76·10	17·40
81·00	2·40
84·47	2·80
87·35	3·30
88·02	3·40
88·90	3·50
91·60	3·90
97·00	8·90
100·00	40·50

measured over the temperature range 0° to 40° C., and the thermoelectric powers of the same alloys were afterwards measured between about 15° and 40° C.

Later the temperature coefficients of all the alloys were determined between 0° and 100° C., and the experimental results are given in Table IV. and plotted in Graph 4. The errors in the results are estimated to be on the average not greater than 0·5 per cent.

The thermoelectric power of each alloy with reference to copper was also measured over the temperature range 15° to 100° C., and the values are given in Table V. and plotted in Graph 5. The errors incurred in their

measurement is estimated to be on the average not greater than 0·4 per cent.

Graph 4.

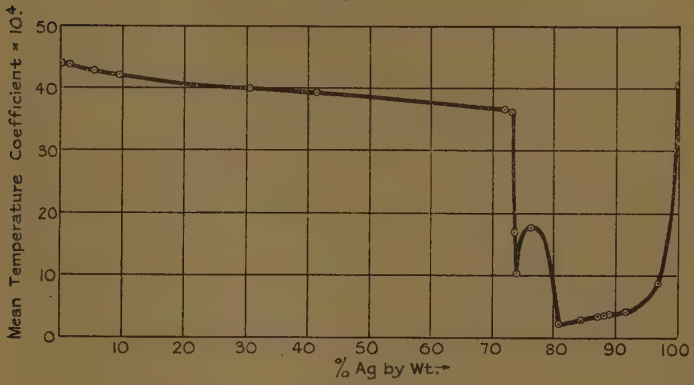

TABLE V.

Composition by weight of Ag.	Mean thermoelectric power (15–100° C.) with reference to copper in microvolts per degree C.
Per cent.	
0·00	−3·19
1·57	−3·16
5·62	−3·06
9·72	−2·96
30·43	−2·29
41·30	−1·82
72·40	−0·61
73·17	−0·58
73·65	+0·24
74·07	+0·68
76·10	−0·57
81·00	−1·64
84·47	−1·70
87·35	−1·74
88·02	−1·86
88·90	−2·16
91·60	−2·78
97·00	−2·38
100·00	−0·29

For the alloys in and near the γ phase it was observed that no measurable difference existed between the values

of these physical constants when determined over the smaller or the larger temperature range.

Graph 5.

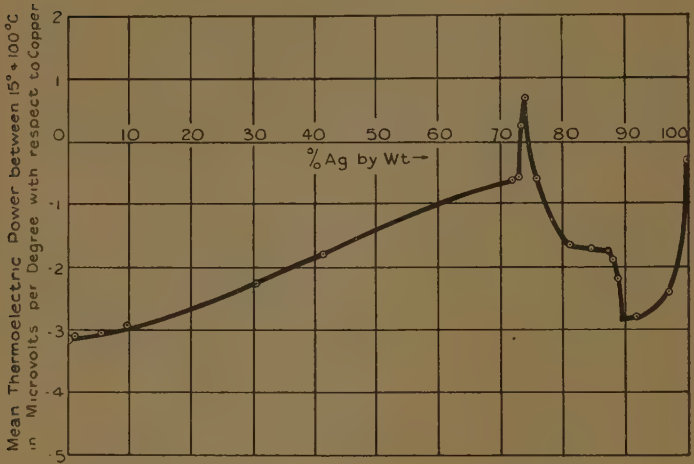

Density.

The values of the density are given in Table VI., and plotted in Graph 6. The experimental error in the determination of the density is estimated to be not more than 0·1 per cent.

Experimental Results.

As is well known the electrical properties of an alloy of two given metals vary markedly with a change in composition. These variations are specially noticeable at or near the phase boundaries in the system. If alloys of suitable composition are prepared and annealed the electrical properties of the system, when plotted against composition, will show the existence of solid solutions, intermetallic compounds, and phase boundaries.

The experimental results obtained in the case of the silver-tin series of alloys will therefore be considered in relation to the equilibrium diagram (Graph 1 B) given by Murphy. This diagram indicates the existence

TABLE VI.

Composition by weight of Ag.	Density in grams per c.c. at 18° C.
Per cent.	
0·00	7·303
1·57	7·33
5·62	7·45
9·72	7·57
30·43	8·29
41·30	8·60
72·40	9·88
73·17	9·90
73·65	9·91
74·07	9·92
76·10	10·01
81·00	10·03
84·47	10·07
87·35	10·17
88·02	10·18
88·90	10·19
91·60	10·27
97·00	10·43
100·00	10·49

Graph 6.

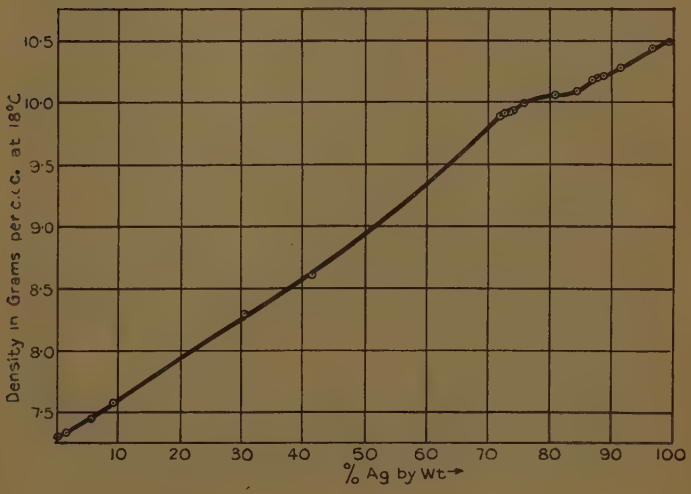

of the compound Ag_3Sn at 73·17 per cent. silver, and the presence of phase boundaries at compositions corresponding to 74, 81, 87·5, and about 89 per cent. silver.

In the first place the results which show the variation of the resistivity with percentage composition by weight (Table II. and Graph 2) will be considered. An examination of Graph 2 shows that the addition of silver to tin causes a slight fall in the resistivity until the composition corresponding to that of the compound Ag_3Sn (73·17 per cent. Ag) is reached. Over this range of composition the resistivity changes almost linearly with composition. Between 73·17 and 74 per cent. silver the curve ascends almost vertically, the final value of the resistivity at a composition which corresponds to the end of the pure γ phase being about three times that of its initial value. The beginning of the $\beta+\gamma$ phase is indicated by a slight initial fall in the resistivity, which is followed by a rapid rise to a sharp peak corresponding to the boundary between the $\beta+\gamma$ and the β phases. From this point the specific resistance falls rapidly to its value for pure silver. The boundaries between the β and $\alpha+\beta$ and between the $\alpha+\beta$ and α phases are not clearly shown in the resistivity curve. The curve, however, shows slight changes of slope near the phase boundaries. The presence of these phase boundaries is shown much more clearly in the curves connecting the other physical properties with composition.

The effect of annealing on the resistivities of the alloys was on the whole rather irregular in both magnitude and direction. In the case of alloys containing 72·4, 73·17, and 76·10 per cent. of silver annealing produced a far greater change in the resistivities than in the case of the other alloys. The addition of silver to tin for unannealed alloys in the $\gamma+$Sn phase produced in general an increase of resistivity. On annealing for a fortnight practically all the resistivities diminished, so that the variation of resistivity with composition was approximately represented by a straight line sloping gradually downwards.

The variation of the Hall coefficients with percentage of silver in the alloy is shown in Graph 3. From the small negative value it has for tin the Hall coefficient decreases and crosses the zero axis at a composition of approximately 5 per cent. of silver. It then increases

slowly, reaching a maximum positive value at 73·17 per cent. silver (Ag_3Sn), and afterwards diminishes rapidly in the γ phase until the boundary between the γ and $\beta+\gamma$ phases is reached. From this point, the coefficient increases slightly and bends back to cross the composition axis at 79 per cent. silver. The negative value of the coefficient then increases rapidly until the boundary between the β and $\alpha+\beta$ phases (87·5 per cent. silver) is reached. The boundary between the $\beta+\gamma$ and the β phases at 81 per cent. silver is not shown on the curve. The presence of the narrow $\alpha+\beta$ field between 87·5 and 89 per cent. silver is, however, clearly indicated. The limit of the α solid solution is shown to be situated at a composition in the neighbourhood of 89 per cent. silver, and this result is in reasonable agreement with that given by Murphy. From Table III. it is seen that within experimental error the Hall coefficients of the alloys are independent of the strength of the magnetic field.

Graph 4 shows how the mean temperature coefficient of resistance varies with the composition. The limits of the γ phase and the boundary between the $\beta+\gamma$ and β phases are very clearly indicated on the curve. On the other hand the phase boundaries between the β and $\alpha+\beta$ and between the $\alpha+\beta$ and α phases are not shown.

In all phases except in the γ+Sn phase an increase in resistivity is accompanied by a decrease in the temperature coefficient of resistance. In the γ+Sn phase the variations in both quantities were comparatively small but in the same direction.

The agreement between the values of the temperature coefficients of alloys in and near the γ phase over the two temperature ranges 0°–40° C. and 0°–100° C. showed that if an allotropic change occurred in these alloys at 60° C. when heated to the higher temperature its effect on the temperature coefficients was small. Similar results were also obtained in measurements of the thermoelectric powers of the alloys over two different temperature ranges.

The variation of the thermoelectric power with composition is indicated in Graph 5. This curve shows all the phase boundaries given by Murphy in his equilibrium diagram.

The curve (Graph 6), showing the variation of density

with composition, lies near the straight line joining the points corresponding to the densities of tin and silver. The greatest deviation from the straight line occurs in the region in the neighbourhood of the compound Ag_3Sn. The values of the densities obtained in the present investigation are higher than those obtained by Maey * and Matthiessen †. The density of the compound Ag_3Sn obtained in this investigation is in agreement with the value calculated from the lattice constants determined by Davies ‡.

The experimental results show that the physical properties of the alloys are intimately connected with their structure, and that the positions of the phase boundaries as deduced from the measurements are in agreement with the observations of Murphy as given in his equilibrium diagram (Graph 1 B).

References.

(1) Phil. Mag. xxii. p. 417 (Sept. 1936).
(2) *Comptes Rendus,* cxxiii. p. 172 (1896).
(3) Bull. Soc. d'Encour. (5) ii. p. 415 (March 1897).
(4) Phil. Trans. Roy. Soc. clxxxix. p. 25 (1897) (A).
(5) *Zeit. Phys. Chem.* xxvii. p. 148 (1898).
(6) Journ. Franklin Inst. cliv. p. 201 (1902).
(7) *Proc. K. Akad. Wet. Amsterdam,* vi. p. 26 (1903).
(8) *Zeit. Anorg. Chem.* liii. p. 200 (1907).
(9) Journ. Chem. Soc. xcix. p. 195 (1911).
(10) Journ. Inst. Metals, xxxv. p. 107 (1926).
(11) 'Metallographie,' Bd. i. T. i. p. 690.
(12) Journ. Inst. Metals, lv. p. 115 (1934).
(13) Pogg. *Ann.* cx. pp. 21, 190 (1860); Phil. Trans. cl. p. 161 (1860).
(14) *Zeit. Phys. Chem.* xxxviii. p. 297 (1901).
(15) Phil. Trans. cl. p. 85 (1860); Pogg. *Ann.* cxvi. p. 369 (1862).
(16) Journ. Franklin Inst. cxcii. pp. 69 & 157 (1921); Phys. Rev. (2) xxiii. p. 307 (1924).
(17) *Zeit. Electro. Chem.* xv. p. 647 (1909).
(18) *Ann. der Physik,* (4) xxxii. p. 261 (1910).
(19) *Zeit. Electro. Chem.* xv. p. 648 (1909).
(20) Phil. Trans. x. p. 203 (1827).
(21) *Atti. Inst. Veneto,* (6) 5, xix. p. 1137 (1887).
(22) *Zeit. Phys. Chem.* xxvii. p. 148 (1898).
(23) *Koll. Zeit.* xxxvi. p. 86 (1925).
(24) Phil. Mag. xvi. p. 329 (1933).

* *Loc. cit.* (see reference 14).
† *Loc. cit.* (see reference 13).
‡ Thesis for Ph.D. degree University of Wales, 1933.

XCIX. *The Crystal Structures of Ni_2Al_3 and $NiAl_3$.* *By* A. J. Bradley, *D.Sc., Royal Society Warren Research Fellow, and* A. Taylor, *Ph.D., Darbishire Research Fellow* *.

AN X-ray examination of the nickel-aluminium alloys [1] has shown the existence of the following structures : Ni_3Al, Ni_2Al_3, and $NiAl_3$, in addition to the solid solutions of aluminium in nickel and nickel in aluminium. Of the intermediate phases Ni_3Al and NiAl have simple structures. Ni_3Al [2] is face-centred cubic with aluminium at cube corners and nickel at the centres of cube faces, while NiAl [3] is body-centred cubic with aluminium at cube corners and nickel at cube centres. The extraordinary changes in lattice spacing which occur in these phases are described elsewhere [1]. In the present paper we shall describe the solution of the more complicated structures Ni_2Al_3 and $NiAl_3$, from X-ray powder photographs.

Ni_2Al_3 is a trigonal crystal, but is best regarded as a deformed CsCl type in which aluminium occupies cube corners and nickel cube centres. The absence of one-third of the number of nickel atoms changes the composition from NiAl to Ni_2Al_3, and produces the debasement from cubic symmetry. This simple relation between NiAl and Ni_2Al_3 is easily seen from the powder photographs and gives a satisfactory means for solving the structure.

$NiAl_3$ has a complicated orthorhombic structure. It was solved completely from X-ray powder photographs taken in a camera of 19 cm. diameter. The first step was to make very accurate measurements of the reflexions of highest spacing from a film taken with cobalt radiation. On arranging the $\sin^2\theta$ values in sequence we noticed arithmetical relationships which gave clues to the indices of the lines. After a few trials a unit cell was selected which accounted for all the measurements. Accurate values of the cell dimensions were found from a film taken with chromium radiation.

The missing reflexions gave the space-group *Pnma* for $NiAl_3$, and the atomic coordinates were found from a rigorous comparison of the X-ray intensities. It was

* Communicated by Prof. W. L. Bragg, F.R.S.

interesting to find that the interatomic distances were almost identical in Ni_2Al_3 and $NiAl_3$ in spite of the complete dissimilarity of structure.

After the structure of $NiAl_3$ had been solved we were surprised to find a resemblance to cementite (Fe_3C), although the axial ratios are quite different. The positions of the aluminium atoms in $NiAl_3$ agree well with those of the iron atoms in cementite. Owing to the low scattering power of carbon it is difficult to be sure of the positions of these atoms, and different structures have been proposed by Hendricks [4], Westgren [5], and Shimura [6]. The nickel distribution in Ni_3Al, determined solely from the X-ray intensities, is not at all like the carbon distribution suggested by Hendricks, but it agrees closely with that proposed by Westgren on spatial grounds.

Ni_2Al_3.

A comparison of the powder photographs of Ni_2Al_3 and NiAl lead to a solution of the structure. The powder pattern of NiAl, which is body-centred cubic, with aluminium at cube corners and nickel at cube centres, greatly resembles the pattern of Ni_2Al_3, but the latter contains extra lines. The lines corresponding to the strong lines of the NiAl pattern are present in almost the same positions but are split up into doublets and triplets, and other weak lines are present. This pattern can be explained by a trigonal structure in which the atoms fit together very like a body-centred cube.

We may think of a structure such a NiAl as being built up from six interpenetrating trigonal lattices, three of nickel and three of aluminium. The mutual positions of the six lattices are such that the structure has cubic symmetry. In Ni_2Al_3 one of the six lattices is missing, so that cubic symmetry is impossible. The unit cell is trigonal and contains two atoms of nickel and three of aluminium. The aluminium atoms fit together to make distorted cubes with almost the same dimensions as in NiAl; two-thirds of the sites at the centres of the distorted cubes are taken up by nickel atoms, the rest are left vacant.

The empty sites in Ni_2Al_3 are regularly distributed in planes perpendicular to the trigonal axis; this gives the effect of a trigonal superlattice, adding additional lines to the powder pattern. It is interesting to contrast the

powder patterns of the aluminium—rich alloys of the NiAl phase. Density and lattice spacing measurements[1] have shown that here also there are empty sites at some of the cube centres. Because the vacancies are at random there is then no distortion of the cubic symmetry, and the powder pattern is scarcely distinguishable from that of NiAl itself.

Figs. 1 and 2 illustrate the structure of Ni_2Al_3. In fig. 1 the nickel and aluminium atoms are shown by

Fig. 1.

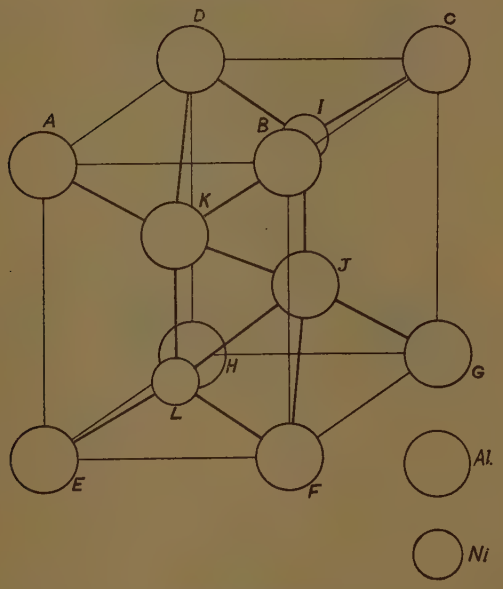

Ni_2Al_3 unit cell.

circles of different sizes. The large circles indicate aluminium atoms, the small circles nickel. The atoms ABCDEFGH lie at the corners of the trigonal unit cell, which also contains the atoms IJKL, situated on three-fold axes. The positions of the atoms at the corners of the cell are of course fixed, but the heights of the atoms IJKL are not determined by symmetry requirements. They were found from the intensity measurements.

The thick lines in fig. 2 outline the pseudo-cubic unit. In the particular one chosen there are aluminium atoms at each of the corners of the pseudo-cube but no nickel atom at the centre. If we had chosen a neighbouring cube for representation on the diagram it would have been seen that it contained a nickel atom almost exactly at the centre. The atoms are shaded to indicate depth, the darkest atoms being nearest the observer. It can

Fig. 2.

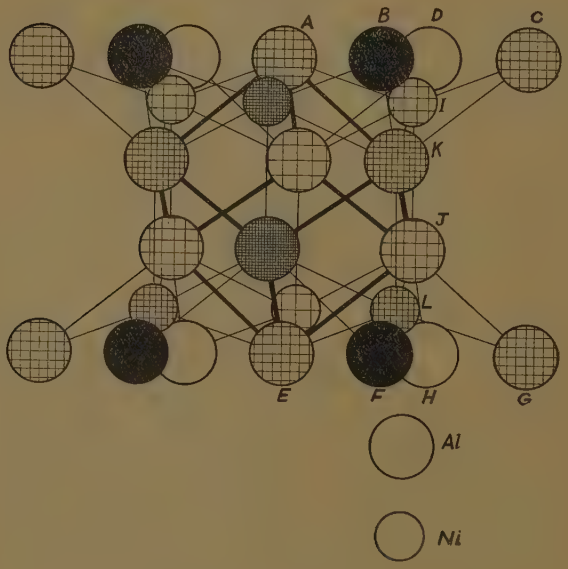

Ni_2Al_3 pseudo-cubic unit.

be seen that the atoms lie in planes perpendicular to the trigonal axis. A plane of nickel atoms lies between two planes of aluminium, but the centre plane in the drawing is missing.

The dimensions of the unit cell were found from a powder photograph taken with chromium radiation, particulars of which are given in Table I. The close agreement between the observed and calculated values of $\sin^2\theta$ for the high order reflexions indicates an accuracy in the spacing measurements of about 1 part in 30,000.

Table II., showing the results from cobalt radiation, confirms the chromium measurements, but it is more difficult to get accurate measurements as there are no strong lines at high angles. The chief value of this powder photograph was for intensity measurements, which are more difficult to obtain from the chromium film.

TABLE I.

Ni_2Al_3.—Powder Photograph.

Chromium Kα Radiation.

Indices *hkil.*		$\sin^2\theta$ observed.	$\sin^2\theta$ calculated.	Indices *hkil.*		$\sin^2\theta$ observed.	$\sin^2\theta$ calculated.
$10\bar{1}4$	α_2	·98382	·98386	$20\bar{2}2$	α	·6482	·6481
	α_1	·98054	·98052	$10\bar{1}3$	α	·5993	·5992
$12\bar{3}2$	α_2	·97252	·97250	$11\bar{2}2$	α	—	·5406
	α_1	·96916	·96920	0003	α	·4841	·4842
$30\bar{3}0$	α_2			$20\bar{2}1$	α		
	α_1	·96543	·96543	$20\bar{3}0$	α	·4295	·4296
$20\bar{2}3$	α_2	·92304	·92340	$11\bar{2}1$	α	·3775	·3768
	α_1	·92023	·92028	$10\bar{1}2$	α	·3269	·3260
0004	α	·8741	·8742	$11\bar{2}0$	α	·3227	·3222
$11\bar{2}3$	α	·8127	·8130	0002	α	—	·2184
$12\bar{3}1$	α_2	·8084	·8082	$10\bar{1}1$	α	·1631	·1621
	α_1	·8053	·8055	$10\bar{1}0$	α	·1083	·1074
$12\bar{3}0$	α_2	·7539	·7535	0001	α	·0556	·0546
	α_1	·7510	·7509				

Cell dimensions :—

$a = 4{\cdot}0282$ Å. $c/a = 1{\cdot}2141$.
$c = 4{\cdot}8906$ Å.

The Atomic Coordinates of Ni_2Al_3.

Theoretically there are eight possible space-groups, but it is only necessary to consider those which explain the relationship to the body-centred cube so clearly shown by the powder photographs. The space-group $D3^3_{3d}$, ($C3m$), has the highest symmetry consistent with all requirements. The atoms must all be placed on the three-fold axes, and in this case the only possible symmetry degradation would remove the centre of symmetry giving C^1_{3v}. In view of the satisfactory intensity checks in Table II. the higher symmetry seems more probable.

Table II.

Ni_2Al_3.—Powder Photograph.
Cobalt Kα Radiation.

Indices *hkil.*		$\sin^2\theta$ observed.	$\sin^2\theta$ calculated.	Intensity observed.	Intensity calculated.
$21\bar{3}4$	α_1	·9915	·9914	Not measured.	
$31\bar{4}2$	α_2	·9889	·9888		
	α_1	·9846	·9845		
$22\bar{4}2$	α_2	—	·9230	—	—
	α_1	—	·9190	—	—
$10\bar{1}5$	α_2	·9018	·9023	60	60·5
	α_1	·8984	·8984		
$30\bar{3}3$	α_2	—	·8930		
	α_1	—	·8904	72	73
$31\bar{4}1$	α_2	·8886	·8884		
	α_1	·8843	·8845		
$31\bar{4}0$	α_2	·8547	·8549	51	49·2
	α_1	·8507	·8512		
0005	α_2	—	·8368	—	—
	α_1	—	·8326		
$22\bar{4}1$	α_2	·8224	·8226	50	53
	α_1	·8185	·8190		
$20\bar{2}4$	α_2	·7982	·7984		
	α_1	·7945	·7950	562	470
$22\bar{4}0$	α_2	·7889	·7891		
	α_1	·7851	·7858		
$21\bar{3}3$	α_2	·7608	·7615	72	63
	α_1	·7574	·7582		
$11\bar{2}4$	α_2	·7327	·7327		
	α_1	·7284	·7257	153	148
$30\bar{3}2$	α_2	·7327	·7295		
	α_1	·7284	·7226		
$30\bar{3}1$	α	·6229	·6235	49	44
$10\bar{1}4$	α	·5993	·5990		
$21\bar{3}2$	α	·5910	·5924	1120	926
$30\bar{3}0$	α		·5902		
$20\bar{2}3$	α	·5619	·5627	39	39
0004	α	·5332	·5334	29	25·6
$11\bar{2}3$	α	faint.	·4970	57	60·6
$21\bar{3}1$	α	·4917	·4925		
$21\bar{3}0$	α	·4593	·4591	41	44·4
$20\bar{2}2$	α	·3959	·3958	383	347
$10\bar{1}3$	α	·3662	·3659	55	62
$11\bar{2}2$	α	—	·3301	—	—
0003	α	·2959	·3003	47	51
$20\bar{2}1$	α		·2958		
$20\bar{2}0$	α	·2624	·2624	44	45·6
$11\bar{2}1$	α	·2317	·2301	122	129
$10\bar{1}2$	α	·1988	·1989	1717	1570
$11\bar{2}0$	α		·1967		
0002	α	—	·1334	—	—
$10\bar{1}1$	α	·0993	·0989	165	172
$10\bar{1}0$	α	·0661	·0656	200	202
0001	α	·0336	·0334	188	161

The atomic coordinates are

Al_a.... 0 0 0.

Al_b.... 1/3, 2/3, z_1 ; 2/3, 1/3, $\bar{z}_1$; where $z_1=0{\cdot}352$.

Ni .... 1/3, 2/3, z_2 ; 2/3, 1/3, $\bar{z}_2$; where $z_2=0{\cdot}149$.

The interatomic distances are given below in Table III.

TABLE III.

Interatomic Distances in Ni_2Al_3.

Type of atom.	No. of neighbours.	Type of neighbours.	Distances in Å.
Ni	3	Al_a	$2{\cdot}43_5$
	1	Al_b	2·44
	1	Al_b	2·45
	3	Al_b	$2{\cdot}52_5$
	3	Ni	$2{\cdot}73_5$
Al_a	6	Ni	$2{\cdot}43_5$
	6	Al_b	$2{\cdot}89_0$
Al_b	1	Ni	2·44
	1	Ni	2·45
	3	Ni	$2{\cdot}52_5$
	3	Al_b	$2{\cdot}73_5$
	3	Al_a	$2{\cdot}89_0$

The interatomic distances fall into two distinct sets—those between like atoms and those between unlike atoms. The general scheme is so close to that of NiAl that it is not surprising to find that the distances are similar. It will be seen later that, in spite of the great difference in structure, the distances in $NiAl_3$ are again of about the same magnitude, the closest neighbours being unlike atoms.

The Unit Cell of $NiAl_3$.

The structure of $NiAl_3$ was solved from a powder photograph taken in a camera of 19 cm. diameter. Chromium and cobalt Kα radiations were used with vanadium and iron screens to remove the β radiations. The innermost lines were stronger and clearer on the

cobalt film, from which the space-group could be found, but at higher angles the lines became so crowded together that it was impossible to decipher them. The chromium photograph, though less suitable for low angles, gave many clearly resolved α-doublets from which the lattice spacings could be accurately measured.

TABLE IV.

$NiAl_3$.—Powder Photograph.

Cobalt K_α Radiation.

Indices *hkl*.		$\sin^2\theta$ observed.	$\sin^2\theta$ calculated.	F(*hkl*) observed.	F(*hkl*) calculated.
011	α	·0496	·0494	8·1	7·9
101	α	·0530	·0529	11·8	11·8
020	α	·0591	·0591	14·9	16·9
111	α	·0678	·0677	11·3	12·5
200	α	—	·0736	0	3·1
210	α	·0882	·0881	14·6	15·0
201	α	·1082	·1079	4·1	4·3
121	α	—	·1110	0	1·2
211	α	·1230	·1227	8·6	7·9
220	α	·1325	·1324	16·2	15·6
002	α	·1386	·1385	16·4	14·8
102	α	·1565	·1567	6·2	6·4
221 / 031	α	·1672	·1670 / ·1675	18·0	16·3
112	α	·1716	·1715	19·2	18·2
131	α	·1858	·1858	21·4	21·4
022	α	·1980	·1974	20·9	21·6
301	α	·1999	·1996	29·9	31·0
230	α	·2063	·2062	29·6	29·0
202	α		·2118	4·7	5·1
311	α	·2156	·2144	13·5	12·8
122	α		·2158	19·3	19·3
212	α	·2266	·2265	14·6	14·5
040	α	·2366	·2362	27·1	30·1
231	α	—	·2408	0	1·6
321	α	·2587	·2589	12·3	11·9

The pattern was clearly inconsistent with high symmetry, and an attempt was therefore made to find an orthorhombic unit cell. A complicating factor was introduced by the missing reflexions, but an arithmetical method was devised by means of which the indices of the lines were found. As the method is of general application in the case of orthorhombic crystals a detailed account may be of some interest.

Table IV. gives a list of the observed values of $\sin^2\theta$

in ascending order of magnitude. For an orthorhombic crystal, where $\sin^2\theta = \left(\frac{\lambda}{2}\right)^2 \left\{ \frac{h^2}{a^2} + \frac{k^2}{b^2} + \frac{l^2}{c^2} \right\}$, it was necessary to separate the three terms depending on a, b, and c. It seemed probable that the 200, 020, or 002 reflexions might be identified among the first few lines. For example, in the case of the third line, a numerical coincidence was observed. Putting $\sin^2\theta_{020}=0{\cdot}0591$, $\sin^2\theta_{010}=0{\cdot}0148$. This number is exactly equal to the difference between two other observed values, 0·0678 and 0·0530. The coincidence was explained by supposing these reflexions to be 111 and 101 respectively; the following equation was satisfied:

$$\sin^2\theta_{111}=\sin^2\theta_{010}+\sin^2\theta_{101}.$$

No further coincidence of this type was detected until the value 0·1386 was reached. Putting $\sin^2\theta_{002}=0{\cdot}1386$, $\sin^2\theta_{001}=0{\cdot}0346_5$. This number is equal to the difference between 0·1227 and 0·0881, which are the values of two lines later identified as 211 and 210.

Assuming 020 and 002 to be correctly identified, it was possible to find 011.

$$\sin^2\theta_{011}=\sin^2\theta_{010}+\sin^2\theta_{001}=0{\cdot}0148+0{\cdot}0346=0{\cdot}0494.$$

This was practically equal to the value for the first line on the film, which was therefore identified as 011. The value for 100 followed immediately.

$$\sin^2\theta_{100}=\sin^2\theta_{111}-\sin^2\theta_{011}=0{\cdot}0678-0{\cdot}0494=0{\cdot}0184.$$

200 was absent, but a check was obtained from 210 and 211, as follows:—

$$\sin^2\theta_{200}=\sin^2\theta_{210}-\sin^2\theta_{010}=0{\cdot}0881-0{\cdot}0148=0{\cdot}0733.$$

This gives $\sin^2\theta_{100}=0{\cdot}0183$, in good agreement with the previous determination.

We were now able to calculate a complete series of $\sin^2\theta$ values, to match every measured line. Many of the calculated reflexions were absent; a list of these is given in Table VI., from which the space-group was found. The $\sin^2\theta$ measurements on the cobalt film were accurately made over the first 20 lines. This is sufficient to fix the unit cell dimensions to about 1 part in 1000. It is essential to the success of the method that each line

should be measured to almost this degree of accuracy and that each line should be clearly resolved; otherwise it is not possible to find the indices. For the solution of the present structure a camera of 19 cm. diameter was required; photographs taken in a smaller camera were quite unsatisfactory.

TABLE V.

$NiAl_3$.—Powder Photograph.

Chromium Kα Radiation.

Indices *hkl*.		$\sin^2\theta$ observed.	$\sin^2\theta$ calculated.	F(*hkl*) observed.	F(*hkl*) calculated.
152	α_1	·8602	·8603	17·5	18·0
	α_2	·8631	·8632		
440	α_1	·8665	·8662	9·2	9·6
	α_2	·8695	·8692		
060	α_1		·8695	24·1	24·1
	α_2	·8725	·8725		
323	α_1	·8759	·8759	14·6	15·2
	α_2	·8789	·8789		
342	α_1	·8828	·8828	5·5	5·1
	α_2	·8857	·8857		
521	α_1	·9028	·9028	17·3	17·3
	α_2	·9060	·9059		
004	α_1		·9057	12·3	11·9
	α_2	·9087	·9088		
441	α	—	·9256	2·6	2·3
432	α	—	·9263	0·0	0·06
143	α_1	·9261	·9259	6·0	4·0
	α_2	·9305	·9291		
351	α_1		·9303	11·0	10·7
	α_2	·9334	·9334		
104	α_1	·9357	·9357	15·9	15·2
	α_2	·9388	·9389		
252	α_1	·9502	·9502	13·3	13·1
	α_2	·9534	·9534		
161	α_1	·9561	·9561	2·0	2·3
	α_2	·9598	·9594		
114	α_1		·9598	15·2	13·9
	α_2	·9630	·9631		

Beyond the limits of Table IV. the pattern becomes more complex with overlapping lines. The measurements of $\sin^2\theta$ were stopped at this point, but more data were obtained by the photometer, and are included in Table VII. Quite good resolution of the high order reflexions was obtained from another film taken with chromium radiation, the results of which are given in Table V.

The cell dimensions were found from the chromium film to an accuracy of at least 1 part in 20,000.

$$a = 6{\cdot}5982 \text{ Å.},$$
$$b = 7{\cdot}3515 \text{ Å.},$$
$$c = 4{\cdot}8021 \text{ Å.}$$

The composition agrees closely to $NiAl_3$. There are 16 atoms per unit cell, of which 4 are nickel and 12 aluminium.

The Space-group.

In Table VI. are summarized all the reflexions which are missing from the chromium and cobalt films. There

TABLE VI.

$NiAl_3$.—Missing Spectra.

Cobalt Kα radiation.						Chromium Kα radiation.		
hkl.	$\sin^2\theta$ calc.	Why absent.	*hkl.*	$\sin^2\theta$ calc.	Why absent.	*hkl.*	$\sin^2\theta$ calc.	Why absent.
010	·0148	*b*	140	·2546	*a*	233	·8478	*c*
100	·0183	*a*	222	·2708	*c*	520	·8512	*a*
110	·0331	*a*	041	·2709	*b*	[350	·8761]	*a*
001	·0347	*b*	032	·2713	*b*	043	·8969	*b*
200	·0733	*c*	330	·2979	*a*	160	·9005	*a*
120	·0774	*a*	003	·3115	*b*	432	·9247	*c*
021	·0937	*a*	050	·3691	*b*	061	·9272	*b*
121	·1120	*c*	023	·3705	*b*	014	·9309	*b*
[030	·1329]	*b*	[150	·3875]	*a*	530	·9720	*a*
130	·1512	*a*	340	·4012	*a*			
012	·1532	*b*	500	·4582	*a*			
300	·1650	*a*	510	·4730	*a*			
310	·1797	*a*	[052	·5076]	*b*			
320	·2240	*a*	520	·5173	*a*			
231	·2408	*c*						

a=*hko* where *h* is odd, *b*=*okl* where *k*+*l* is odd.
c="accidentally" missing Brackets indicate overlapping lines.

are two sets of systematic absences, $-hk$O, where h is odd, and Okl, where $k+l$ is odd. In addition there are a number of lines which are too weak to be observed; these help to fix the atomic coordinates. The possible space-groups are D_{2h}^{16} (P*nma*), and C_{2v}^{9} (P*na*). The former has the higher symmetry and is the more probable, giving a satisfactory explanation of all the observed lines.

There are several different ways of arranging the atoms to give the required symmetry. Groups of four and eight are possible. The four groups may lie either at centres of symmetry or on symmetry planes. The groups of eight are in general positions. Intensity agreement can be obtained by putting four nickel atoms and four aluminium atoms on symmetry planes and eight aluminium atoms in general positions.

The atomic coordinates are :—

4−Ni : $x_1, \frac{3}{4}, z_1$; $x_1, \frac{1}{4}, \bar{z}_1$; $\frac{1}{2}+x_1, \frac{3}{4}, \frac{1}{2}-z_1$; $\frac{1}{2}-x_1, \frac{1}{4}, \frac{1}{2}+z_1$.

4−Al : $x_2, \frac{1}{4}, z_2$; $\bar{x}_2, \frac{3}{4}, \bar{z}_2$; $\frac{1}{2}+x_2, \frac{1}{4}, \frac{1}{2}-z_2$; $\frac{1}{2}-x_2, \frac{3}{4}, \frac{1}{2}+z_2$.

8−Al : x_3, y_3, z_3 ; $x_3, \frac{1}{2}-y_3, z_3$; $\frac{1}{2}+x_3, y_3, \frac{1}{2}-z_3$; $\frac{1}{2}+x_3, \frac{1}{2}-y_3, \frac{1}{2}-z_3$;

$\bar{x}_3, \bar{y}_3, z_3$; $\bar{x}_3, \frac{1}{2}+y_3, \bar{z}_3$; $\frac{1}{2}-x_3, \bar{y}_3, \frac{1}{2}+z_3$; $\frac{1}{2}-x_3, \frac{1}{2}+y_3, \frac{1}{2}+z_3$.

$x_1=0{\cdot}131, \quad y_1=0{\cdot}75, \quad z_1=0{\cdot}055,$

$x_2=0{\cdot}011, \quad y_2=0{\cdot}25, \quad z_2=0{\cdot}415,$

$x_3=0{\cdot}174, \quad y_3=0{\cdot}053, \quad z_3=0{\cdot}856.$

The Choice of Coordinates.

The coordinates given above were found as the result of a careful study of the observed intensities of the lines, with special reference to the absent spectra. The structure contains planes of symmetry, $y=\frac{1}{4}$, and $y=\frac{3}{4}$. It is not difficult to decide which atoms lie in these planes, and which are between them. Any atoms lying between these planes must be fairly near a midway position ; otherwise pairs of atoms which are mirror images of each other would be too close together. For this reason the y coordinates must be near 0 and $\frac{1}{2}$ unless the atoms are on the mirror planes. The large structure factor of 040 confirms this conclusion.

On spatial grounds it is probable that eight atoms will lie on the mirror planes and eight atoms between them. It is then possible to obtain the correct intensity for 020. There are two possibilities for the atoms between the mirror planes : either they lie at centres of symmetry or they form an eight group of atoms in general positions. The former solution does not give the correct intensities ; 060 must then have the same structure factor as 020,

which is certainly wrong. The only satisfactory solution must include a group of eight aluminium atoms in general positions. The remaining four aluminium atoms together with the four nickel atoms then lie on the mirror planes.

There was one y parameter to fix, that of the eight group, (y_3). This was found from 020 and 040, but a more accurate value was afterwards obtained from the high order reflexions on the chromium film.

Knowing y_3, it was possible to find x_3 and z_3. This was done by comparing reflexions hkl with $hk+2l$. The total contribution of the atoms on the planes of symmetry is identical for the two sets of planes ; that of the other eight aluminium atoms is approximately equal in magnitude but opposite in sign. For example, in a comparison of 101 with 121 the contributions α, of the four nickel atoms, and β, of the four aluminium atoms, are the same. For 101 the contribution γ_{101} of the eight aluminium atoms is opposite in sign to γ_{121}, which is their contribution to 121, *i. e.*,

$$\gamma_{121}=-\gamma_{101}.$$

The structure factors F_{101} and F_{121} can now be related to each other.

$$F_{101}=\alpha+\beta+\gamma_{101}, \quad . \quad . \quad . \quad . \quad . \quad . \quad (1)$$

$$F_{121}=\alpha+\beta+\gamma_{121}=\alpha+\beta-\gamma_{101}. \quad . \quad . \quad (2)$$

121 is absent, so that $F_{121}=0$, and we find that

$$\alpha_{101}+\beta_{101}=\gamma_{101}=\tfrac{1}{2}F_{101}. \quad . \quad . \quad . \quad (3)$$

This approximate relationship enables the two parameters x_3 and z_3, which determine the value of γ, to be found independently of the values of x_1, x_2, z_1, and z_2.

Similar considerations apply to the two reflexions 200 and 220. In this case 200 is absent, and the formula is therefore slightly different :

$$F_{200}=\alpha_{200}+\beta_{200}+\gamma_{200}=0, \quad . \quad . \quad . \quad . \quad (4)$$

$$F_{220}=\alpha_{220}+\beta_{220}+\gamma_{220}$$

$$=\alpha_{200}+\beta_{200}-\gamma_{200}, \quad . \quad . \quad . \quad . \quad (5)$$

$$\alpha_{200}+\beta_{200}=-\gamma_{200}=\tfrac{1}{2}F_{220}. \quad . \quad . \quad . \quad . \quad (6)$$

From this equation the value of x_3, which determines γ_{200}, can be found independently of the other parameters.

The above methods may be extended to other planes until approximate values have been found for all seven

parameters. It is not possible to get exact values by this means, because the experimental errors in the intensity values cause difficulties, and some of the parameters cannot be found independently of one another by this method of deduction.

The final process of fixing the exact values of the parameters is done from a complete comparison of all

TABLE VII.

$NiAl_3$.—Intensity Comparison for Cobalt Radiation.

Intensity.			Intensity.			Intensity.		
hkl.	Obs.	Calc	*hkl.*	Obs.	Calc.	*hkl.*	Obs.	Calc.
011	23	22	040	17	21	421	4	4
101	44	44	321	12	11	123	7	7
020	31	40	141	8	10	142	1	1
111	60	74	132			213	6	5
210	37	40	400	6	5	051	4	5
201	2	2	302	2	2	151		
211	17	15	410	2	2	430		
220	27	25	240			402	31	32
002	13	11	312	4	4	341		
102	3	3	013	3	3	332		
221	44	42	401	4	5	250		
031			103	0	0	223		
112	53	48	331	7	7	033	18	15
131	58	58	411	37	37	412		
022	26	27	241			242		
301	52	56	113			431	2	2
230	45	43	232			133		
202	1	1	420	8	9	303	5	5
311	19	17	322	2	1	251		
122	38	38	042	6	7	422		
212	20	20	203	3	2	313	6	5
						501		
						511	2	2

the observed and calculated intensities, starting with the lowest order reflexions and concluding with the resolved α-doublets on the chromium film. At the beginning some of the values were almost correct, especially y_3 and x_3, which were found in the direct manner described above. Others were in error by as much as 0·1 of the unit cell dimensions. The corrections had to be made by the simultaneous adjustment of all seven parameters to give the best possible agreement between observed and calculated intensities.

The most accurate values of the parameters were found by a new method which is of general application and will be described elsewhere. The agreement between the observed and calculated intensities in Tables IV., V., and VII. is a proof of the soundness of the deductions. The scale of the observed intensities is adjusted to that of the calculated values by a graphical method, as in the case of Cr_2Al and Cr_5Al_8 [7]. Fig. 5 shows the graph for $NiAl_3$ with cobalt radiation. Log (F calc./F obs.) is plotted against $\sin^2\theta/\lambda^2$. If there were no experimental error and the temperature factors for the aluminium and nickel atoms were identical all the points should lie on a straight line, the slope of which depends on the temperature factor. By the use of this graph the observed

Fig. 3.

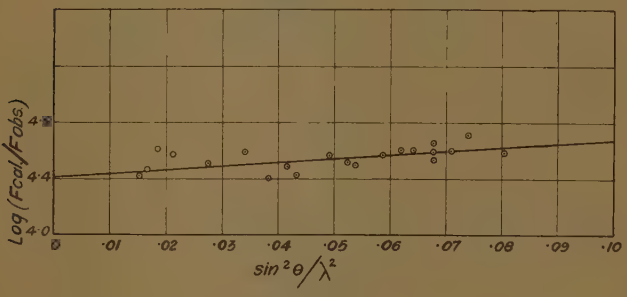

Cobalt Kα radiation.

values are easily brought to the scale of the calculated values, making the appropriate allowance for the temperature factor. While the parameters are being adjusted the graph is used to test the direction of the displacements from the original approximate positions of the atoms.

Discussion of the Structure of $NiAl_3$.

Projections of the structure of $NiAl_3$ are shown in figs. 4 and 5. Fig. 4 is a projection on the 001 face. The edges of the unit cell are outlined and the atoms are indicated by circles of different sizes and with different shading. The larger circles represent aluminium atoms, the smaller nickel. The shading indicates depth ; the lower the atom the lighter the shading. The *a* axis is

Fig. 4.

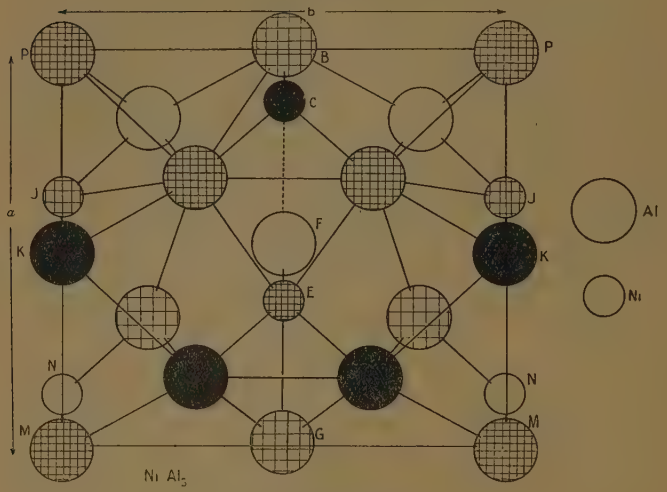

Projection on 001 face.

Fig. 5.

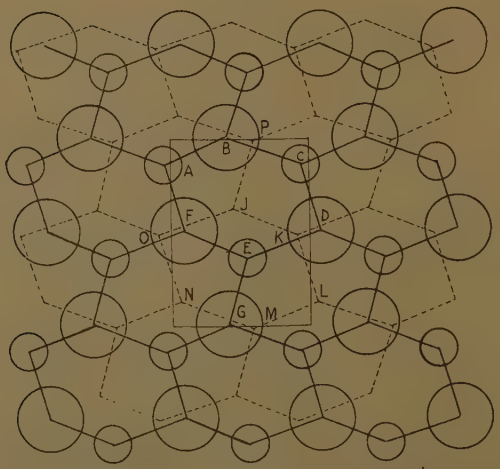

$NiAl_3$. Relative positions of atoms on the mirror planes (010).

the shorter of the two, and the mirror planes lie in this direction. The main feature of the structure, as seen from this drawing, is the distribution of the nickel atoms, which are so placed that they are as far away from one another as possible, no two making direct contact with one another.

Fig. 5 is a projection on the 010 face, showing only the atoms on the mirror planes. The unit cell is the small oblong in the centre of the diagram, but the drawing has been extended to include a large number of neighbouring atoms. By this means a characteristic feature of the structure is brought out—the presence of distorted hexagonal rings consisting of alternate aluminium and nickel

TABLE VIII.

Interatomic Distances in $NiAl_3$.

Type of atom.	Type of neighbours.	Distances.			
Ni	Al_a	2·44	2·46	2·72	
	Al_b	2·42	2·44	2·52	
		2·42	2·44	2·52	
Al_a	Ni	2·44	2·46	2·72	
	Al_b	2·78	2·86	2·87	3·06
		2·78	2·86	2·87	3·06
Al_b	Ni	2·42	2·44	2·52	
	Al_a	2·78	2·86	2·87	3·06
	Al_b	2·72	2·72	2·80	2·90

atoms. The ring ABCDEF is lettered to show the corresponding atoms in fig. 4. The hexagons shown by the dotted lines lie midway between the completed hexagons. The ring JKLMNO is also lettered to show the corresponding atoms in fig. 4.

The structure is a type of close-packing intermediate between the face-centred cubic type, where each atom has twelve neighbours, and the body-centred cubic type, where there are eight neighbours to each atom. Here the nickel atoms have nine neighbours, and the aluminium atoms have eleven. The interatomic distances are surprisingly consistent, aluminium to nickel distances being much smaller than aluminium to aluminium, as can be seen from Table VIII.

It is interesting to compare these values with the interatomic distances in Ni_2Al_3 and NiAl. The Ni—Al distances are surprisingly similar. If we omit the one large value of 2·72 we find that nickel has eight aluminium neighbours of average distance 2·46 Å. in $NiAl_3$; in Ni_2Al_3 nickel has again eight aluminium neighbours of distance 2·46; whereas in NiAl the eight aluminium neighbours of the nickel atoms are at 2·49 Å. The nickel to nickel distances in NiAl and Ni_2Al_3 are much greater than in the pure metal; probably they do not represent any points of real contact between the atoms, since here, as in $NiAl_3$, the nickel atoms are so distributed that they are as far apart as possible. The aluminium–aluminium distances vary slightly with the circumstances. When there are twelve or more neighbours the distances are about equal to those in the pure metal (2·86 Å.); with only eleven neighbours two or three of these are nearer (2·72–2·78 Å.). In all cases the average distance is very near that in the pure metal. It may perhaps be legitimate to infer from these features that the state of the aluminium atom in the alloys is exactly the same as in the element except in its relation to the nickel atoms. Here the distances are far shorter than would be expected from an additive law. This suggests a strong interaction between aluminium and nickel. The very high melting-point of NiAl and the great heat of combination are [8] facts pointing in the same direction.

Acknowledgments.

We desire to thank Professor W. L. Bragg, F.R.S., for his kind interest in the work. One of us (A. T.) is indebted to the Permanent Magnet Association for a grant which enabled the work to be carried out. The aluminium used in the alloys was kindly supplied by Aluminium Française.

SUMMARY.

Ni_2Al_3 is trigonal, space-group D^3_{3d} (C3*m*). There are two nickel and three aluminium atoms in the unit cell, of which the dimensions are

$$\left.\begin{array}{l} a=4\cdot0282 \text{ Å.} \\ c=4\cdot8906 \text{ Å.} \end{array}\right\} c/a=1\cdot2141.$$

The aluminium atoms lie at the corners of a deformed cube, and the nickel atoms are very near to the centres of two-thirds of these pseudo-cubes. One-third of them are empty.

$NiAl_3$ is orthorhombic, space-group D_{2h}^{16} ($Pnma$).

$a = 6{\cdot}5982$ A.

$b = 7{\cdot}3515$ A.

$c = 4{\cdot}8021$ A.

The unit cell contains four nickel and twelve aluminium atoms arranged in a peculiar type of close-packing. The nickel atoms and four of the aluminium atoms form distorted hexagonal nets lying in the mirror planes of the structure. The other eight aluminium atoms are to be found almost midway between these planes.

The interatomic distances Ni–Al are almost the same in NiAl, Ni_2Al_3, and $NiAl_3$ (2·42–2·49 Å.); these are much smaller than the sums of the atomic radii. The Al–Al distances are on the average about the same as in the element (2·86 Å.).

References.

(1) A. J. Bradley and A. Taylor, Proc. Roy. Soc. A, clix. p. 56 (1937).
(2) A. Westgren and W. Ekman, *Arkiv. f. Kem. o. Ast.* 10 B. no. 11 (1930).
(3) K. Becker and F. Ebert, *Zeit. f. Phys.* xvi. p. 165 (1923).
(4) St. B. Hendricks and P. R. Kostiny, *Z. Krist.* lxxiv. p. 534 (1930).
(5) A. Westgren, *Jernkont. Ann.* p. 457 (1932).
(6) S. Shimura, Fac. Eng. Tokyo Univ. xx. p. 1 (1931).
(7) A. J. Bradley and S. S. Lu, *Z. Krist.* (A) xcvi. p. 20 (1937).
(8) F. Körber [with W. Oelsen, W. Middel, and H. Lichtenberg] Stahl u. Eisen, lvi. (48), p. 1401 (1936).

C. *The Raman Spectra of some Acid Chlorides.*

By V. N. Thatte *and* M. S. Joglekar, *M.Sc.**

[Plates XII. & XIII.]

IN this paper are reported the Raman spectra of a number of acid chlorides belonging to the aliphatic and aromatic classes. The substances studied include oxalyl chloride, succinyl chloride, and phthalyl chloride, which are of some interest in deciding their molecular

* Communicated by the Authors.

structure. The majority of the acid chlorides studied here were obtained from British drug houses. Oxalyl, succinyl, and phthalyl chlorides were obtained from Kahlbaum. The apparatus and experimental technique employed were similar to those recommended by Wood *. A mercury arc-lamp was used as a source of light. An aqueous solution of sodium nitrite was used as a filter,

TABLE I.

α-Chlor-propionyl Chloride.

Wave-length in air (Å.).	Intensity.	Exciting line (Å.).	Wave number difference. $\Delta\nu$ cm.$^{-1}$.
5015·5	1	4358·3	3005
5000·8	2	,,	2947
4984·1	0	,,	2880
4652·8	0	,,	1452
4606·8	2	4046·6	3003
4592·8	3	,,	2938
4581·6	0	,,	2885
4571·6	0	4358·3	1070
4499·5	3	,,	719
4464·1	2 *b*	,,	543
4444·5	4 *d*	,,	445
4257·0	0	,,	−545
4179·9	1 *b*	4046·6	788
4168·6	3 *b*, *d*	,,	723
4155·2	1 *b*	4077·6	451
4139·2	2 *b*, *d*	4046·6	553
4122·0	4 *d*	,,	452
4095·8	2	3654·8	2946
4089·3	3	3650·1	2942

$\Delta\nu$ =	3004, (1)	2943, (2)	2882, (0)	1452, (0)	1070, (0)	788, (1)	721, (3)	547, (26)	449. (4 *d*)

which considerably reduced the intensity of the fluorescent background in the region of the modified radiation due to 4358° Å. The spectra were photographed on a E_3 quartz spectrograph of Adam Hilger. The results obtained are shown in Tables I. to XI. The intensity was estimated visually, and gives a relative idea of the intensity of Raman lines in a spectrum. Broad and diffuse lines are marked *b* and *d* respectively.

* R. W. Wood, Phil. Mag. vi. p. 729 (1928).

TABLE II.

α-Chlor-butyryl Chloride (iso).

Exciting line 4358·3 Å.

Wave-length in air (Å.).	Intensity.	Wave number difference. $\Delta\nu$ cm.$^{-1}$.
4725·6	0	1782
4654·0	1	1457
4476·1	0	603
4463·2	3	538
4452·6	1	485
4440·5	1	424
4424·9	1	344
4411·3	1	275
4395·1	2	192

TABLE III.

Caproyl Chloride.

Exciting line 4358·3 Å.

Wave-length in air (Å.).	Intensity.	Wave number difference. $\Delta\nu$ cm.$^{-1}$.
4999·1	4	2940
4991·8	4	2911
4728·0	3	1793
4650·8	5 *b*	1442
4641·5	1	1399
4629·1	1	1342
4620·4	3	1301
4579·2	2	1106
4569·8	2	1061
4523·5	2	838
4491·5	3	680
4470·7	3	576
4441·4	10	429
4428·3	1	362
4278·3	2	−429
4230·6	1	−693

TABLE IV.

Oxalyl Chloride.

Exciting line 4358·3Å.

Wave-length in air (Å.).	Intensity.	Wave number difference. $\Delta\nu$ cm.$^{-1}$.
4724·1	2	1776
4572·9	1 *d*	1076
4478·7	6	617
4460·6	2 *d*	526
4447·2	4 *b*, *d*	458
4424·9	1	345
4409·9	2	268
4394·3	1	187
4307·1	0	−273

TABLE V.

Succinyl Chloride (symmetrical).

Exciting line 4358·3Å.

Wave-length in air (Å.).	Intensity.	Wave number difference. $\Delta\nu$ cm.$^{-1}$.
4999·7	1	2942
4730·3	1	1803
4644·0	1	1411
4603·5	0	1221
4571·6	0	1070
4516·5	1	803
4494·2	3	693
4446·1	5	452
4406·0	2	248
4314·1	1	−235
4276·2	2	−441

TABLE VI.

Ortho-Chlor-benzoyl Chloride.

Exciting line 4358·3 Å.

Wave-length in air (Å.).	Intensity.	Wave number difference. $\Delta\nu$ cm.$^{-1}$.
5032·1	0	3071
4725·6	3	1782
4682·1	4	1586
4657·1	0	1471
4618·0	0	1290
4597·8	3	1195
4585·9	0	1138
4566·0	4	1043
4529·9	0	868
4485·4	3	649
4463·5	3	540
4444·4	3	444
4427·8	0	360
4407·6	1	256
4395·7	1	195
4383·3	2	130
4372·7	4	75

TABLE VII.

Meta-Chlor-benzoyl Chloride.

Exciting line 4358·3 Å.

Wave-length in air (Å.).	Intensity.	Wave number difference. $\Delta\nu$ cm.$^{-1}$.
5032·1	1	3071
4721·6	10	1765
4683·5	10	1592
4648·2	0	1430
4621·5	0	1306
4598·3	10	1197
4578·2	0	1101
4558·1	7	1005
4542·3	0	929
4488·2	5	664
4460·4	4 *d*, *b*	525
4442·8	2 *d*, *b*	436
4422·7	2 *d*, *b*	334
4399·6	3	215
4387·9	3	153
4375·9	5	91

TABLE VIII.

Para-Chlor-benzoyl Chloride.

Exciting line 4358·3 Å.

Wave-length in air (Å.).	Intensity.	Wave number difference. $\Delta\nu$ cm.$^{-1}$.
4723·9	2	1775
4715·5	2	1737
4682·8	5	1589
4600·1	2	1205
4593·3	2	1173
4576·6	3	1093
4500·2	2	722
4481·4	0	630
4468·1	3	563
4447·0	1	457
4437·1	1	407
4409·2	2	264

TABLE IX.

(Ortho) Phthalyl Chloride.

Exciting line 4358·3 Å.

Wave-length in air (Å.).	Intensity.	Wave number difference. $\Delta\nu$ cm.$^{-1}$.
4716·2	1 *b, d*	1740 *
4682·5	2	1588
4659·5	0	1482
4601·6	2	1212
4591·7	0	1165
4578·4	0	1102
4566·5	1	1045
4512·7	0	784
4485·8	1	651
4466·8	1	557
4457·4	0 *b*	509
4447·2	1	458
4387·6	3	153
4379·3	3	109
4328·4	0	−159

* Probably double.

Table X.

Anisoyl Chloride.

Wave-length in air (Å.).	Intensity.	Exciting line (Å.).	Wave number difference. $\Delta\nu$ cm.$^{-1}$.
4723·3	2	4358·3	1772
4715·7	2	,,	1738
4686·0	5	,,	1604
4649·2	0	,,	1435
4626·0	0	,,	1327
4601·8	1	,,	1214
4591·5	3	,,	1165
4513·6	1	,,	788
4477·7	2	,,	611
4450·2	0	,,	473
4428·2	0	,,	351
4327·1	5	4046·6	1600
4257·1	1 *b*	,,	1221
4246·8	3	,,	1165
4179·8	0	,,	787
4149·0	2	,,	610

$\Delta\nu$=1772, 1738, 1602, 1435, 1327, 1217, 1165, 788, 611, 473, 351.
(2) (2) (5) (0) (0) (1) (3) (1) (2) (0) (0)

Table XI.

α-Furoyl Chloride.

Exciting line 4358·3 Å.

Wave-length in air (Å.).	Intensity.	Wave number difference. $\Delta\nu$ cm.$^{-1}$.
4717·8	3 *d*	1748
4677·6	0	1565
4654·8	5 *b*	1460
4639·6	2	1391
4607·3	0	1239
4590·7	2	1161
4573·6	1	1080
4562·5	2	1026
4548·0	1	956
4534·2	1	889
4521·4	1	827
4464·8	3	547
4440·9	2	426
4422·3	2	331
4392·7	2	179
4322·6	0	−190

α-Chlor-propionyl Chloride.

The prominent lines in the scattered spectrum of this liquid are due to the aliphatic C—H bond. Of the four frequencies $\Delta\nu=3004$, 2943, 2882, and 1452, which can be attributed to the C—H vibration 2943 is the strongest. Caproyl chloride gives the shift of the same magnitude, namely 2940, in addition to 2911, both of which are equally strong The shift $\Delta\nu=1442$ in caproyl chloride appears, however, more prominently than the corresponding shift in α-chlor-propionyl chloride. The Raman spectrum of α-chlor-propionyl chloride gives a faint continuous radiation between $\lambda=4358$ Å. and $\lambda=4916$ Å., which masks the faint lines appearing in this region. This probably accounts for the absence of the shift in the neighbourhood of $\Delta\nu=1800$ attributed to C=O in the acid chlorides. This shift is noticed in the α-chlor-butyryl chlorides at $\Delta\nu=1782$.

Caproyl Chloride (*normal*).

The molecule of caproyl chloride contains a long chain of carbon atoms. The shifts * $\Delta\nu=838$, 1061, and 1106 arise out of the C—C oscillations in the chain. A very prominent line of the spectrum is $\Delta\nu=1442$. The large intensity of this line is probably due to a number of CH_2 groups in the molecule, the corresponding line in other aliphatic compounds being comparatively of a smaller intensity. The large number of carbon atoms in the chain has not, however, resulted in the complexity of the bond at $3{\cdot}5\,\mu$. There are only two shifts, $\Delta\nu=2911$ and 2940, characteristic of the aliphatic C—H oscillation.

Oxalyl Chloride.

Oxalic acid is represented by the following structural formula: $\begin{matrix} OH-C=O \\ | \\ OH-C=O \end{matrix}$; the structural formula for oxalyl-chloride may therefore be shown as $\begin{matrix} Cl-C=O \\ | \\ Cl-C=O \end{matrix}$. It is,

* Venkateswaran and S. Bhagvantam, Ind. Jour. Physics, v. p. 140 (1930).

however, suggested that a teutomeric arrangement of the acid is possible, as the structural formula given above does not explain all its properties. The suggested structure for oxalic acid is $\begin{matrix} OH-C-O \\ \| \\ OH-C-O \end{matrix}$, and the corresponding acid chloride $\begin{matrix} Cl-C-O \\ \| \quad | \\ Cl-C-O \end{matrix}$ would contain a double bond linking the two carbon atoms. The Raman spectrum of this liquid does not contain the shift $\Delta\nu=1630$ which is characteristic of C=C group in ethylene and its derivatives. The appearance of two shifts, $\Delta\nu=1776$ and 1076, characteristic of C=O and C−C bonds respectively, gives support to the first formula.

Succinyl Chloride.

The most prominent line of the spectrum is $\Delta\nu=458$, which is present more or less in the same position in all the spectra of acid chlorides. The shifts $\Delta\nu=1411$ and 2942 are the well-known aliphatic C—H shifts. The characteristic frequency of the C=O linkage is 1803, its corresponding value in oxalyl chloride being considerably smaller, namely, 1776. The shift 1070 is faint, as in oxalyl chloride, and is probably due to C−C oscillation.

Ortho-Chlor-benzoyl Chloride.

The frequencies $\Delta\nu=868$, 1043, 1195, 1586, and 3071 can be identified with 849, 991, 1178, 1584, and 3060 of benzene. The Raman spectrum for this liquid shows three faint lines in this region corresponding to $\Delta\nu=1138$, 1290, and 1471. The appearance of such faint lines in this region accompanied by a number of low-frequency shifts seems to be the result of substitution. There is a very small shift, $\Delta\nu$ 75, which can be clearly seen on the negative, as there is no wing accompanying the incident line $\lambda=4358$ Å. A similar shift $\Delta\nu=91$ appears in the spectrum of meta-chlor-benzoyl chloride. Such short shifts have already been observed by several investigators *†. Gross and Vuks studied the Raman spectra in single crystals of some organic substances, and have

* Gross, E., and Vuks, M., ' Nature,' cxxxv. pp. 100, 431, 998 (1935).
† Sirkar, S. C., Ind. Jour. Phys. x. pp. 109 & 189 (1936).

shown that they are due to the characteristic oscillations of the crystal lattice. Sirkar finds that such short shifts persist in some cases even in solution and that their magnitude and intensity is considerably affected by temperature. He attributes them to the intermolecular oscillations in polymerized groups of molecules not of a crystalline nature. It would therefore be interesting to study these substances more closely to arrive at a satisfactory explanation as regards the origin of such short shifts observed by us in these liquids.

Meta-Chlor-benzoyl Chloride.

The Raman spectra of ortho- and meta-chlor-benzoyl chlorides are similar in nature. Even in the appearance of faint shifts (which have no corresponding values in the benzene spectrum) we have a line to line correspondence. The faint lines due to $\Delta\nu=1138$, 1290, and 1471 of the ortho compound correspond to $\Delta\nu=1101$ 1306, and 1430 of the meta derivative. The shift $\Delta\nu=3071$, which is the characteristic shift of the aromatic C—H linkage, is in the same position in the two spectra. The frequency $\Delta\nu=991$ of benzene, which is attributed to the symmetric oscillation of the benzene ring, is, however, considerably affected in the ortho compound, which gives $\Delta\nu=1043$, whereas the meta form gives $\Delta\nu=1005$.

Para-Chlor-benzoyl Chloride.

The incident line $\lambda=4358$ Å. has a wing accompanying it, which is prominent on its red side. The very short shifts observed with ortho- and meta-chlor-benzoyl chlorides cannot therefore be seen in the spectrum. The lines $\Delta\nu=407$, 457, and 563 are quite sharp here, whereas the corresponding lines in the meta compound are broad and diffuse.

Phthalyl Chloride.

There are two strong lines in the spectrum which correspond to $\Delta\nu=1212$ and 1588; they can be easily identified with 1178 and 1584 of benzene. The line corresponding to $\Delta\nu=1740$ is broad as well as diffuse on its red side. The reading was taken practically on its short wave-length side, which is quite prominent

and sharp. It is very probable that this line is double the other part of the doublet, having a value near about $\Delta\nu=1770$.

Anisoyl Chloride.

The scattered spectrum of anisoyl chloride gave a faint continuous radiation between $\lambda=4046$ and $\lambda=4916$ Å. The lines reported here are therefore those which could be seen against this background. The shift $\Delta\nu=1604$ is very prominent and sharp. We have here two shifts, $\Delta\nu=1738$ and 1772, characteristic of the C=O linkage. The line $\Delta\nu=473$, which is quite strong in the spectra of other acid chlorides, is rather faint here.

Furoyl Chloride.

The Raman spectrum of this substance has already been reported by Matsuno and Kwan Han *. The most prominent shifts are $\Delta\nu=1460$ and 1748. The latter is the well-known characteristic shift of the C=O oscillation, whereas the former, which is broad, is the strongest line of the spectrum.

General Discussion.

The study of the Raman spectra of these substances shows clearly the existence of two Raman lines, which are quite prominent in all the spectra recorded here. The origin of these shifts is therefore to be found in the group $-COCl$, which is characteristic of an acid chloride molecule. This group, however, forms merely a part of the molecule of an acid chloride. The characteristic frequencies of this group will therefore be affected to some extent by the nature of the other part of the molecule. This is borne out by the fact that the characteristic frequency of the carbonyl group varies within a certain range. In the aliphatic acid chlorides it has a fairly constant value $\Delta\nu=1790$; succinyl and oxalyl chlorides, though they are the derivatives of dibasic acids, give values $\Delta\nu=1776$ and 1803 respectively. The aromatic acid chlorides have a shift of about $\Delta\nu=1774$, with the exception of phthalyl chloride, which gives 1740 cm.$^{-1}$. Whether this shift is characteristic of the chloride of the

* Matsuno and Kwan Han, Bull. Chem. Soc. Japan, ix. p. 327 (1934).

dibasic aromatic acid cannot be decided here as this is the only substance belonging to its class studied by us. Para-chlor-benzoyl chloride and anisoyl chloride deserve mention here. Both have the group $-COCl$ in the para position, and in both we have a double shift characteristic of the C=O linkage. The former gives $\Delta\nu=1775(2)$ and 1737 (2), while in the latter the shifts are $\Delta\nu=1772$ (2) and 1738 (2). It will be interesting to study some other acid chorides in which the $-COCl$ group happens to be in the para position to decide whether the occurrence of this double shift is characteristic of it. In the case of furoyl chloride we have a strong shift which is also broad corresponding to $\Delta\nu=1748$ cm.$^{-1}$. The value of this shift is of the same magnitude as that of the shorter shift observed in para-chlor-benzoyl chloride and anisoyl chloride.

The characteristic frequency shift of the C—Cl linkage in COCl group is quite prominent in all the spectra reported here. The magnitude of this shift, 448 cm.$^{-1}$, is just the same as that of the intense line (459 cm.$^{-1}$) of Raman spectrum of carbon tetra-chloride. This shift has the minimum value of 424 cm.$^{-1}$ in α-chlor-butyryl chloride, whereas phthalyl chloride gives the maximum value of 473 cm.$^{-1}$.

In addition to these two frequencies, which are conserved in all these compounds, there are others that appear more or less regularly which need mention here. Their mean values are $\Delta\nu=664$, 548, and 347. Their intensities are generally in the decreasing order of magnitude in a given spectrum. Thus in the low-frequency shift region we have $\Delta\nu=644, 548, 448$, and 347, separated by about 100 wave numbers.

Our thanks are due to the authorities of the Nagpur University for a research grant to meet the expenses of this investigation. We wish also to thank Principal De for facilities for work in the Physics Laboratory of the College of Science, Nagpur.

College of Science, Nagpur.
January 1937.

CI. *The Theory of Electrocapillarity.*—Part VI. *A Note on Electrophoresis. By* S. R. Craxford, O. Gatty, *and* H. A. C. McKay *.

A DETAILED treatment of electrophoresis is necessarily a matter of some complication, involving a consideration of lines of flow and coefficients of slip and, in particular, the electrophoretic force on a particle is not directly proportional to the potential gradient causing electrophoresis. But in one special case, namely, when the interphase between the two phases is completely polarizable, and when the potential gradient causing electrophoresis is vanishingly small, it is possible to reach useful conclusions by means of arguments of a more general nature.

In general there will be a tendency for the charges on an electrophoresing particle to leave it at one end in the form of ions, and for corresponding ions to enter it at the other. The rate at which this double electrolysis occurs at any potential gradient will clearly be a determining factor for the velocity of electrophoresis, but it is only known in the limiting case of a completely polarizable interphase where the ions cannot cross a certain impenetrable boundary in the interphase at all, and then the rate is, in fact, zero. An example of such a case is a drop of mercury electrophoresing in a solution containing no mercurous ions, when the potential between the mercury and the solution lies within an appropriate range. It would therefore be expected that the electric charge actually involved in electrophoresis would be that part of the charge which lies on the inner side of the impenetrable boundary between the two phases. The electrophoretic force F on a particle would accordingly be $Q.\frac{\Delta V}{\Delta x}$, where $\frac{\Delta V}{\Delta x}$ is the electrical potential gradient causing electrophoresis and Q is the net charge on the particle as measured by electrocapillary or other methods. This result can be deduced rigorously by means of an isothermal cycle, of which the following is an outline: this can, if necessary, be expanded to the full detail of the complete argument.

* Communicated by Sir Harold Hartley, F.R.S.

Consider an indefinitely long tube containing a solution, and let a small finite potential difference be set up between the ends of the tube so as to produce a uniform but vanishingly small potential gradient down the tube. If the solution is free from mercurous ions and reducible impurities such as dissolved oxygen, a drop of mercury in it can be considered to have a completely polarizable surface if its potential against the solution lies within a certain range of potential. The cycle is now as follows. The mercury drop is discharged, *i. e.*, brought to the potential of the electrocapillary maximum relative to the solution, and its charge is allowed to flow on to a condenser during this process. The mercury drop is then removed from the solution, and the mercury and its charge brought to a point further along the tube. The mercury is then reinserted into the solution and its charge allowed to flow on to it again from the condenser. Finally, the mercury drop is allowed to undergo infinitely slow electrophoresis back to the point from which it started. Thus an isothermal reversible cycle has been performed on the drop, and the net work involved must be zero. If F denotes the electrophoretic force, which is uniform between the two points considered, which are separated by a distance Δx, the net work done during the infinitely slow electrophoresis must equal $F\Delta x$. The net work necessary for removing and replacing the mercury is zero, because the surface tension and other mechanical properties of the drop are the same in both positions. The discharging and charging of the mercury also involve amounts of compressional work which cancel to zero. There remains the difference between the work of discharging the drop in the first position and charging it in the second. If the potential difference between these points is ΔV, the net work for these two processes is $Q\Delta V$. Hence, by completing the cycle,

$$F\Delta x = Q\Delta V$$

$$F = Q.\frac{\Delta V}{\Delta x}.$$

The above argument may easily be made more precise by adding fuller details to the outline given here, but this is perhaps unnecessary for the present purpose. The result is general for electrically conducting particles with

completely polarizable interphases against the given solution.

The following four results follow from the equation $F=Q.\frac{\Delta V}{\Delta x}$:—

(1) The electrophoretic null point is the same as the electrolytic null point as determined from the electrocapillary maximum or the zero of the dropping electrode. This agrees with the experimental results obtained by one of us (S. R. C., Phil. Mag. (7) xvi. p. 268 (1933)), who found that the potential of the electrophoretic null point for mercury is approximately the same as that of the electrocapillary maximum for a series of solutions, including those containing salts strongly specifically adsorbed at the mercury surface at the potential of the null point.

(2) By combining the above equation for the electrophoretic force with the electrocapillary equation, F is given as the product of the surface area of the particle and the slope of its electrocapillary curve at that potential and $\frac{\Delta V}{\Delta x}$. Thus the electrophoretic force on a symmetrical particle is proportional to the difference of surface tension at its two ends *.

(3) Electrophoresis at vanishingly small potential gradients cannot arise from a double layer of specifically adsorbed salt, or from any other type of double layer situated entirely on one side of the impenetrable boundary in the interphase.

(4) If the capacity C per unit area of the double layer over any potential range that includes the electrolytic

* *Cf.* The deformation of mercury drops in electrical potential gradients (Christiansen, *Ann. d. Physik* (4) xii. p. 1072 (1903)), also the motion of mercury drops with one side in contact with acid dichromate (Bernstein, *Pflug. Arch.* lxxx. p. 628 (1900), and Quincke, *Wied. Ann.* xxxv. p. 580 (1888)). If the difference in surface tension is maintained by continuous chemical or physical change at a particle the particle moves owing to surface forces. The camphor boat and other cases are discussed in Freundlich, 'Colloid and Capillary Chemistry,' Methuen, p. 70 (1926). Given suitable chemical and physical changes surface forces may be operating during the intracellular movements of mitosis.

null point is constant *, and if ϕ is the potential difference across the interphase at any point in this range, and ϕ_{null} is the potential across the double layer at the electrolytic null point,

$$F = s.C.(\phi - \phi_{\text{null}}).\frac{\Delta V}{\Delta x},$$

where s is the surface area of the electrophoresing particle.

Finally, it must be emphasized that these results hold essentially only for very small potential gradients. For higher rates of flow complicated questions of viscosity arise.

The Laboratory of Physical Chemistry,
Balliol College and Trinity College,
Oxford.

CII. *Notes on Two-Dimensional Potential Theory.*—III. *The Line Source Influence Problems.* *By* Rosa M. Morris, *B.Sc.*†

THESE are essentially the problems of finding the influence of a line source outside and parallel to the generators of a cylinder. They take various forms, and we shall here mention three only :—

(i.) A line charge outside an electrical conducting cylinder

(ii.) A solid cylinder in an infinite fluid in motion due to a line source.

(iii.) A solid cylinder in an infinite fluid in motion due to a line vortex.

For certain forms of cylinders the solutions for the potential and also the force and couple on the cylinder are known. These solutions include :

(i.) Circular cylinder in all three cases.

* This condition does not hold for solution, mercury interphases, nor for interphases of the type considered by Stein. For such interphases, however,

$$\frac{dF}{d\phi} = S.C.\frac{\Delta V}{\Delta x}$$

at some points of the electrocapillary curve.

† Communicated by Prof. G. H. Livens.

(ii.) Elliptic cylinder in the electrical case, which has to a certain extent been developed by Bateman *. No formula for the force and couple in this case appears to have been obtained.

(iii.) Another case has been worked out in its simple hydrodynamical aspects by D. Wrinch † who, using the familiar results of aerofoil theory, calculates the forces involved.

A discussion covering, mainly in their hydrodynamical aspects, some of these cases and also certain others of a general character, has also been given by Bickley ‡ but his method is very cumbrous and somewhat less directly applicable than that here employed.

The reason for the success achieved in the solutions of these cases is due to a particular form which the transformations defining the surfaces take ; they all appear to belong to a general class of surface.

It is now proposed to show how the complete results of all these cases—and others of similar type—can be much more elegantly deduced by the consistent use of the complex potential throughout.

I. *Electrical Cases.*

(i.) *Circular Cylinder.*

The processes involved can perhaps best be illustrated by working out the details for the circular cylinder case.

Suppose the line charge of strength E is at a point z_0 outside the cylinder. The undisturbed complex potential function is given by

$$\Omega_0=\phi_0+i\psi_0=(\mathrm{E}/2\pi)\log(z-z_0).$$

The circular cylinder is defined by the transformation §

$$z=ae^{-i\zeta}\ ;\ \eta=0,$$

$\eta=+\infty$ being at infinity.

* ' Partial Differential Equations ' (Bateman). In this book reference is made to a paper by C. Neumann in the Leipzig *Ber.* Bd. lxii., which I have not yet seen.

† " Fluid Circulation round Cylindrical Obstacles," by D. M. Wrinch, Phil. Mag. vol. xlix. p. 240 (1925).

‡ Phil. Trans. Roy. Soc. A.

§ The sign is chosen to conform to our general convention that $\eta=+\infty$ corresponds to the infinitely distant parts of the z-plane. This point must be remembered in comparing our work with that of other authors who have not been quite so consistent in the matter.

In terms of the complex variable ζ we then have

$$\Omega_0=(E/2\pi)\log a(e^{-i\zeta}-e^{-i\zeta_0})$$

$$\Omega_0=\text{const.}+(E/2\pi)\log(1-e^{-i(\zeta-\zeta_0)}).$$

The new potential when the cylinder is introduced must be such that it is purely imaginary on the cylinder, *i. e.* when $\eta=0$, and the undisturbed form must be preserved where the presence of the cylinder is unnoticed, i. e. $\eta=+\infty$.

To make a complex function from $F(\zeta)$ which is purely imaginary when $\eta=0$, all we have to do is to subtract the conjugate function $F(\zeta)$. But in doing this we may introduce terms into Ω which become infinite when $\eta\to\infty$: to avoid this we must really divide $F(\zeta)$ into two parts, including in the one, $F_1(\zeta)$, the terms whose conjugates do not tend to infinity, and in the other, $F_2(\zeta)$, all the terms whose conjugates tend to infinity. To make up the complete Ω we then subtract the actual terms $F_2(\zeta)$, thus removing them altogether, and the conjugates of $F_1(\zeta)$, which are regular at infinity. Thus we take

$$\Omega=\{F_1(\zeta)+F_2(\zeta)\}-\{\overline{F_1}(\zeta)+F_2(\zeta)\}$$

$$=F_1(\zeta)-\overline{F}_1(\zeta).$$

At infinity $F_1(\zeta)$ is of course the controlling part of Ω_0, as $F_2(\zeta)$ tends to zero there, so that the new Ω does in effect tend to Ω_0 at infinity, and all the conditions of the problem are satisfied.

In this case of the circular cylinder the conjugate does reduce to zero when $\eta=+\infty$, and so we subtract

$$(E/2\pi)\log\{1-e^{i(\zeta-\overline{\zeta}_0)}\}\ ;\ \overline{\zeta}_0=\xi_0-i\eta_0,$$

and then we have for the complex potential

$$\Omega=\text{const.}+(E/2\pi)\log\left\{\frac{1-e^{-i(\zeta-\zeta_0)}}{1-e^{i(\zeta-\overline{\zeta}_0)}}\right\}.$$

To find the forces and couple on the cylinder we require the value of $\dfrac{\partial\Omega}{\partial\overline{\zeta}}$. This is easily found to be

$$\frac{-E}{2\pi}\left[1-\frac{\sinh\eta_0}{\cosh\eta_0-\cos(\zeta-\xi_0)}\right].$$

The components X, Y of the force on the cylinder are now given by *

$$Y+iX=\frac{1}{8\pi}\int_C \left(\frac{\partial\Omega}{\partial z}\right)^2 dz,$$

integrated round the curve of cross-section C of the cylinder.

Now

$$\left(\frac{\partial\Omega}{\partial z}\right)^2 dz=\left(\frac{\partial\Omega}{\partial\zeta}\right)^2 d\zeta\Big/\left(\frac{dz}{d\zeta}\right)$$

and

$$dz/d\zeta=-iae^{-i\zeta}.$$

On the cylinder $\eta=0$ and ξ changes from 0 to 2π. We therefore want

$$\int_0^{2\pi}\left[1-\frac{\sinh\eta_0}{\cosh\eta_0-\cos(\zeta-\xi_0)}\right]^2\frac{d\zeta}{-iae^{-i\zeta}}.$$

A similar integral to this appears in Dr. Wrinch's paper, and to evaluate it she transforms to a new plane. This process seems completely unnecessary, however, as the integral can be completed in a simple contour integral in the ζ-plane, viz., the rectangle of sides $\xi=0$, $\xi=2\pi$; $\eta=0$; $\eta=+\infty$ The integrand has the same value at two corresponding points $i\eta$ and $2\pi+i\eta$, so that the integrals along $\xi=0$ and $\xi=2\pi$ cancel out. When $\zeta=\xi+i\mathrm{R}$ where R is large, then the integrand tends to zero with R, so that the integral along $\eta=+\infty$ is zero †.

The only pole inside the contour is $\zeta=\zeta_0$, and thus we have merely to evaluate the residue there.

Writing $\zeta=\zeta_0+t$, where t is small, we have then

$$\begin{aligned}\cosh\eta_0-\cos(\zeta-\xi_0)&=\cosh\eta_0(1-\cos t)+i\sinh\eta_0\sin t\\&=\sinh\eta_0(it+\tfrac{1}{2}t^2\coth\eta_0).\end{aligned}$$

Thus

$$\begin{aligned}1-\frac{\sinh\eta_0}{\cosh\eta_0-\cos(\zeta-\xi_0)}&=1-\frac{1}{it}\left(1-\frac{t}{2i}\coth\eta_0\right)\\&=\frac{-1}{it}\{1-it(1-\tfrac{1}{2}\coth\eta_0)\}.\end{aligned}$$

* See the first note in this series.

† The contour can equally be completed by going to infinity in the negative direction, but there is then some doubt as to the number of poles inside it in view of the fact that the complete transformation from the ζ- to the z-plane gives a very complex Riemann surface over the z-plane. The contour taken in reality means that the force on the cylinder is here calculated as the equal reaction force on the pole.

The square of this expression is, to the same order in t,

$$\frac{-1}{t^2}[1-2it(1-\tfrac{1}{2}\coth\eta_0)].$$

Further,

$$\frac{dz}{d\zeta}=-iae^{-i\zeta}=-iae^{-i\zeta_0}(1-it);$$

$$\therefore\quad\left(\frac{dz}{d\zeta}\right)^{-1}=\frac{-e^{i\zeta_0}}{ia}(1+it),\quad\text{approx.}$$

Multiplying these two together, and picking out the term in t^{-1}, we get the residue at $\zeta=\zeta_0$ of the form

$$\frac{e^{i\zeta_0}}{ia}\{i-2i(1-\tfrac{1}{2}\coth\eta_0)\},$$

so that the components of the force are given by

$$Y+iX=\frac{iE^2e^{i\zeta_0}}{16\pi^2a}\{1-\coth\eta_0\},$$

which can be easily seen to agree with the well-known result if we take $\xi_0=0$ and $c=ae^{\eta_0}$ for the distance of the charge from the cylinder.

To find the couple on the cylinder in these cases of line charge we can use the contour integral, but it is easier to remember that the forces on the cylinder are equal and opposite to the forces on the line charge. The resultant of the forces on the cylinder must therefore act through the point z_0, so that its moment about the centre or the couple on the cylinder in the usual sense is

$$Yx_0-Xy_0,$$

which is the real part of

$$(Y+iX)(x_0+iy_0)=(Y+iX)z_0.$$

In this case the couple on the cylinder is therefore the real part of

$$\frac{iE^2}{16\pi^2}(1-\coth\eta_0),$$

which is, of course, zero.

(ii.) *Elliptic Cylinder.*

The undisturbed field of the line charge at z_0 is, as before,

$$\Omega_0=(\mathrm{E}/2\pi)\log(z-z_0).$$

The transformation for the elliptic cylinder we take as

$$z=c\cos(\zeta+i\alpha)\,;\ \eta=0.$$

This form of definition is different from that usually employed, but it is made to secure complete consistency throughout the work, in which the surface involved is always taken as the surface $\eta=0$. Also the definition in this form greatly facilitates the process of finding the new potential function by our methods.

The undisturbed potential in terms of ζ is, in this form of the problem,

$$\begin{aligned}\Omega_0&=(\mathrm{E}/2\pi)\log c\{\cos(\zeta+i\alpha)-\cos(\zeta_0+i\alpha)\}\\&=(\mathrm{E}/2\pi)\log\tfrac{1}{2}c+(\mathrm{E}/2\pi)\log\sin\tfrac{1}{2}(\zeta+\zeta_0+2i\alpha)\sin\tfrac{1}{2}(\zeta-\zeta_0)\\&=(\mathrm{E}/2\pi)\log\tfrac{1}{2}c-(i\mathrm{E}/2\pi)(\zeta_0+i\alpha)+\mathrm{E}/2\pi\log\{1-e^{i(\zeta+\zeta_0+2i\alpha)}\}\\&\qquad+(\mathrm{E}/2\pi)\log\{1-e^{-i(\zeta-\zeta_0)}\}.\end{aligned}$$

There is an alternative resolution of Ω_0 which gives the opposite signs for the arguments of the exponentials in the two logarithms. This could be used to solve the problem, but in reality it solves not the given problem but a similar one on another sheet of the Riemann surface defined by the transformation. The one chosen does give an Ω which has a proper pole at $\zeta=\zeta_0$.

In the same way as for the circular cylinder, to find the new potential we construct from this function another function which is purely imaginary on the cylinder, and reduces to the same form as Ω_0 at infinity. The conjugate of the first logarithm term diverges with η, and we must therefore subtract this term altogether. We therefore add

$$-(\mathrm{E}/2\pi)\log\{1-e^{i(\zeta+\zeta_0+2i)\alpha}\}-(\mathrm{E}/2\pi)\log\{1-e^{i(\zeta-\bar{\zeta}_0)}\}$$

and then finally we have

$$\Omega=\text{const.}+(\mathrm{E}/2\pi)\log\left[\frac{1-e^{-i(\zeta-\zeta_0)}}{1-e^{i(\zeta-\bar{\zeta}_0)}}\right].$$

This is the same as for the circular cylinder, as must be the case for the problem in the ζ-plane, which is identical in all cases.

Now

$$dz/d\zeta = -c \sin(\zeta + i\alpha),$$

and so we want for the force

$$\int_0^{2\pi} \left[1 - \frac{\sinh \eta_0}{\cosh \eta_0 - \cos(\zeta - \xi_0)}\right]^2 \frac{d\zeta}{\sin(\zeta + i\alpha)}.$$

This can again be completed round the same contour as before, the integrand having the same value at corresponding points $i\eta$ and $2\pi + i\eta$, and reducing to zero when $\zeta = \xi + i\mathrm{R}$ and R tends to infinity.

The only pole inside the contour is $\zeta = \zeta_0$, so we have to evaluate the residue there.

Writing $\zeta = \zeta_0 + t$, then, as before,

$$\left[1 - \frac{\sinh \eta_0}{\cosh \eta_0 - \cos(\zeta - \xi_0)}\right] = \frac{-1}{t^2}\left[1 - 2it\left(1 - \tfrac{1}{2}\cosh \eta_0\right)\right]$$

and

$$\{\sin(\zeta + i\alpha)\}^{-1} = [\sin(\zeta_0 + i\alpha)\{1 + t\cot(\zeta_0 + i\alpha)\}]^{-1}$$
$$= \{\sin(\zeta_0 + i\alpha)\}^{-1}\{1 - t\cot(\zeta_0 + i\alpha)\}.$$

Multiplying these two together, and picking out the term in t^{-1}, we get the residue at $\zeta = \zeta_0$ equal to

$$[2i - i\coth \eta_0 + \cot(\zeta_0 + i\alpha)]/\sin(\zeta_0 + i\alpha).$$

The components of the force are thus given by

$$\mathrm{Y} + i\mathrm{X} = \frac{-\mathrm{E}^2}{16\pi^2 c \sin(\zeta_0 + i\alpha)}[2i - i\coth \eta_0 + \cot(\zeta_0 + i\alpha)],$$

and the couple is then the real part of

$$\frac{-\mathrm{E}^2}{16\pi^2}\cot(\zeta_0 + i\alpha)[2i - i\coth \eta_0 + \cot(\zeta_0 + i\alpha)],$$

and is, therefore, immediately derivable.

(iii.) *A General Cylinder.*

Suppose the cylinder is defined by the transformation

$$z = ae^{-i\zeta} + a_1 e^{i\alpha_1 + i\zeta} + a_2 e^{i\alpha_2 + 2i\zeta} + \ldots; \quad \eta = 0,$$

which is such that $\eta = +\infty$ at infinity *. The undisturbed potential is

$$\mathfrak{L}_0 = (\mathrm{E}/2\pi)\log(z - z_0),$$

* This general class of cylinder appears to be all inclusive; at least it covers all cases for which solutions are known.

which in terms of ζ is

$$\Omega_0=(\mathrm{E}/2\pi)\log\{ae^{-i\zeta}+a_1e^{i\alpha_1+i\zeta}+a_2e^{i\alpha_2+2i\zeta}+\ldots$$
$$-(ae^{-i\zeta_0}+a_1e^{i\alpha_1+i\zeta_0}+\ldots)\}$$
$$=(\mathrm{E}/2\pi)\log(e^{-i\zeta}-e^{-i\zeta_0})\{a-a_1e^{i\alpha_1+i\zeta+i\zeta_0}$$
$$-a_2e^{i\alpha_2}(e^{i\zeta+2i\zeta_0}-e^{i\zeta_0+2i\zeta})\ldots\}$$
$$=\text{const.}+(\mathrm{E}/2\pi)\log\{1-e^{-i(\zeta-\zeta_0)}\}$$
$$+(\mathrm{E}/2\pi)\log\{a-a_1e^{i\alpha_1+i\zeta+i\zeta_0}\ldots\}.$$

We find the new potential in the same way as in (i.) and (ii.). The conjugate of the second logarithm diverges to infinity with η, and we therefore subtract it altogether. We therefore add

$$-(\mathrm{E}/2\pi)\log\{1-e^{i(\zeta-\bar{\zeta}_0)}\}-(\mathrm{E}/2\pi)\log\{a-a_1e^{i\alpha_1+i\zeta+i\zeta_0}\ldots\},$$

and then finally we have

$$\Omega=\text{const.}+\frac{\mathrm{E}}{2\pi}\log\left[\frac{1-e^{i(\zeta-\zeta_0)}}{1-e^{i(\zeta-\bar{\zeta}_0)}}\right],$$

which is the same as in (i.) and (ii.).

Now

$$z=ae^{-i\zeta}+a_1e^{i\alpha_1+i\zeta}+\ldots;$$

$$\therefore\quad\frac{dz}{d\zeta}=-iae^{-i\zeta}+ia_1e^{i\alpha_1+i\zeta}+\ldots,$$

and so in this case we want

$$\int_0^{2\pi}\left[1-\frac{\sinh\eta_0}{\cosh\eta_0-\cos(\zeta-\xi_0)}\right]^2\frac{d\zeta}{\{-iae^{-i\zeta}+ia_1e^{i\alpha_1+i\zeta}+\ldots\}},$$

and again we have to find the residue at $\zeta=\zeta_0$. Writing $\zeta=\zeta_0+t$, we get, as before,

$$\left\{1-\frac{\sinh\eta_0}{\cosh\eta_0-\cos(\zeta-\xi_0)}\right\}^2=\frac{-1}{t^2}\left[1-2it(1-\tfrac{1}{2}\coth\eta_0)\right],$$

and

$$-iae^{-i\zeta}+ia_1e^{i\alpha_1+i\zeta}+2ia_2e^{i\alpha_2+2i\zeta}+\ldots$$
$$=-iae^{-i\zeta_0}(1-it)+ia_1e^{i\alpha_1+i\zeta_0}(1+it)$$
$$+2ia_2e^{i\alpha_2+2i\zeta_0}(1+2it)+\ldots$$
$$=\mathrm{A}+\mathrm{B}t,$$

where

$$A=-iae^{-i\zeta_0}+ia_1e^{i\alpha_1+i\zeta_0}+2ia_2e^{i\alpha_2+2i\zeta_0}\ \dots\ ,$$

$$B=-ae^{-i\zeta_0}-a_1e^{i\alpha_1+i\zeta_0}-4a_2e^{i\alpha_2+2i\zeta_0}+\ \dots\ ;$$

so that the a's must be restricted in such a way that these series are convergent if they extend to infinity.
Then

$$\{-iae^{-i\zeta}+ia_1e^{i\alpha_1+i\zeta}+\ \dots\ \}^{-1}=(A+Bt)^{-1}=\frac{1}{A}\left\{1-\frac{Bt}{A}\right\}.$$

Multiplying the two together, and picking out the term in t^{-1}, we get the residue at $\zeta=\zeta_0$ to be

$$-\frac{1}{A}\left\{i\coth\eta_0-2i-\frac{B}{A}\right\},$$

and the components of the force on the cylinder are given by

$$Y+iX=\frac{E^2}{16\pi^2A}\left\{\coth\eta_0-2+\frac{iB}{A}\right\},$$

and the couple is the real part of

$$\frac{E^2}{16\pi^2A}\left\{\coth\eta_0-2+\frac{iB}{A}\right\}\{ae^{-i\zeta_0}+a_1e^{i\alpha_1+i\zeta_0}+\ \dots\ \}.$$

The first of these expressions agrees with that given by Dr. Wrinch, but she does not give the formula here deduced for the couple.

II. *Hydrodynamical Cases.*

(i.) *Circular Cylinder.*

Suppose the line source of strength m is at a point z_0 outside the cylinder. The undisturbed stream is given by

$$\Omega_0=\phi_0+i\psi_0=(m/2\pi)\log(z-z_0).$$

The circular cylinder is defined by the transformation

$$z=ae^{-i\zeta};\ \eta=0,$$

$\eta=+\infty$ being at infinity.
In terms of the complex variable ζ we then have

$$\Omega_0=\text{const.}+(m/2\pi)\log\{1-e^{-i(\zeta-\zeta_0)}\}.$$

The new potential when the cylinder is introduced must be such that it is purely real on the cylinder, *i. e.*, $\eta=0$, and the undisturbed form must be preserved where the presence of the cylinder is unnoticed, *i. e.*, $\eta=+\infty$. To make a complex function from $F(\zeta)$, which is purely real when $\eta=0$, all we have to do is to add the conjugate function $\overline{F}(\zeta)$. But in doing this we may again introduce terms into Ω which become infinite when $\eta\to\infty$: to avoid this we divide $F(\zeta)$, as before, into two parts, including in the one, $F_1(\zeta)$, the terms whose conjugates do not tend to infinity, and in the other, $F_2(\zeta)$, all the terms whose conjugates tend to infinity. To make up the complete Ω we then subtract the actual terms $F_2(\zeta)$ and add the conjugates of $F_1(\zeta)$, which are regular at infinity. Thus

$$\begin{aligned}\Omega_0&=\{F_1(\zeta)+F_2(\zeta)\}+\{\overline{F}_1(\zeta)-F_2(\zeta)\}\\&=F_1(\zeta)+\overline{F}_1(\zeta).\end{aligned}$$

At infinity $F_1(\zeta)$ is of course the controlling part of Ω_0, as $F_2(\zeta)$ tends to zero there, so that the new Ω does in effect tend to Ω_0 at infinity, and all the conditions of the problem are satisfied.

In this case of the circular cylinder the conjugate does reduce to zero at $\eta=\infty$, and so we add

$$(m/2\pi)\log\{1-e^{-i(\zeta-\overline{\zeta}_0)}\},$$

and then we have for the potential

$$\Omega=\text{const.}+(m/2\pi)\log\{1-e^{-i(\zeta-\zeta_0)}\}\{1-e^{i(\zeta-\overline{\zeta}_0)}\}.$$

To find the force and couple on the cylinder we require the value of $\partial\Omega/\partial\zeta$, which is easily found to be

$$\frac{mi}{2\pi}\left[\frac{\sin(\zeta-\xi_0)}{\cosh\eta_0-\cos(\zeta-\xi_0)}\right].$$

The components X, Y of the force on the cylinder are given by

$$Y+iX=\tfrac{1}{2}\rho\int_C\left(\frac{\partial\Omega}{\partial\overline{z}}\right)^2dz$$

integrated around C, the curve of cross-section of the cylinder. Now

$$\left(\frac{\partial\Omega}{\partial\overline{z}}\right)^2dz=\left(\frac{\partial\Omega}{\partial\zeta}\right)^2d\zeta\Big/\left(\frac{dz}{d\overline{\zeta}}\right)$$

and

$$\frac{dz}{d\zeta} = -iae^{-i\zeta}.$$

The integral around the curve C then becomes the integral along $\eta=0$ from $\xi=0$ to 2π. We therefore want

$$\int_0^{2\pi} \left[\frac{\sin(\zeta-\xi_0)}{\cosh\eta_0-\cos(\zeta-\xi_0)}\right]^2 \frac{d\zeta}{-iae^{-i\zeta}}.$$

This integral can, as before, be completed around the rectangle $\xi=0$, $\xi=2\pi$, $\eta=0$, $\eta=+\infty$, the integrand, having the same value at corresponding points $+i\eta$, $2\pi+i\eta$, where η is the same, and tending to zero when $\eta=\infty$. The only pole inside is again $\zeta=\zeta_0$, and thus we have merely to evaluate the residue there.

Writing $\zeta=\zeta_0+t$, where t is small, we have

$$\begin{aligned}
&\frac{\sin(\zeta-\xi_0)}{\cosh\eta_0-\cos(\zeta-\xi_0)} \\
&\quad= \frac{i\sinh\eta_0\cos t+\cosh\eta_0\sin t}{\cosh\eta_0(1-\cos t)+i\sinh\eta_0\sin t} \\
&\quad= \frac{i\sinh\eta_0+t\cosh\eta_0}{it\sinh\eta_0+\frac{1}{2}t^2\cosh\eta_0} \\
&\quad= \frac{(i\sinh\eta_0+t\cosh\eta_0)}{it\sinh\eta_0}\left(1-\frac{t}{2i}\coth\eta_0\right) \\
&\quad= \frac{1}{t}(1-it\coth\eta_0)(1+\tfrac{1}{2}it\coth\eta_0) \\
&\quad= \frac{1}{t}(1-\tfrac{1}{2}it\coth\eta_0)
\end{aligned}$$

to our order in t. The square of this is

$$\frac{1}{t^2}(1-it\coth\eta_0).$$

$$1\Big/\left(\frac{dz}{d\zeta}\right) = -\frac{e^{i\zeta_0}}{ia}(1+it).$$

Multiplying these two together, and picking out the term in t^{-1}, we get the residue

$$+ie^{i\zeta_0}\{i-i\coth\eta_0\}/a,$$

so that the components of the force are given by

$$Y+iX=im^2\rho e^{i\zeta_0}(1-\coth\eta_0)/4\pi a.$$

In the same way as for the electrical cases the couple on the cylinder will be the real part of

$$(Y+iX)z_0,$$

so that in this case the couple is the real part of

$$im^2\rho(1-\coth\eta_0)/4\pi,$$

which is, of course, zero.

(ii.) *Elliptic Cylinder.*

The undisturbed velocity potential of the stream due to a line source at z_0 is

$$\Omega_0=\phi_0+i\psi_0=(m/2\pi)\log(z-z_0).$$

The transformation for the elliptic cylinder is

$$z=c\cos(\zeta+i\alpha)\ ;\ \eta=0,$$

so that in terms of ζ the undisturbed potential is

$$\begin{aligned}\Omega_0&=(m/2\pi)\log c\{\cos(\zeta+i\alpha)-\cos(\zeta_0+i\alpha)\}\\&=\text{const.}+(m/2\pi)\log\{1-e^{i(\zeta+\zeta_0+2i\alpha)}\}\\&\qquad+(m/2\pi)\log\{1-e^{-i(\zeta-\zeta_0)}\}.\end{aligned}$$

The new potential will be, in the same way as for the circular cylinder,

$$\Omega=\text{const.}+(m/2\pi)\log\{1-e^{-i(\zeta-\zeta_0)}\}\{1+e^{i(\zeta-\bar{\zeta}_0)}\},$$

and we therefore want the coefficient of t^{-1} in the product of

$$\frac{1}{t^2}(1-it\coth\eta_0)$$

and

$$\{1-t\cot(\zeta_0+i\alpha)\}/\sin(\zeta_0+i\alpha),$$

giving

$$-\{i\coth\eta_0+\cot(\zeta_0+i\alpha)\}/\sin(\zeta_0+i\alpha),$$

and the components of the force are then given by

$$Y+iX=\frac{m^2\rho}{4\pi c\sin(\zeta_0+i\alpha)}\{\coth\eta_0-i\cot(\zeta_0+i\alpha)\},$$

and the couple is the real part of

$$m^2\rho \cot(\zeta_0+i\alpha)\{\coth\eta_0 - i\cot(\zeta_0+i\alpha)\}/4\pi.$$

(iii.) *A General Cylinder.*

Suppose the cylinder, as in the electrical case, is defined by the transformation

$$z=ae^{-i\zeta}+a_1e^{i\alpha_1+i\zeta}+a_2e^{i\alpha_2+2i\zeta}+\ldots.$$

Then we have, as before,

$$\Omega_0\text{—const.}+(m/2\pi)\log\{1-e^{-i(\zeta-\zeta_0)}\}$$
$$+(m/2\pi)\log\{a-a_1e^{i\alpha_1+i\zeta+i\zeta_0}-\ldots\},$$

and we have to subtract the second logarithm altogether and add the conjugate of the first, giving, as before,

$$\Omega=\text{const.}+(m/2\pi)\log\{1-e^{-i(\zeta-\zeta_0)}\}\{1-e^{i(\zeta-\bar{\zeta}_0)}\},$$

and also

$$\frac{dz}{d\zeta}=\mathrm{A}+\mathrm{B}t,$$

where

$$\mathrm{A}=-iae^{-i\zeta_0}+ia_1e^{i\alpha_1+i\zeta_0}+2ia_2e^{i\alpha_2+2i\zeta_0}+\ldots,$$
$$\mathrm{B}=-ae^{-i\zeta_0}-a_1e^{i\alpha_1+i\zeta_0}-4a_2e^{i\alpha_2+2i\zeta_0}-\ldots.$$

We then require the coefficient of t^{-1} in the product of

$$\frac{1}{t^2}(1-it\coth\eta_0)$$

and

$$\frac{1}{\mathrm{A}}\left(1-\frac{\mathrm{B}}{\mathrm{A}t}\right),$$

giving a residue at $\zeta=\zeta_0$ of

$$-\frac{1}{\mathrm{A}}\left\{i\coth\eta_0+\frac{\mathrm{B}}{\mathrm{A}}\right\}.$$

The components of the force are then given by

$$\mathrm{Y}+i\mathrm{X}=\frac{m^2\rho}{4\pi}\left\{\coth\eta_0-\frac{i\mathrm{A}}{\mathrm{B}}\right\},$$

and the couple is the real part of

$$\frac{m^2\rho}{4\pi}\left\{\coth\eta_0-\frac{i\mathrm{B}}{\mathrm{A}}\right\}\{ae^{-i\zeta_0}+a_1e^{i\alpha_1+i\zeta_0}+\ldots\}.$$

(iv.) *Cylinders in a Stream due to a Line Vortex.*

The undisturbed velocity potential for a line vortex at the point z_0 is

$$\Omega = \frac{im}{2\pi} \log (z - z_0).$$

In terms of the complex variable ζ it will, in each case, be of the form

$$\Omega_0 = i\{F_1(\zeta) + F_2(\zeta)\}.$$

Forming the new velocity potential in the usual way, we get

$$\Omega = i\{F_1(\zeta) - \bar{F}_1(\zeta)\},$$

which is the same form as for the electrical cases apart from the factor i outside. Thus in every case the components of the force, and the couple, will be of the same form as in the electrical cases, the only difference being the constant factor $-\frac{1}{2}\rho m^2$ instead of $E^2/8\pi$.

Conclusion.

We can now see the connexion between all these cases. The potential function, apart from a constant, is the same in all the electrical cases, and the hydrodynamical with the line vortex, and is the same for the three hydrodynamical cases with the line source.

This means that when we are evaluating the integral for the force on the cylinder we have one factor, $\left(\frac{\partial \Omega}{\partial \zeta}\right)^2$, which is independent of the type of surface and depends only on the type of problem—electrical, hydrodynamical, etc. The only part of the integral which depends on the type of cylinder is $\left(\frac{dz}{d\zeta}\right)^{-1}$. Thus, if the general transformation for the cylinder was

$$z = f(\zeta); \ \eta = 0,$$

then provided $f(\zeta)$ could be expanded in the form

$$a_0 e^{-i\zeta} + \sum_{n=1}^{n=\infty} a_1 e^{in\zeta},$$

or something like this, the force integral would be

$$\int_0^{2\pi} \left(\frac{\partial \Omega}{\partial z}\right)^2 d\zeta \Big/ \left(\frac{dz}{d\zeta}\right),$$

$dz/d\zeta$ being the only part of the integral depending on the surface. Being able to expand $f(\zeta)$ in this form means that the contour of the given section can be mapped on to a unit circle by functions which admit of Fourier expansions. In another form we can say, with Wilton, that the success of the methods depends on the peculiar type of unicursal representation of the curve of section, the parameter being, of course, always the angle of the corresponding point in the circle. We easily see from this why the potential function is the same for different types of surfaces: it is because in the plane of the circle it is simply the problem of a line source outside a circular cylinder.

Cardiff.
15th December, 1936.

CIII. *The Stability and some other Properties of the Corona Discharge. By* L. G. H. Huxley, *M.A., D.Phil., F.Inst.P., F. W. Bennett Lecturer in Physics, University College, Leicester, and* J. H. Bruce, *B.A., B.Sc., Balliol College, Oxford* *.

I. *Introduction.*

ELECTRICAL discharges in gases may be conveniently classified according as the potential necessary to maintain a current is less than or exceeds the smallest potential required to start the discharge.

Examples of the former class are the spark discharge between parallel plates, arcs, and Geissler discharges, and of the latter corona and brush discharges from wires and points, and the high-frequency discharge.

Since many of the properties of the corona discharge serve to illustrate the principal features of discharges in fields which are not uniform it is proposed to discuss the corona discharge in relation to the general theory of discharges, and in particular to examine the conditions which determine the transformation of the stable corona discharge from wires and the brush discharge from points, into the unstable disruptive form, when the current is appropriately increased.

* Communicated by the Authors.

To this end a preliminary review is given of the general theory, originally developed by Townsend [1], [2a], of discharges in fields which are not uniform.

II. *Condition for the Self-maintenance of a Discharge.*

Consider an elementary "tube of flow" along which ions travel between surface elements dS_1 and dS_2 situated respectively on the cathode and anode. Let distances measured along the tube from dS_1 on the cathode be denoted by x. The electric field X is directed along the axis of the tube, but may be a function of x.

Let $n_1\,dx$ and $n_2\,dx$ be respectively the number of negative ions (electrons) and positive ions contained between the normal sections of the tube at x and $(x+dx)$, the field strength at x being X. Let u be the velocity of drift of the electrons, and $\alpha\,dx$ the number of molecules ionized by each electron on the average in a displacement dx along the tube, v and $\beta\,dx$ being the corresponding quantities for the positive ions. Suppose, further, that when N positive ions impinge on the element of surface dS_1 γN electrons are liberated by them, the field at dS_1 being X_0 and the coefficient γ a function of X_0/p, where p is the pressure of the gas.

It is known that the quantities u, v, α/p, and β/p are functions of the ratio X/p of the electric force X to the pressure p of the gas.

The current i across any section at distance x along the tube is given by,

$$n_1u+n_2v=i/e=c,$$

where e is the ionic charge.

For the current i to remain steady the following conditions are necessary: the net number of ions c crossing a section of the tube per second is the same for all sections, or

$$n_1u+n_2v=c=\text{constant}; \quad . \quad . \quad . \quad . \quad (1)$$

also

$$\left.\begin{aligned} \frac{dn_1}{dt} &= -\frac{d}{dx}(n_1u)+\alpha n_1u+\beta n_2v=0, \\ \frac{dn_2}{dt} &= \frac{d}{dx}(n_2v)+\alpha n_1u+\beta n_2v=0; \end{aligned}\right\} \quad . \quad . \quad (2)$$

whence

$$\left.\begin{aligned}\frac{d}{dx}(n_1u)-(\alpha-\beta)n_1u&=\beta c,\\ \frac{d}{dx}(n_2v)-(\alpha-\beta)n_2v&=-\alpha c,\end{aligned}\right\} \quad . \quad . \quad . \quad (3)$$

at the section dS_1 ($x=0$) let $(n_1u)_0$ and $(n_2v)_0$ be the values of the variables (n_1u) and (n_2v), their values at the element dS_2 at the anode ($x=d$) being $(n_1u)_d$ and $(n_2v)_d$ respectively.

The solutions of (3) are

$$\left.\begin{aligned}(n_1u)_x&=Z(x)\left[(n_1u)_0+c\int_0^x\frac{\beta\,dx}{Z(x)}\right],\\ (n_2v)_x&=Z(x)\left[(n_2v)_0-c\int_0^x\frac{\alpha\,dx}{Z(x)}\right],\end{aligned}\right\} \quad . \quad . \quad (4)$$

in which

$$Z(x)=e^{\int_0^x(\alpha-\beta)\,dx}.$$

Of the $(n_1u)_0$ electrons emitted per second from the element dS_1 of the cathode suppose that

(1) a number c_0 are liberated per second by the action of some external agent, such as a source of ultra-violet light, or by thermionic emission;

(2) a number $\gamma(n_2v)_0$ are liberated by the $(n_2v)_0$ positive ions which impinge in one second on the element dS_1.

Consequently

$$(n_1u)_0=c_0+\gamma(n_2v)_0,$$

whence

$$(n_1u)_0=\frac{\gamma c+c_0}{(1+\gamma)}$$

and

$$(n_2v)_0=\frac{(c-c_0)}{(1+\gamma)},$$

while at the anode

$$(n_2v)_d=0, \quad \text{and} \quad (n_1u)_d=c.$$

It follows from equation (4) that

$$\left.\begin{aligned}c=(n_1u)_d&=Z(d)\left[\frac{\gamma c+c_0}{(1+\gamma)}+c\int_0^d\frac{\beta\,dx}{Z(x)}\right],\\ 0=(n_2v)_d&=Z(d)\left[\frac{c-c_0}{(1+\gamma)}-c\int_0^d\frac{\alpha\,dx}{Z(x)}\right],\end{aligned}\right\} \quad . \quad . \quad (5)$$

and from either equation it may be seen that

$$c=\frac{c_0}{1-(1+\gamma)\int_0^d \frac{\alpha\,dx}{Z(x)}}, \quad \ldots \quad (6)$$

where

$$Z(x)=e^{\int_0^x(\alpha-\beta)\,dx}.$$

In the particular instance of a uniform field the formula reduces to the well known [2b], [4] forms which have been used to interpret experiments on the conductivity of gases between parallel plates.

This formula relates the number of electrons c which reach the element dS_2 of the anode with the number c_0 independently liberated from the element dS_1 of the cathode, the electric field being of arbitrary form.

Equation (b) shows that the current, proportional to c, will remain finite when c_0 becomes infinitesimal only when the denominator of the expression vanishes, so that the necessary condition for the self-maintenance of a current through the gas between the surface elements dS_1 and dS_2 is

$$(1+\gamma)\int_0^d \frac{\alpha\,dx}{Z(x)}=1. \quad \ldots \quad (7)$$

When $\gamma=0$ this condition assumes the form first given by Townsend [1] the subsequent generalization to the above form to include the coefficient γ being due to H. A. Wilson [3].

III. *Action of Positive Ions in Discharge.*

When the following substitutions are made,

$$\alpha'=\alpha(1+\gamma),$$

$$(\alpha-\beta)=(\alpha'-\beta'),$$

i. e.,

$$\beta'=(\gamma\alpha+\beta),$$

equation (6) assumes the form

$$c=\frac{c_0}{1-\int_0^d \alpha' e^{-\int_0^x(\alpha-\beta)\,dx}\,dx}, \quad \ldots \quad (8)$$

which is analytically equivalent to (6) with $\gamma=0$.

On the other hand the substitutions

$$(\alpha-\beta)=\alpha'',$$
$$\alpha(1+\gamma)=\alpha''(1+\gamma''),$$

i. e.,

$$\gamma''=\gamma\alpha+\beta,$$

reduces (6) to the form

$$c=\frac{c_0}{1-(1+\gamma'')\int_0^x \alpha'' e^{-\int_0^x \alpha'' dx}\,dx}, \quad . \quad . \quad . \quad (9)$$

which is analytically equivalent to formula (6) with $\beta=0$. Formulæ (6), (8), and (9) show that any one of the following hypotheses concerning the action of the positive ions may be adopted with equal success to explain the electrical conductivity of gases :

(*a*) the positive ions produce new ions solely by ionizing the molecules of the gas ($\gamma=0$),
(*b*) the positive ions do not ionize the molecules of the gas ($\beta=0$), but liberate electrons from the cathode,
(*c*) the positive ions operate in both these ways,

as is well known [2b], [4] from experiments on the conductivity of gases between parallel plate electrodes.

Certain properties of discharges in fields which are not uniform indicate that in air and some diatomic gases the process represented by the coefficient β must play an important part in the maintenance of discharges ; for example, when $\beta=0$ the condition (7) reduces to

$$e^{-\int_0^d \alpha dx}=1-\frac{1}{1+\gamma}$$

and cannot be satisfied if γ is also zero. It would be difficult to explain the brush discharge from an isolated positively charged point or wire unless β appears in expression (7).

IV. *Similarity Theorems.*

Townsend [2c] has given the following general theorem relating to discharges between geometrically similar pairs of conductors of the same material.

If V be the potential difference which first produces a discharge through a gas at pressure p between a pair of

electrodes the same potential will initiate a discharge between a second pair of conductors whose linear dimensions and separations are increased by a factor m relative to the first pair, when the pressure of the gas is p/m.

The following extension of the theorem by Holm [6] relates to the maintenance of current between similar pairs of electrodes.

If potential V maintains a current I between the first pair of electrodes when the pressure of the gas is p, then the same potential maintains the same current in the second system when the pressure of the gas is p/m.

Paschen's Law of sparking in uniform fields and the phenomena of the cathode fall of potential afford special examples of these theorems, but, as is shown below, the most accurate experimental tests of their validity are probably obtained from observations of the potentials required to maintain currents in a corona discharge between a wire and coaxial cylinder.

The theorems may be briefly established as follows :— Let the " dashed " symbols refer to the second system, and consider two corresponding " tubes of flow," one in each system. The potential at any point P in the first system is

$$V_P = \underset{\text{conductors}}{\int} \frac{\sigma\, ds}{r} + \underset{\text{tubes}}{\int} \frac{\rho\, dx\, ds}{r},$$

σ and ρ being the densities of surface and space charges respectively.

The potential at the corresponding point P′ in the second system is

$$V_{P'} = \underset{\text{electrodes}}{\int} \frac{\sigma'\, ds'}{r'} + \underset{\text{tubes}}{\int} \frac{\rho'\, dx'\, ds'}{r'}.$$

Since all dimensions $r' = mr$, the conditions that $V_{P'} = V_P$ are

$$(a) \quad \sigma' = \sigma/m,$$

$$(b) \quad \rho' = \rho/m^2.$$

Since

$$\rho = \frac{(n_2 - n_1)e\, dx}{ds\, dx}$$

within the one tube, and

$$\rho' = \frac{(n_2' - n_1')e\,dx'}{ds'\,dx'}$$

within the other, it follows that because

$$ds' = m^2\,ds$$

$$(n_2 - n_1) = (n_2' - n_1').$$

It follows that if the electric force at P is X then that at the corresponding point P′ is $X' = X/m$ and that the potentials V and V′ between the electrodes are identical. Let the pressure $p' = p/m$; then at corresponding points P and P′ it follows that

$$X/p = X'/p' \; ; \; u = u' \; ; \; v = v' \; ; \; \alpha/p = \alpha'/p' \text{ and } \beta/p = \beta'/p',$$

and also at the cathodes $\gamma = \gamma'$.

It may be easily verified that the integrals and the quantity $Z(x)$ which appear in equations (4), (6), and (7) are equal for the two systems when referred to corresponding coordinates x and x'.

Further, at the cathodes

$$\frac{(n_1 u)_0}{(n_2 v)_0} = \gamma = \gamma' = \frac{(n_1' u')_0}{(n_2' v')_0}.$$

Since the velocities are equal in the above equality, and also

$$(n_1 - n_2)_0 = (n_1' - n_2')_0,$$

therefore

$$(n_1)_0 = (n_1')_0 \quad \text{and} \quad (n_2)_0 = (n_2')_0.$$

Hence by equation (4), recalling that $(n_1 - n_2)_x = (n_1' - n_2')_{x'}$, it follows that $(n_1)_x = (n_1')_{x'}$ and $(n_2)_x = (n_2')_{x'}$ for corresponding values of x and x' ; consequently $c = c'$. Conversely, if it be assumed that $c = c'$ and that $p' = p/m$, it may be shown that $V = V'$. The theorem is thus established.

V. *The Corona Discharge.*

In the corona discharge the ionization is confined to a small region of intense field strength near the wire. The current flows out as a stream of similarly charged ions which produce a space charge in the gas, and in order to increase the current the potential difference between the

electrodes must be further increased, since the force at the surface of the wire cannot be diminished below the value X_0 if the discharge is to be maintained.

The relation between the potentials and the currents maintained by them between a wire and coaxial cylinder has been derived by Townsend [2d], [7] on the assumption that the discharge is confined to the immediate vicinity of the wire and that the velocity of the ions in the field is proportional to the electric force. The theory is given below in outline.

Let i be the current per unit length of the system, A the radius of the cylinder and a that of the wire, kX the velocity of the ions through the gas under an electric force X, and ρ the charge density at a distance r from the axis.

Let V be the potential difference between the electrodes which maintains the current i, and V_0 that which just starts the discharge ($i \to 0$), so the force X_0 at the surface of the wire is equal to $V_0/a \log A/a$, electrostatic units being adopted.

Let ϕ be the potential at a distance r from the axis, and suppose ϕ to be zero at the cylinder (r=A), its value at r=a being therefore V.

The current is given by $2\pi\rho rk\mathrm{X}=i$.

From Poisson's equation

$$\frac{d}{dr}\left(r\frac{d\phi}{dr}\right)=-4\pi\rho r,$$

whence

$$\left(r\frac{d\phi}{dr}\right)^2-\frac{2i}{k}=\text{constant},$$

or

$$r^2\left(\mathrm{X}^2-\frac{2i}{k}\right)=a^2\left(\mathrm{X}_0{}^2-\frac{2i}{k}\right)$$

and

$$\left(\frac{d\phi}{dr}\right)^2=\mathrm{X}^2=\frac{2i}{k}\left[1+\frac{a^2}{r^2}\left(\frac{k^2\mathrm{X}_0{}^2}{2i}-1\right)\right]$$

$$=\mathrm{C}^2\left[1+\frac{\mathrm{B}^2}{r^2}\right], \quad \ldots\ldots\ldots\ldots \quad (10)$$

where

$$\mathrm{C}^2=\frac{2i}{k} \quad \text{and} \quad \mathrm{B}^2=a^2\left(\frac{k\mathrm{X}_0{}^2}{2i}-1\right).$$

When (10) is integrated in conformity with the boundary conditions stated above the following expression is obtained for ϕ:

$$\frac{\phi}{BC} = \log A/r + \log \frac{1+\left(1+\frac{r^2}{B^2}\right)^{1/2}}{1+\left(1+\frac{A^2}{B^2}\right)^{1/2}} - \left(1+\frac{r^2}{B^2}\right)^{1/2} + \left(1+\frac{A^2}{B^2}\right)^{1/2}. \quad (11)$$

The term $BC = aX_0\left(1-\frac{2i}{kX_0^2}\right)^{1/2}$, but in practice $\frac{2i}{kX_0^2}$ is negligible compared with unity, so that in effect

$$BC = aX_0 = \frac{V_0}{\log A/a}.$$

Put

$$\theta = \frac{A^2}{B^2} = \frac{A^2}{a^2X_0^2}\cdot\frac{2i}{k},$$

and introduce what may be termed "reduced" variables, $z=r/A$ and $z_a=a/A$.

Equation (9) now becomes

$$y = \frac{\phi}{V_0}\log A/a = (1+\theta)^{1/2} - \log\left[1+(1+\theta)^{1/2}\right] - \log z - (1+z^2\theta)^{1/2} + \log\left[1+(1+z^2\theta)^{1/2}\right]. \quad (12)$$

It expresses the "reduced" potential $\frac{\phi}{V_0}\log A/a$ in terms of the "reduced" axial distance z and the parameter θ.

Let $Z = \left(\frac{dy}{dz}\right)_\theta$ be termed the reduced force. Then from (12)

$$Z = \left(\frac{AX}{aX_0}\right) = -\frac{(1+z^2\theta)^{1/2}}{z}, \quad . \quad . \quad . \quad (13)$$

its value at the outer cylinder, $z=1$, being

$$\bar{Z}_A = -(1+\theta)^{1/2}. \quad . \quad . \quad . \quad . \quad . \quad (14)$$

From equation (12) and the condition $\phi=V$ at $r=a$ it follows that

$$\left(\frac{V}{V_0}-1\right)\log A/a = (1+\theta)^{1/2} - \log\left[1+(1+\theta)^{1/2}\right] - (1+z_a^2\theta)^{1/2} + \log\left[1+(1+z_a^2\theta)^{1/2}\right]. \quad (15)$$

Since in practice $z_a < \frac{1}{20}$, $z_a^2 << 1$, this equation may be written in the following form given by Townsend [7]:

$$\left(\frac{V}{V_0} - 1\right) \log A/a = (1+\theta)^{1/2} - 1 - \log\left[1+(1+\theta)^{1/2}\right] + \log 2. \quad . \quad . \quad . \quad (16)$$

Equation (16) relates the currents $i\left(= \frac{k\theta}{2} \cdot \frac{a^2 X_0^2}{A^2}\right)$ with the potentials V which maintain them.

Put $y = \left(\frac{V}{V_0} - 1\right) \log A/a$ in equation (15), then

$$\frac{dy}{d\theta} = \frac{1}{2}\left[\frac{1}{1+(1+\theta)^{1/2}} - \frac{z_a^2}{1+(1+Z_a^2\theta)^{1/2}}\right].$$

In practice the second term in the brackets may be neglected, so that $\left(\frac{dy}{d\theta}\right)_{\theta \to 0} \to \frac{1}{4}$, and for small values of θ equation (15) reduces to $y = \theta/4$, the error already being less than 5 per cent. when $\theta = 0{\cdot}25$ and about 10 per cent. when $\theta = 0{\cdot}5$.

Substitution for y and θ gives

$$V_0(V - V_0) = \frac{iA^2}{2k} \log A/a, \quad . \quad . \quad . \quad . \quad (17)$$

a well-known formula [2d] which is in good agreement with observation at the higher pressures where θ is usually small.

For the larger values of θ, Z approaches $\theta^{1/2}$ at $z = 1$,

i. e., $\qquad X^2 \doteq \frac{2i}{k}$ when $r = A$.

The ratio $R = \frac{Z}{Z_A}$ of the force at distance z to its value at the outer surface $z = 1$ is given by

$$R = \frac{\left(\theta + \frac{1}{z^2}\right)^{1/2}}{(1+\theta)^{1/2}}.$$

The following table illustrates the variation of R with z for various values of θ :—

TABLE I.

R.

z \ θ	0.	5.	10.	15.	20.	25.
0·1	10·0	4·16	3·16	2·66	2·40	2·01
0·2	5·00	2·22	1·78	1·57	1·47	1·37
0·3	3·33	1·63	1·38	1·27	1·22	1·16
0·4	2·50	1·36	1·21	1·14	1·12	1·09
0·5	2·00	1·22	1·12	1·08	1·05	1·04
0·6	1·67	1·13	1·07	1·05	1·03	1·02
0·7	1·43	1·07	1·05	1·03	1·02	1·01
0·8	1·25	1·04	1·03	1·01	1·01	1·00
0·9	1·11	1·02	1·01	1·00	1·00	1·00
1·0	1·00	1·00	1·00	1·00	1·00	1·00

It is clear that with θ large (large currents) the field tends to uniformity in the outer regions and, indeed, for a considerable fraction of the distance between the outer cylinder and the wire.

The distribution of the field in a corona discharge between a wire and a large coaxial cylinder has been investigated experimentally by Hoover [8], whose conclusions are in substantial agreement with the expression given above.

VI. *Measurement of Mobilities of Ions* [2d], [7], [9], [10].

The quantity $\left(\frac{V}{V_0}-1\right)\log A/a$ which appears in equation (16) may be obtained experimentally by observing the potentials V_0 and V which start a discharge and maintain a current i respectively between a wire and a coaxial cylinder.

The corresponding value of θ is then obtained from equation (16) and as the current is known the mobility k of the ions under the prevailing conditions is obtained immediately from the relation

$$\theta = \frac{2i}{k}\cdot\frac{A^2}{a^2X_0^2}.$$

The appropriate value of θ is most conveniently found from a curve [9] representing $\left(\frac{V}{V_0}-1\right)\log A/a$ as a function of θ according to equation (16).

A table of corresponding values of $\left(\frac{V}{V_0}-1\right)\log A/a$ and θ is given, and may be used to construct the curve.

TABLE II.

θ.	·5.	1.	2.	3.	4.	5.	6.	7.	8.
$\left(\frac{V}{V_0}-1\right)\log\frac{A}{a}$	·118	·226	·420	·594	·755	·904	1·04	1·175	1·300

θ.	9.	10.	12.	14.	16.	18.	20.	30.	40.
$\left(\frac{V}{V_0}-1\right)\log\frac{A}{a}$	1·423	1·540	1·765	1·975	2·17	2·36	2·54	3·36	4·07

At reduced pressures the corona discharge is obtained only when the wire is positively charged, the negative discharge being disruptive, but the values found for the mobilities of the positive ions by the above procedure in a number of gases with various currents at various pressures are extremely concordant.

It is justifiable to regard such results as affording an accurate experimental verification of equation (16).

For example, the velocities $W=kX$ of positive ions in dry air which were deduced from the present series of observations over a range of pressures from 20 to 50 millimetres of mercury were found to be in excellent agreement with the experimental curve given by Boulind [10] for experiments at lower pressures. In these measurements, as has already been explained, the ions move under a constant force for the greater portion of the distance.

VII. *The Corona Discharge and the General Similarity Theorems.*

In corona discharges in which the region of ionization by collision does not extend to the outer cylinder the

Townsend similarity theorem for potentials reduces to the statement that the quantity aX_0 is a function of the product ap [2e].

This consequence of the theorem has been tested by a number of experimenters [2e], [9], [10], and the results of the present series of measurements are shown in fig. 1, where the sets of points furnished by two wires of different diameters can be seen to lie closely about the same curve.

Fig. 1.

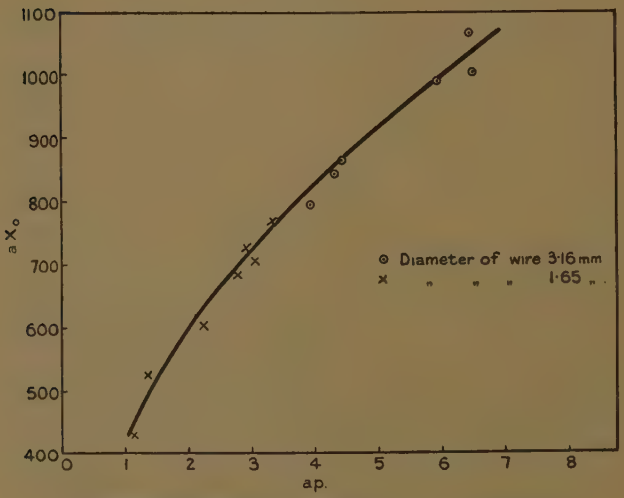

aX_0 shown as a function of ap for air; a in centimetres; X_0 in volts per centimetre; p in millimetres of mercury.

The similarity theorem for currents is also accurately and conveniently verified by the corona discharge.

Equation (15) may be written

$$\left(\frac{V}{V_0}-1\right)=-f(\theta)\log z_a,$$

where

$$\theta=\frac{2i}{k}\cdot\frac{A^2}{a^2X_0^2}=\frac{2i}{k}\cdot\left(\frac{A}{V_0}\log A/a\right)^2$$

and $z_a=a/A$, i being the current per cm.

Consider two corona systems whose dimensions are respectively a, A and ma, mA. Let the first contain gas at pressure p and the second gas at pressure p/m.

It follows that since the products kp and ap and the quantity z_a are the same in each system the quantity $aX_0 = -V_0/\log z_a$ is also the same.

The same potential V_0 will therefore suffice to start the discharge in each system. Equation (15) shows that when a potential V is applied to each system the current i per centimetre in each system is obtained from the same value of θ.

For the first system we find that the current per length l is

$$I = li = \frac{lk\theta}{A^2} \cdot \text{constant}$$

and the current I′ per length $l' = ml$ in the second system is

$$I' = \theta \cdot \frac{(ml).(mk)}{(mA)^2} \cdot \text{constant} = I.$$

As the results of experiments on the currents in corona discharges are in close agreement with equation (15) it follows that such experiments also are an accurate test of the similarity theorem for currents.

VIII. *Transition of Corona to Disruptive Discharge.*

It has been shown above that when the current i becomes large the field X between the electrodes everywhere tends to uniformity except in the immediate vicinity of the wire.

The whole field may be considered to be constituted as follows :—

(1) A cylindrical portion $\left(X = \frac{aX_0}{r}\right)$ extending from the surface of the wire a short distance $r = b$ into the gas.

(2) A field $X \doteqdot \left(\frac{2i}{k}\right)^{1/2}$, approximately constant, extending from $r = A$ to $r = b$.

At first the ionization is confined within the distance $r = b$ of the wire, and the condition (7) for the maintenance

of the discharge between the electrodes over the distance $d=(A-a)$ becomes

$$\frac{1}{(1+\gamma)} = \int_0^d \frac{\alpha\, dx}{Z(x)} = \int_{(d-b)}^{d} \frac{\alpha\, dx}{Z(x)} + \int_0^{(d-b)} \frac{\alpha\, dx}{Z(x)} = \int_{(d-b)}^{d} \frac{\alpha\, dx}{Z(x)},$$

the coefficients α and β being zero over the path $(b-d)$, and the coefficient γ negligible when the wire is positive. When, however, the outer field increases to a value such that α and β become appreciable over the whole distance the second term is no longer zero, and

$$\int_{(d-b)}^{d} \frac{\alpha\, dx}{Z(x)} < \frac{1}{1+\gamma}.$$

Consequently the mean field in the vicinity of the wire is reduced when ionization appears in the outer regions and, moreover, the field near the surface of the outer cylinder somewhat increased. Therefore, as the current is increased a condition is reached in which the field between the electrodes tends to uniformity for virtually the whole distance $(A-a)$, so that condition (7) becomes the same as that necessary for sparking in uniform fields. In this condition the discharge is unstable, since a fortuitous increase in current concentrates the force at cathode, and the potential required to maintain the current is diminished [1], [2f].

It would be anticipated therefore that the transition from the stable corona to the disruptive discharge should happen when the total potential V between the wire and cylinder is nearly equal to the sparking potential between parallel plates appropriate to the value $p(A-a)$ of the sparking parameter (pressure $\times$ separation).

A set of measurements in dry air at reduced pressures with two wires of diameters 1·65 mm. and 3·16 mm. stretched along coaxial cylinders, with guard cylinders all of diameter 4·6 cm., were in good agreement with this expectation.

In fig. 2 the potentials V at which the disruptive discharge occurs are plotted against the sparking parameter $p(A-a)$. The source of voltage was a Westinghouse metal rectifier circuit with adequate smoothing capable of delivering 5000 volts.

The points furnished by each apparatus, with the wires at positive potentials, lie closely about the dotted curve,

which is the standard sparking potential curve for uniform fields in air. The lower curve gives the corona starting potentials for one of the wires, and it can be seen that for values of $p(A-a)$ less than about 10 the corona discharge is not obtained in air, and also that the range of stable currents increases rapidly with greater values of $p(A-a)$.

Fig. 2.

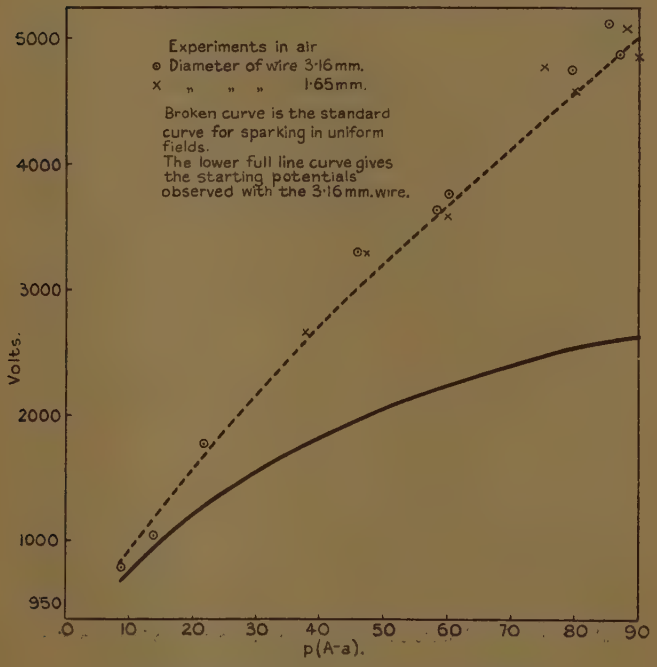

p in millimetres of mercury ; $(A-a)$ in centimetres.

The transformation of a brush discharge from a small sphere to a plane into a disruptive discharge can also be explained on the same principles. As in the corona discharge so in the brush discharge the current is maintained by the ions generated in a small region of intense electric force near the point or small sphere, the force at its surface preserving a fixed value X_0 whatever the current. It is clear that progressive increment of the

total potential V between the electrodes, with increasing current, first affects the field near the plane electrode, so that a region of uniform field of increasing strength extends progressively towards the sphere from the plane. Sparking again appears when the total potential difference V between the electrodes approaches the value for uniform fields appropriate to the same value of *pd*.

A series of measurements on discharges between a small sphere and a large plane electrode, at various pressures

Fig. 3.

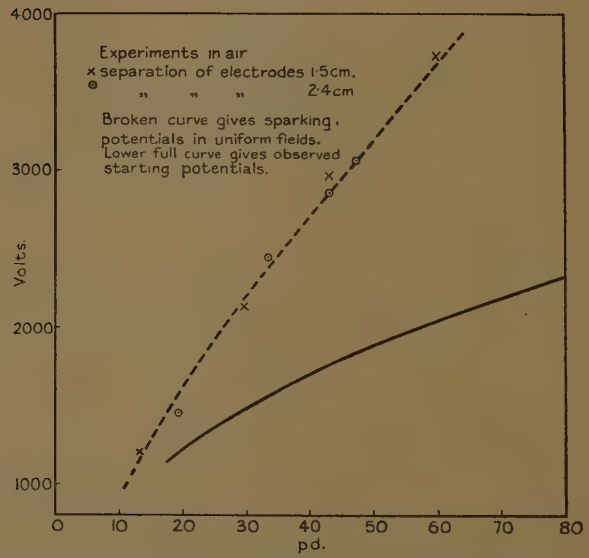

Pressure p in millimetres of mercury; d, the electrode separation in centimetres.

and separations, gave results in satisfactory agreement with this view of the process.

The results are again shown graphically in fig. 3, where the points are seen to lie near the standard sparking potential curve. The lower curve shows the least potential which starts the brush discharge.

Peek [11] has investigated the breakdown at atmospheric pressure of the stable discharges between wires and coaxial cylinders and between parallel wires. The

values of the breakdown potential were notably lower than the corresponding sparking voltages in uniform fields, but as alternating potentials were used the conditions are not the same as those which prevailed in the present experiments.

In brush discharges between parallel wires using direct current there is already a concentration of electric force at the cathode, and it would be anticipated that the breakdown would occur at a voltage less than the corresponding sparking voltage in uniform fields, but we have no information on this point.

Several investigators [12] have studied the factors which may affect the transformation of a discharge into one of another form. For instance, Jurriaanse and Druyvesteyn have observed, among other matters, that the transition of a glow discharge to an arc is facilitated by supplying ions to the vicinity of the cathode. In the present experiments the formation of an auxiliary discharge near the cathode caused the breakdown of the corona. This is consistent with the theory given above, as the field near the cathode becomes further disturbed by the additional ionization.

We are indebted to Mr. E. B. Waterson for technical assistance.

References.

(1) Townsend, J. S., Phil. Mag. ix. p. 289 (1905); 'The Theory of Ionization of Gases by Collision,' chap. iv. (Constable & Co., 1910).
(2) Townsend, J. S., 'Electricity in Gases' (Oxford, 1915):
(*a*) Chap. xi. § 293.
(*b*) Chap. ix.
(*c*) Chap. x. § 251.
(*d*) Chap. x. § 257.
(*e*) Chap. x. § 252.
(*f*) Chap. xi. § 295.
(3) Wilson, H. A., 'Modern Physics,' chap. xvi. p. 272 (Blackie & Son, 1928).
(4) Townsend, J. S., and MacCallum, S. P., Phil. Mag. ser. 7, xvii. p. 690 (1934).
(5) Townsend, J. S. and Jones, F. Ll., Phil. Mag. xv. p. 282 (1933); Townsend, J. S., and Yarnold, G. D., Phil. Mag. xviii. p. 594 (1934); Jones, F. Ll., and Willott, W. H., Proc. Phys. Soc. xlviii. p. 830 (1936).
(6) Holm, R., *Phys. Zeit.* xxv. p. 504 (1924).
(7) Townsend, J. S., Phil. Mag. xxviii. p. 83 (1914).
(8) Hoover, W. G., Elect. Engineering (New York), lv. 5, p. 448 (1936).
(9) Huxley, L. G. H., Phil. Mag. v. p. 721 (1928).

(10) Huxley, L. G. H., Phil. Mag. x. p. 185 (1930); Bruce, J. H., Phil. Mag. x. p. 476 (1930); Boulind, H. F., Phil. Mag. xviii. p. 909 (1934).
(11) Peek, 'Dielectric Phenomena in High Voltage Engineering,' 3rd ed. chap. v. pp. 109–116 (McGraw-Hill).
(12) Jurriaanse, T., and Druyvesteyn, M. J., 'Physica,' iii. p. 825 (1936), and references given therein; Newman, F. H., Phil. Mag. xxiii. p. 239 (1937).

General References.

Townsend, 'Electricity in Gases' (Oxford).
Darrow, 'Electrical Phenomena in Gases' (Williams & Wilkins).
Schumann, 'Elektrische Durchbruchfeldstärke von Gasen' (Springer).
Von Engel and Steenbeck, 'Elektrische Gasentladungen' (Springer).
Laporte, 'Les Phénomènes Élémentaires de la Décharge Electrique dans les Gaz' (Les Presses Universitaires de France).

CIV. *Wires under Tension and Transverse Forces* *.

By J. E. Doyle, *M.Sc.* †

THE following investigations have been suggested by the manner of failure of the wires in wire ropes which run over pulleys, or over which loads travel as in aerial ropeways. The breakage of the wires suggests fatigue in a large number of cases and that the stresses caused by the bending of the wires are larger than are generally realized.

To a first approximation, the total load may be considered as divided more or less equally among the individual wires composing the rope, and we are thus led to a consideration of the case of a wire stretched between two points on the same level and carrying various loads. It is shown that the bending moments can be much reduced by distributing the loads.

The deflexions and inclinations are taken as small, except where otherwise stated, and R, the radius of curvature of the axis of the wire, is represented by $-\dfrac{1}{\dfrac{d^2y}{dx^2}}$, following the method usually adopted for beams. Stretch of the wire is neglected, as is also, in most cases, the difference in length between the arc and the chord.

* Based on a Thesis submitted at Queen's University, Belfast.
† Communicated by the Author.

Previous Investigations.

The general equations applicable to a wire which is under tension, and is also acted on by other forces, in the form suitable to an element of the wire, are well known (*e. g.*, Routh, ' Analytical Statics ').

Morley (Phil. Mag. ser. 6, xv. p. 711, 1908) gives solutions for small deflexions of the cases of a tie-rod pivoted at the ends, under tension and carrying :

(*a*) a uniformly distributed lateral load only over its whole length ;

(*b*) a central lateral load only.

For (*a*) the Bending Moment obtained at the centre, where it is a maximum, is

$$\frac{w\mathrm{EI}}{\mathrm{P}}\left(1-\operatorname{sech}\frac{l}{2}\sqrt{\frac{\mathrm{P}}{\mathrm{EI}}}\right), \quad \text{or} \quad \frac{w}{a^2}(1-\operatorname{sech} a\mathrm{L}),$$

and for (*b*) the Bending Moment at the centre is

$$\frac{\mathrm{W}}{2}\sqrt{\frac{\mathrm{EI}}{\mathrm{P}}}\tanh\frac{l}{2}\sqrt{\frac{\mathrm{P}}{\mathrm{EI}}}, \quad \text{or} \quad \frac{\mathrm{W}}{2a}\tanh a\mathrm{L},$$

where w is the distributed load per unit length, W the central lateral load, l the total length between ends, P the tension, E Young's Modulus, I the Moment of Inertia of a cross-section of the wire or rod, $a^2=\frac{\mathrm{P}}{\mathrm{EI}}$, $\mathrm{L}=\frac{l}{2}$.

Young (Phil. Mag. ser. 6, xxix. p. 96, 1915) solves a problem similar to (*a*) with regard to a surveyor's metal tape, arriving at essentially similar results. He also solves the problem for small deflexions in the case where the ends are clamped horizontally at the same level, obtaining for the Bending Moment at the centre

$$\frac{w}{a^2}(1-a\mathrm{L}\operatorname{cosech} a\mathrm{L})$$

when expressed in our present notation. w, the transverse load per unit length, is in this case the weight per unit length of the tape. For the Bending Moment at the supports, he obtains

$$\frac{w}{a^2}(1-a\mathrm{L}\coth a\mathrm{L}), \quad \text{or} \quad \frac{w}{a^2}(1-a\mathrm{L}), \text{ nearly}, \quad \text{or} \quad -\frac{w}{a}\mathrm{L}$$

practically.

The results obtained by Morley and Young also appear as particular cases of the more general problems which follow.

Single Concentrated Load at any Point.

Fig. 1.

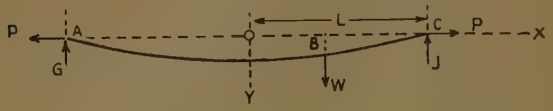

Let the uniform wire AC, pivoted freely at A and C, be under a tension P and carry a load W at the point B. The weight of the wire itself is neglected in the first instance. The vertical forces at A and C are represented by G and J respectively. The origin is taken at O, the middle point of AC, the positive direction of y being downwards and of x to the right.

The Bending Moment at a point X_1 in AB will be denoted by M_{AB}, while that at a point X_2 in BC will be denoted by M_{BC}. This is necessary, as a discontinuity exists at B and the sections AB and BC require different equations. y_{AB} and y_{BC}, also $\dot{y}_{AB}$ or $\frac{d}{dx}(y_{AB})$ will be used similarly.

For small deflexions and inclinations the simple theory of bending is used, *i. e.*, $\frac{M}{I} = \frac{E}{R}$, where M is the Bending Moment, E is Young's Modulus, R is the radius of curvature of the axis of the wire, and I the Moment of Inertia of the cross-section of the wire.

We then have

$$M_{BC} = J(L-x) - Py_{BC}, \qquad M_{AB} = G(L+x) - Py_{AB},$$

a bending moment, which tends to cause concavity on the upper side of the wire, being taken as positive.

Hence

$$\frac{d^2M_{AB}}{dx^2} = -\frac{Pd^2y_{AB}}{dx^2} = \frac{P}{R_{AB}} = \frac{PM_{AB}}{EI} = a^2M_{AB},$$

where a^2 is used for $\frac{P}{EI}$.

Thus

$$\frac{d^2M_{AB}}{dx^2} = a^2M_{AB} \quad \text{and} \quad \frac{d^2M_{BC}}{dx^2} = a^2M_{BC}.$$

Solving these equations and adjusting the four arbitrary constants in the solutions so as to make the Bending Moments zero at A and C (the y's will then be zero there), and so as to make the slope, $\dot{y}$, and Bending Moment at B have the same values respectively for AB and BC, we find

$$M_{AB} = \frac{W}{a} \operatorname{cosech} 2aL \sinh aBC \sinh aAX_1,$$

or

$$\frac{W}{a} \operatorname{cosech} aAC \sinh aBC \sinh aAX_1,$$

$$M_{BC} = \frac{W}{a} \operatorname{cosech} 2aL \sinh aAB \sinh aCX_2,$$

or

$$\frac{W}{a} \operatorname{cosech} a\ AC \sinh aAB \sinh aCX_2.$$

At B, the Bending Moment, as deduced from either, is

$$\frac{W}{a} \operatorname{cosech} aAC \sinh aAB \sinh aBC,$$

or

$$\frac{W}{2a} \operatorname{cosech} 2aL(\cosh 2aL - \cosh 2aOB).$$

For a given position of B, as $\sinh z$ increases with z, it follows that the Bending Moments increase from zero at A and C to the value at B.

Again, the Bending Moment at B,

$$\frac{W}{2a} \operatorname{cosech} 2aL(\cosh 2aL - \cosh 2aOB),$$

will increase as OB decreases, that is, as the load is moved nearer to the point O. Hence the greatest Bending Moment caused by a concentrated load moving slowly along the wire will occur when it is at the middle point of AC, and its value will then be $\frac{W}{a} \operatorname{cosech} 2aL \sinh^2 aL$, or $\frac{W}{2a} \tanh aL$, agreeing with the result obtained by

Morley for a tie-rod loaded transversely at its middle point.

In ordinary cases aL will be large, so that tanh aL will be less than unity by only a very small amount. The maximum Bending Moment due to a concentrated load W is thus practically $\frac{W}{2a}$ or $\frac{W}{2}\sqrt{\frac{EI}{P}}$.

From the equation $M_{AB}=G(L+x)-Py_{AB}$, the value of y_{AB}, giving the curve of deflexion, may now be obtained, and a similar result may also be obtained for BC from the equation $M_{BC}=J(L-x)-Py_{BC}$.

The weight of the wire may be taken into account by adding the Bending Moment due to it to that obtained above. If the weight of the wire is w per unit length the Bending Moment due to it at a distance x from the centre is $\frac{w}{a^2}(1-\text{sech } aL \cosh ax)$, as shown by Morley

(see p. 1115).

Single Concentrated Load on a Wire whose Ends are clamped horizontally.

Fig. 2.

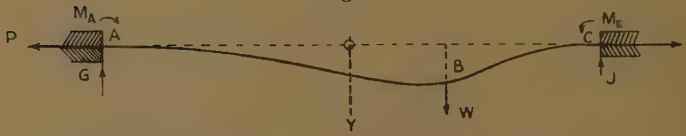

Let the uniform wire AC, whose ends are clamped horizontally at the same level, be under tension P and carry a load W at the point B. The weight of the wire is neglected in the first instance. The vertical forces at A and C respectively are represented by G and J. Bending Moments will be caused at A and C by the clamping, which are represented by M_A and M_C respectively, acting on the wire as shown, they will be found to be negative.

Using the same notation and conventions as in the last case we then have :

$$M_{AB}=G(L+x)-Py_{AB}+M_A, \quad M_{BC}=J(L-x)-Py_{BC}+M_C,$$

$$\frac{d^2M_{AB}}{dx^2}=a^2M_{AB}, \qquad \frac{d^2M_{BC}}{dx^2}=a^2M_{BC},$$

where $$a^2 = \frac{P}{EI}.$$

Solving and determining the arbitrary constants so that $M_{BC}=M_{AB}$ at B, $\dot{y}_{l\,C}=\dot{y}_{AB}$ at B, $\dot{y}_{AB}=0$ at A ($x=-L$), $\dot{y}_{BC}=0$ at C ($x=L$), we obtain the following :

$$M_{AB} = \frac{W}{2a}\operatorname{cosech} aL \cosh ax \{\cosh a(L-d)-1\} + \frac{W}{2a}\operatorname{sech} aL \sinh ax \left\{ \cosh a(L-d)-1+\frac{2G}{W} \right\},$$

$$M_{BC} = \frac{W}{2a}\operatorname{cosech} aL \cosh ax \{\cosh a(L+d)-1\} - \frac{W}{2a}\operatorname{sech} aL \sinh ax \left\{ \cosh a(L+d)-1+\frac{2J}{W} \right\},$$

where d is the value of x at B.

$$J = \frac{W}{2}\left(1+\frac{ad\cosh aL-\sinh ad}{aL\cosh aL-\sinh aL}\right),$$

$$G = \frac{W}{2}\left(1-\frac{ad\cosh aL-\sinh ad}{aL\cosh aL-\sinh aL}\right).$$

M_{AB} and M_{BC} may also be written as follows :

$$M_{AB} = \frac{G}{a}\operatorname{sech} a(L-z_{AB})\sinh a(z_{AB}+x),$$

$$M_{BC} = \frac{J}{a}\operatorname{sech} a(L-z_{BC})\sinh a(z_{BC}-x),$$

where z_{AB} is the distance from O of the point of inflexion in AB and z_{BC} the distance from O of the point of inflexion in BC (numerical values).

Thus the numerical value of the Bending Moment falls from $\frac{G}{a}\tanh a(L-z_{AB})$ at A to zero at the point of inflexion and then rises to the same value at $y_{max.}$. It then continues to increase as far as B, where its value is

$$\frac{G}{a}\operatorname{sech} a(L-z_{AB})\sinh a(z_{AB}+d).$$

Again, starting at C, the Bending Moment decreases until the point of inflexion in BC is reached. From here it again increases as far as B, but, since BC does not

contain any point except C where the slope is zero, the Bending Moment does not rise to so high a value as at C. Hence we conclude that the Bending Moment at C is the largest one in the wire (for a position of the load as shown where B is in OC).

The maximum numerical value of M_C is reached when the load is at a distance d from O such that

$$\tanh a\frac{L-d}{2}=\coth aL-\frac{1}{aL},$$

or
$$a(L-d)=\log_e\frac{e^{2aL}(2aL-1)+1}{e^{2aL}-2aL-1}.$$

When aL is large, the load will thus be comparatively near C when the Bending Moment at C is a maximum.

The maximum Bending Moment in the wire is thus greater than if the ends were free, but it is less than $\frac{J}{a}$ or $\frac{W}{a}$, that is, it is less than twice as large.

To take the weight of the wire into account, we may add the Bending Moment for a wire under the action of a uniform load w (the weight per unit length of the wire) which gives $\frac{w}{a}\left(\frac{1}{a}-L\ \text{cosech}\ aL\cosh ax\right)$, as shown by Young (Phil. Mag. p. 96, 1915). With W in the centre, the Bending Moment at C will in this case be $-\frac{wL}{a}-\frac{W}{2a}$ approximately. This will also represent approximately the Bending Moment over the supports where a wire is stretched over several supports at the same level, each span being of length 2L and carrying a load W at the centre. This result may also be obtained by dividing the reaction at each support, $2wL+W$, by $2a$.

Load distributed over Portion of Stretched Wire.

Fig. 3.

Let the wire AD, stretched between two points on the same level A and D, carry a load v per unit length over

the portion BC. The length BC will be denoted by $2k$. Then, with the same notation as in previous cases,

$$M_{AB}=G(L+x)-Py\ ;\ M_{BC}=J(L-x)-\frac{v}{2}(OC-x)^2-Py\ ;$$

$$M_{CD}=J(L-x)-Py.$$

$$\frac{d^2M_{AB}}{dx^2}=a^2M_{AB}\ ;\quad \frac{d^2M_{BC}}{dx^2}=a^2M-v\ ;\quad \frac{d^2M_{CD}}{dx^2}=a^2M_{CD}.$$

Solving and determining the constants so that

(1) $M_{AB}=0$ at $x=-L$,

(2) $M_{CD}=0$ at $x=L$,

(3) $M_{AB}=M_{BC}$ at $x=OB$,

(4) $M_{BC}=M_{CD}$ at $x=OC$,

(5) $\dot{y}_{AB}=\dot{y}_{BC}$ at $x=OB$,

(6) $\dot{y}_{BC}=\dot{y}_{CD}$ at $x=OC$,

the following values are obtained for the Bending Moments :

$$M_{AB}=\frac{v}{a^2}\operatorname{cosech} 2aL(\cosh aBD-\cosh aCD)\sinh a(L+x),$$

$$M_{BC}=\frac{v}{a^2}-\frac{v}{a^2}\operatorname{cosech} 2aL\cosh aCD\sinh a(L+x)$$

$$-\frac{v}{a^2}\operatorname{cosech} 2aL\cosh aAB\sinh a(L-x),$$

$$M_{CD}=\frac{v}{a^2}\operatorname{cosech} 2aL(\cosh aAC-\cosh aAB)\sinh a(L-x).$$

From the value given for M_{BC} it follows that if the load is movable, the greatest Bending Moment it causes is $\frac{v}{a^2}\{1-\operatorname{sech} aL\cosh a(L-k)\}$ and occurs at the middle point of the wire.

Combined Loads and Constant Curvature Loading.

Fig. 4.

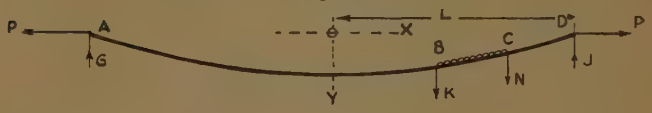

Let the wire AD, stretched between the two points A and D at the same level by the forces P, weigh w per unit length and carry a distributed load of v per unit length over the portion BC, and two concentrated loads, K at B and N at C. The vertical forces at A and D are denoted by G and J respectively. The same notation is used as in previous cases, $a^2 = \frac{P}{EI}$, etc.

By proceeding as in the previous case and forming equations for each of the three portions AB, BC, CD, or by adding the Bending Moments produced by the various loads separately, as shown below, the same results are obtained.

(1) The load w per unit length over the whole wire gives a Bending Moment $\frac{w}{a^2} - \frac{w}{a^2}$ sech aL cosh ax. This applies to the whole length.

(2) A Bending Moment $\frac{K}{a}$ cosech $2a$L sinh aBD sinh a(L$+x$) over AB and

(3) a B.M. $\frac{K}{a}$ cosech $2a$L sinh aAB sinh a(L$-x$) over BD

are caused by the load K at B.

(4) A B.M. $\frac{N}{a}$ cosech $2a$L sinh aCD sinh a(L$+x$) over AC and

(5) a B.M. $\frac{N}{a}$ cosech $2a$L sinh aAC sinh a(L$-x$) over CD

are caused by the load N at C.

(6) A B.M. over AB,

$$\frac{v}{a^2}\operatorname{cosech} 2aL(\cosh aBD-\cosh aCD)\sinh a(L+x),$$

(7) a B.M. $\frac{v}{a^2}-\frac{v}{a^2}\operatorname{cosech} 2aL\cosh aAB\sinh a(L-x)$

$$-\frac{v}{a^2}\operatorname{cosech} 2aL\cosh aCD\sinh a(L+x)$$ over BC,

and

(8) a B.M. over CD

$$\frac{v}{a^2}\operatorname{cosech} 2aL(\cosh aAC-\cosh aAB)\sinh a(L-x)$$

are caused by the load v per unit length which is distributed over BC.

Adding together the various Bending Moments which refer particularly to AB, and doing the same for BC and CD respectively, we obtain the following results :

$M_{AB}=(1)+(2)+(4)+(6)$

$$=\frac{w}{a^2}(1-\operatorname{sech} aL\cosh ax)$$

$$+\frac{1}{a}\operatorname{cosech} 2aL(K\sinh aBD+N\sinh aCD)\sinh a(L+x)$$

$$+\frac{v}{a^2}\operatorname{cosech} 2aL(\cosh aBD-\cosh aCD)\sinh a(L+x),$$

$M_{BC}=(1)+(3)+(4)+(7)$

$$=\frac{w}{a^2}(1-\operatorname{sech} aL\cosh ax)$$

$$+\frac{1}{a}\operatorname{cosech} 2aL\{K\sinh aAB\sinh a(L-x)$$

$$+N\sinh aCD\sinh a(L+x)\}$$

$$+\frac{v}{a^2}-\frac{v}{a^2}\operatorname{cosech} 2aL\{\cosh aAB\sinh a(L-x)$$

$$+\cosh aCD\sinh a(L+x)\},$$

$$M_{CD}=(1)+(3)+(5)+(8)$$

$$=\frac{w}{a^2}(1-\operatorname{sech} a\mathrm{L}\cosh ax)$$

$$+\frac{1}{a}\operatorname{cosech} 2a\mathrm{L}(\mathrm{K}\sinh a\mathrm{AB}+\mathrm{N}\sinh a\mathrm{AC})\sinh a(\mathrm{L}-x)$$

$$+\frac{v}{a^2}\operatorname{cosech} 2a\mathrm{L}\,(\cosh a\mathrm{AC}-\cosh a\mathrm{AB})\sinh a(\mathrm{L}-x).$$

To consider the case where the curvature over BC is constant we may find values of K and N which make the coefficients of sinh x and cosh x in M_{BC} each equal to zero. This gives

$$\mathrm{K}=\frac{w}{a}\operatorname{cosech} a\mathrm{AB}+\frac{v}{a}\coth a\mathrm{AB}$$

and

$$\mathrm{N}=\frac{w}{a}\operatorname{cosech} a\mathrm{CD}+\frac{v}{a}\coth a\mathrm{CD}.$$

The value of M_{BC} will then be $\frac{w+v}{a^2}$.

We thus have possible conditions of equilibrium for a load supported on a stretched wire by means of, say, a circular pulley. The forces exerted by the pulley on the wire will be (*a*) a vertical load of v per unit length, and (*b*) concentrated loads at the points where the pulley leaves the wire of magnitudes given above. The loads being all vertical, the pulley must be supposed to be prevented from running down to the middle point of the wire by friction of its rim on the wire, the necessary moment being supplied at the axle by forces internal to the pulley-load system. Under these circumstances the maximum Bending Moment is that over BC, namely $\frac{w+v}{a^2}$, since that due to w may be neglected in ordinary cases, and in AB, that due to the load is proportional to sinh $a(\mathrm{L}+x)$ or increases from A to B, while in CD the Bending Moment due to the load increases from D to C. The maximum Bending Moment may thus be effectively reduced as compared with that produced by a concentrated load.

If the values of y are now found by substituting these values of M in the equations for M_{AB} etc., it is naturally

found that the equation for BC indicates an arc of a parabola. For small deflexions the circle and the parabola are equivalent.

Constant Curvature in a Wire under Tension.

In the preceding article it has been found that at the points separating a portion of a stretched wire where constant curvature exists from portions where the curvature is variable, definite concentrated forces act on the wire. This may be shown to be the case generally, both for small deflexions as hitherto considered and also by the more exact method suitable for large deflexions.

Fig. 5.

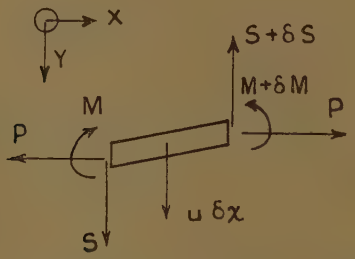

Consider an element of a wire under a tension P and a total vertical load u per unit length. The shearing forces are S and S+δS, and the Bending Moments M and M+δM, in directions acting on the element as shown. Then

$$u=\frac{dS}{dx} \quad S=-\frac{dM}{dx}-P\frac{dy}{dx},$$

$$u=-\frac{d^2M}{dx^2}-P\frac{d^2y}{dx^2},$$

$$u=-\frac{d^2M}{dx^2}+\frac{P}{R},$$

where R is the radius of curvature.

The last equation may also be written

$$\frac{d^2M}{dx^2}=a^2M-u,$$

in which form it has already been met with ($a^2=P/EI$).

If M is constant over a certain portion then $u = \frac{P}{R}$ and $S = -P\frac{dy}{dx}$. Thus over this portion u is constant and the value of S depends only on P and the inclination.

Just beyond the portion where M is constant, in the direction of x increasing,

$$S = -\frac{dM}{dx} - P\frac{dy}{dx}.$$

The value of $\frac{dy}{dx}$ is the same for both portions at the point dividing them, hence the difference between the two values of S or $-\frac{dM}{dx}$ for the variable curvature section is the value of the force which must act downwards on the wire at the point of junction. This explains why, in the case considered in the preceding article, if BC is circular, the downward force at B is $\frac{dM_{AB}}{dx}$, taken at B, and that at C is $-\frac{dM_{CD}}{dx}$, taken at C.

Constant Curvature. More Exact Method for Large Deflexions.

Fig. 6.

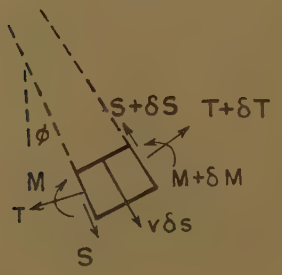

Considering an element of the wire bounded by two planes cutting the wire normally and passing through

the centre of curvature, denoting by T, M, and S the tension, bending moment, and normal shearing force respectively at one end as shown, and by $T+\delta T$, $M+\delta M$, and $S+\delta S$ the corresponding quantities at the other end, the length of the element being δs and v the radial pressure per unit length, we have, neglecting the weight of the wire,

$$T.\delta\phi+\delta S=v.\delta s, \quad \delta T=S.\delta\phi, \quad S.\delta s=-\delta M,$$

or

$$\frac{T}{\rho}+\frac{dS}{ds}=v, \qquad S=\frac{dT}{d\phi}, \qquad S=-\frac{dM}{ds}.$$

(ρ=radius of curvature.)

Hence, if the curvature is constant over a particular portion of the wire and therefore M is also constant there, we must have $S=0$ over that length, T=constant, and $\frac{T}{\rho_c}=v$ where ρ_c is the (constant) radius of curvature of this length. On passing beyond the end of the constant-curvature portion we find that S is not zero, and the difference will represent a concentrated load of magnitude $-\frac{dM}{ds}$, normal to the wire at the junction of the two portions.

This concentrated pressure may be compared with the expression $-\frac{dM}{dx}$ already obtained for small deflexions.

Load divided into a Number of Equal Parts.

Let three loads, each W, separated by a distance d be carried on a stretched wire of length 2L, whose ends are pivoted at the same level. The centre weight of the three is supposed to be at the middle point of the wire. The weight of the wire itself is neglected.

The Bending Moment over the space between the two weights on the left is represented by ;

$$\frac{W}{a}\operatorname{cosech} 2aL\{\sinh a(L-d)\sinh a(L-x)$$
$$+\sinh aL\sinh a(L+x)+\sinh a(L-d)\sinh a(L+x)\}$$

$$= \frac{W}{a} \operatorname{cosech} 2aL\{2 \sinh a(L-d) \sinh aL \cosh ax + \sinh aL \sinh a(L+x)\}$$

$$= \frac{W}{2a} \operatorname{sech} aL\{2 \sinh a(L-d) \cosh ax + \sinh a(L+x)\}.$$

At the middle point of the wire the B.M. is

$$\frac{W}{2a} \operatorname{sech} aL\{2 \sinh a(L-d) + \sinh aL\},$$

or

$$\frac{W}{2a}\{2 \tanh aL \cosh ad - 2 \sinh ad + \tanh aL\},$$

which, if aL is large and d not nearly equal to L, is practically

$$\frac{W}{2a}(2 \cosh ad - 2 \sinh ad + 1) \quad \text{or} \quad \frac{W}{2a}(2e^{-ad} + 1).$$

If ad is more than a few units this is practically $\frac{W}{2a}$, or the other loads have practically no effect at the centre. The Bending Moment at the centre, which is the greatest in the wire, is thus only about one-third of what it would be if the three loads were concentrated.

Similarly, if the total load is divided into n equal fractions separated by a suitable distance d, the maximum Bending Moment in the wire is only about $1/n$th of its value if the load were concentrated.

Tensile Stress.

The Bending Moment having been found in various cases as shown above, the maximum tensile stress caused in the wire by this Bending Moment may be calculated, and to this must be added the average tensile stress due to the tension in the wire. In this way the greatest tensile stress which can occur being found it will be seen whether the wire is capable of resisting it, remembering that a given fibre may sometimes tend to compression and sometimes to extension due to moving loads, thus the effect in tending to produce fatigue is increased. It will be found that in some cases, increasing the tension in the wire decreases the maximum tensile stress, at least up to a certain value.

CV. *The Frequency of Transverse Vibration of a Loaded Fixed-Free Bar.*—IV. *The Effect of Shearing of the Bar.*

By R. M. Davies, *M.Sc., F.Inst.P., Lecturer in Physics, University College of Wales, Aberystwyth* *.

Notation.

ρ=Density of the bar.
E=Young's Modulus of the material of the bar.
G=Rigidity Modulus of the material of the bar.
l=Length of the bar.
k=Radius of gyration of the cross-section of the bar about an axis through the centre of gravity, perpendicular to the plane of motion.
$\beta=k/l$.
A=Area of cross-section of the bar.
$M'=\rho Al$=Mass of the bar.
M=Mass of the load fixed to the free end of the bar.
$c=M/M'$.
κ=Radius of gyration of the load about an axis through the point of attachment of the load to the bar and perpendicular to the plane of motion.
$I=M\kappa^2$=Moment of inertia of the load about this axis.
$d=I/M'l^2=c\kappa^2/l^2$.
n=Natural frequency of vibration of the bar when vibrating in its fundamental mode.
$\omega=2\pi n$=Natural pulsatance of the bar for this mode.
m=Frequency parameter, defined by the equation $m^4=\rho\omega^2/Ek^2$.
$z=ml$; $\alpha=z^4=\rho\omega^2l^4/Ek^2$.

THE present paper is a continuation of the work described in three previous papers [1], [2], [3] on the frequency of transverse vibration of loaded fixed-free bars. The aim of these papers has been to evaluate the parameter z (defined above) in terms of the dimensions and masses of the bar and of its load. In the first paper [1] (hereafter quoted as D.1) the load was treated as a point mass and the rotatory inertia of the load was neglected. In the second paper [2] (hereafter quoted as D.2) the rotatory inertia of the load was taken into

* Communicated by Vice-Principal Gwilym Owen, M.A., D.Sc.

account whilst that of the bar was neglected. In the third paper [3] (hereafter quoted as D.3) the rotatory inertia of both bar and load were taken into account. The general procedure in each case has been to find a solution of the differential equation of motion of the bar which satisfies the boundary conditions at the free and fixed ends of the bar; the form of this solution is an implicit transcendental equation involving z and the dimensions and masses of the bar and the load. By a method of expansion in series this equation can be transformed into an algebraic relation giving z explicitly in terms of the dimensions and masses of the bar and the load. This algebraic relation is approximate in that terms involving z^{12} and higher powers of z are neglected; the error in z committed by neglecting these terms is only of the order of 1 in 10,000, and an error of this order of magnitude is unlikely to be important in any practical application of the result. For example, in the dynamical method developed in this laboratory for the determination of Young's Modulus [1], [5] the experimental error is such that it is sufficient to be able to calculate z to an accuracy of 1 in 2000.

The object of the present paper is to extend the results given in the previous, papers so as to include the effect of the shearing of the elements of the vibrating bar. The importance of this effect was first shown by Timoshenko [6], [7], who deduced the differential equation of motion of the bar when shear is permitted; he also showed that in the simplest case—that of a bar with hinged ends—the correction for shear in the frequency equation is about four times that due to the rotatory inertia of the bar. The case of an unloaded bar free at both ends has been investigated by Goens [8], but the case of a fixed-free bar, whether loaded or unloaded, does not appear in the literature.

Let the axis of the bar (assumed straight when in equilibrium) be taken as the axis of x, and let the direction of the displacement of the bar be taken as the axis of y. It will be assumed that the bar is uniform and that the displacements are small. In fig. 1 let ABCD represent the equilibrium position of an element of the bar bounded by two planes abscissæ x and $x+dx$ perpendicular to the x-axis. If the effect of shear forces is neglected the motion of this element consists of a linear displacement

y of its centre of gravity and a rotation of the faces of the element through an angle $\partial y/\partial x$; the shape of the element remains unaltered during the displacement. This corresponds to the case treated in D.3, whilst in the cases treated in D.1 and D.2 the thickness of the bar is supposed to be so small that the effect of the rotation of the element is negligible. If, however, shear forces are operative, a distortion of the element by these forces occurs in addition to the linear displacement and rotation of the element. Thus the total slope of the axis of the bar in its displaced position ($\partial y/\partial x$) is the sum of the angle ψ through which the element is rotated and the

Fig. 1.

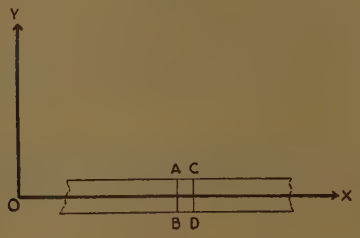

angle α through which the element is sheared at its axis. Hence

$$\frac{\partial y}{\partial x} = \alpha + \psi. \quad . \quad . \quad . \quad . \quad . \quad . \quad (1)$$

If the shear stress were uniform over the cross-section the angle of shear would be constant at all points on the cross-section and the angle of shear of the element would be F/AG, where F is the resultant shearing force, A the cross-sectional area, and G the rigidity modulus. Actually the shearing force is not uniform over a cross-section, and its distribution depends on the shape of the cross-section (*v.* Prescott [9], § 53, and Southwell [10], § 226); in the case of a bar of rectangular section, for example, the distribution of shearing stress over the cross-section is parabolic, the stress being a maximum at the axis. It follows that the angle of shear will also vary from point to point over the cross-section. It is, however,

possible to show that the angle of shear α at the axis of the element is proportional to F/AG, and thus

$$\alpha = RF/AG \quad \text{and} \quad F = AG\alpha/R, \quad . \quad . \quad . \quad (2)$$

where R is a constant of proportionality depending on the shape of the cross-section. (In Timoshenko's work R is denoted by $1/\lambda$.) According to Föppl [11] and Goens [8] the value of R is 6/5 for a rectangular cross-section and 10/9 for a circular cross-section.

The sign convention used in the present work, as well as in D.1, D.2, and D.3, is that given in Prescott [9], ch. ix., *i. e.*, the Ox and Oy axes are taken as shown in fig. 1; the shearing force F is positive when the portion of the bar to the left of an element ABCD exerts a downward force on the face AB, whilst the bending moment M_b is positive when the portion of the bar to the left of ABCD exerts a clockwise couple across the face AB. With this sign convention and in our present notation equations (4), (5), and (6) of Timoshenko's paper [6] become

$$M_b = EAk^2 \frac{\partial \psi}{\partial x}; \quad F = AG\alpha/R = \frac{AG}{R}\left(\frac{\partial y}{\partial x} - \psi\right), \quad . \quad (3)$$

$$F + \frac{\partial M_b}{\partial x} = \rho A k^2 \frac{\partial^2 \psi}{\partial t^2} \quad \text{or} \quad F = Ak^2\left[\rho \frac{\partial^2 \psi}{\partial t^2} - E \frac{\partial^2 \psi}{\partial x^2}\right], \quad (4)$$

$$\rho \frac{\partial^2 y}{\partial t^2} = \frac{G}{R}\left(\frac{\partial^2 y}{\partial x^2} - \frac{\partial \psi}{\partial x}\right). \quad . \quad . \quad . \quad . \quad (5)$$

Equation (4) is deduced from the equation of rotational motion of an element, whilst equation (5) follows from a consideration of the translational motion of an element. If the effect of shear is negligible equation (4) reduces to equation (9) of D.3.

Eliminating ψ from equations (4) and (5) the differential equation connecting y with x and t is

$$\frac{Ek^2}{\rho}\frac{\partial^4 y}{\partial x^4} + \frac{\partial^2 y}{\partial t^2} - k^2\left(1 + \frac{RE}{G}\right)\frac{\partial^2 y}{\partial x^2 \partial t^2} + \rho \frac{k^2 R}{G}\frac{\partial^4 y}{\partial t^4} = 0 \quad (6)$$

(*v.* Timoshenko [6], equation (8)).

If we write $\epsilon = RE/G$ this equation becomes

$$\frac{Ek^2}{\rho}\frac{\partial^4 y}{\partial x^4} + \frac{\partial^2 y}{\partial t^2} - k^2(1+\epsilon)\frac{\partial^4 y}{\partial x^2 \partial t^2} + \rho \frac{k^2 \epsilon}{E}\frac{\partial^4 y}{\partial t^4} = 0. \quad (7)$$

In this equation the effect of shear is represented by the terms involving ϵ, and if ϵ is zero equation (7) reduces to the well-known equation of motion, which includes the effect of the rotatory inertia of the bar (equation (3) of D.3).

It is clear that the numerical value of ϵ depends on the material of the bar and on the shape of its cross-section. As to the value of the ratio E/G, Goens [8] gives 2·1 and 3·5 as the extreme values for isotropic materials; these values correspond to values of Poisson's ratio of 0·05 and 0·75 respectively. For most metals the value of the ratio is about 2·6, corresponding to a value of 0·3 for Poisson's ratio. Assuming the value of E/G to be 2·6, the value of ϵ is found to be 3·12 for a bar of rectangular cross-section and 2·89 for a bar of circular cross-section. For the purpose of rough calculation the value of ϵ may thus be taken as 3.

To solve equation (7) let it be assumed that for a simple harmonic vibration of pulsatance ω, y is of the form $y=ue^{i\omega t}$, where $i=\sqrt{-1}$ and where the normal or characteristic function u is a function of x only.

Substituting this expression for y in equation (7) the following differential equation for u is obtained :—

$$\frac{\partial^4 u}{\partial x^4}+m^4k^2(1+\epsilon)\frac{\partial^2 u}{\partial x^2}-m^4(1-\epsilon m^4k^4)u=0, \quad . \quad (8)$$

where $m^4=\rho\omega^2/Ek^2$.

The particular integrals of this equation are of the form $u=e^{\lambda mx}$; substituting in equation (8), we obtain the following equation for λ :—

$$\lambda^4+\lambda^2m^2k^2(1+\epsilon)-(1-m^4k^4\epsilon)=0. \quad . \quad . \quad (9)$$

Thus

$$\lambda^2=-\frac{m^2k^2}{2}(1+\epsilon)\pm\sqrt{1+\frac{m^4k^4}{4}(1-\epsilon)^2}$$
$$=-\tfrac{1}{2}\beta^2z^2(1+\epsilon)\pm\sqrt{1+\tfrac{1}{4}\beta^4z^4(1-\epsilon)^2},$$

where $\beta=k/l$ and $z=ml$.

The permissible values of λ may therefore be written $\pm\gamma$ and $\pm i\delta$, where

$$\left.\begin{matrix}\delta\\ \gamma\end{matrix}\right\}=+\{\sqrt{1+\tfrac{1}{4}\beta^4z^4(1-\epsilon)^2}\pm\tfrac{1}{2}\beta^2z^2(1+\epsilon)\}^{\frac{1}{2}}. \quad . \quad (10)$$

The general solution of equation (8) is thus

$$u = Ce^{\lambda mx} + De^{-\lambda mx} + C'e^{i\delta mx} + D'e^{-i\delta mx},$$

or, in terms of hyperbolic and trigonometrical functions,

$$u = P \cosh \gamma mx + P' \sinh \gamma mx + Q \cos \delta mx + Q' \sin \delta mx, \quad . \quad . \quad . \quad (11)$$

where C, C' . . . Q, Q' are integration constants to be determined from the boundary conditions.

It is seen that equation (11) is of the same form as equation (6) of D.3 ; when the effect of shear is neglected (*i. e.*, when $\epsilon = 0$) the values of γ and δ given in equation (10) reduce to the values of equation (5) of D.3.

The frequency equation is determined by eliminating the integration constants P, P', Q, Q' of equation (11) ; this is done by introducing the boundary conditions at the free and fixed ends. Let the origin be taken at the fixed end of the bar.

Taking first the conditions at the fixed end of the bar ($x = 0$), consider the element of the bar adjacent to the clamp ; this element will undergo no linear or rotational displacement, although there is nothing to prevent it from being sheared. It follows that, although α and $\partial y/\partial x$ will differ from zero, y (or u) and ψ will be permanently zero at this end.

The condition that $u = 0$ at $x = 0$ for all values of t gives

$$P + Q = 0. \quad . \quad . \quad . \quad . \quad . \quad . \quad . \quad . \quad (12)$$

The angle ψ is of the form $\psi = \phi e^{i\omega t}$, where the function ϕ is a function of x only. ϕ or ψ can be evaluated from equation (5), which can be written

$$\frac{\partial \psi}{\partial x} = \frac{\partial^2 y}{\partial x^2} - \frac{\epsilon \rho}{E} \frac{\partial^2 y}{\partial t^2},$$

or, in terms of u and ϕ,

$$\frac{\partial \phi}{\partial x} = \frac{\partial^2 u}{\partial x^2} + \epsilon k^2 m^4 u. \quad . \quad . \quad . \quad . \quad . \quad . \quad (13)$$

Using the values of u and $\partial^2 u/\partial x^2$ given by equation (11), and integrating, it is found that

$$\phi = \frac{mC}{\gamma}(P \sinh \gamma mx + P' \cosh \gamma mx) - \frac{mD}{\delta}(Q \sin \delta mx - Q' \cos \delta mx), \quad . \quad (14)$$

where

$$C = \gamma^2+\epsilon\beta^2z^2 = \delta^2-\beta^2z^2;\ D = \delta^2-\epsilon\beta^2z^2 = \gamma^2+\beta^2z^2;\ CD=1. \quad . \quad . \quad (15)$$

The condition that $\psi=\phi=0$ at $x=0$ for all values of t thus gives

$$Q' = -(\delta CP')/(\gamma D). \quad . \quad . \quad . \quad . \quad . \quad (16)$$

It follows that the normal functions u and ϕ are given by the equations

$$\left.\begin{aligned} u &= P(\cosh\gamma mx-\cos\delta mx)+P'\left(\sinh\gamma mx-\frac{\delta C}{\gamma D}\sin\delta mx\right),\\ \phi &= mP\left(\frac{C}{\gamma}\sinh\gamma mx+\frac{D}{\delta}\sin\delta mx\right)\\ &\qquad +\frac{mP'C}{\gamma}(\cosh\gamma mx-\cos\delta mx). \end{aligned}\right\} \quad . \quad . \quad . \quad (17)$$

Consider next the boundary conditions at the free end of the bar ($x=l$).

(i.) The product of the mass M of the load into its linear acceleration is equal to the reversed shearing force, *i. e.*,

$$M\frac{\partial^2y}{\partial t^2} = -F = -\frac{AG}{R}\left(\frac{\partial y}{\partial x}-\psi\right), \quad . \quad . \quad . \quad (18)$$

using the value of the shearing force F given in equation (2), or, using equation (4), we obtain

$$M\frac{\partial^2y}{\partial t^2} = -F = -Ak^2\left[\rho\frac{\partial^2\psi}{\partial t^2}-E\frac{\partial^2\psi}{\partial x^2}\right]. \quad . \quad (19)$$

In terms of u and ϕ equation (18) becomes

$$cu = \left(\frac{\partial u}{\partial x}-\phi\right)\Big/(\epsilon lk^2m^4), \quad . \quad . \quad . \quad . \quad (20)$$

whilst equation (19) similarly becomes

$$\frac{\partial^2\phi}{\partial x^2} = -m^4(k^2\phi+clu). \quad . \quad . \quad . \quad . \quad (21)$$

If the effect of shear is negligible (*i. e.*, if $\epsilon=0$) ϕ is equal to $\partial u/\partial x$, and equation (21) reduces to equation (10) of D.3.

(ii.) The second condition which is satisfied at $x=l$ is that the product of the moment of inertia I of the load into its rotational acceleration $\partial^2\psi/\partial t^2$ is equal to the reversed bending moment. Using the expression given in equation (3) for the bending moment M_b, we find that

$$-M_b=-EAk^2\frac{\partial\psi}{\partial x}=I\frac{\partial^2\psi}{\partial t^2}. \quad . \quad . \quad . \quad (22)$$

In terms of ϕ and d this equation becomes

$$\frac{\partial\phi}{\partial x}=z^4d\phi/l, \quad . \quad . \quad . \quad . \quad . \quad . \quad (23)$$

which reduces to equation (11) of D.3 when $\epsilon=0$.

Using equation (20) and the values of u, $\partial u/\partial x$, and ϕ from equation (17), it is found that

$$P\left[\left(\frac{1}{\gamma}\sinh\gamma ml-\frac{1}{\delta}\sin\delta ml\right)+cz(\cosh\gamma ml-\cos\delta ml)\right]$$
$$=-\frac{P'}{\gamma}[(\cosh\gamma ml+C^2\cos\delta ml)$$
$$+cz(\gamma\sinh\gamma ml-\delta C^2\sin\gamma ml)]. \quad . \quad (24)$$

Similarly from equation (23) we obtain

$$P\left[(\cosh\gamma ml+D^2\cos\delta ml)-dz^3\left(\frac{1}{\gamma}\sinh\gamma ml+\frac{D^2}{\delta}\sin\delta ml\right)\right]$$
$$=-\frac{P'}{\gamma}[(\gamma\sinh\gamma ml+\delta\sin\delta ml)$$
$$-dz^3(\cosh\gamma ml-\cos\delta ml)]. \quad . \quad (25)$$

When shear is neglected, $\epsilon=0$, $C=\gamma^2$, $D=\delta^2$, and $CD=\gamma^2\delta^2=1$; equations (24) and (25) then reduce to equations (12) and (13) of D.3.

Eliminating P and P′ from equations (24) and (25) by cross multiplication, we obtain

$$1+\tfrac{1}{2}(C^2+D^2)\cosh\gamma z\cos\delta z+\left(\frac{\gamma^2-\delta^2}{2\gamma\delta}\right)\sinh\gamma z\sin\delta z$$
$$=\tfrac{1}{2}cz(C+D)(\delta C\cosh\gamma z\sin\delta z-\gamma D\sinh\gamma z\cos\delta z)$$
$$+\frac{dz^3}{2}(C+D)\left(\frac{D}{\delta}\cosh\gamma z\sin\delta z+\frac{C}{\gamma}\sinh\gamma z\cos\delta z\right)$$

$$-cdz^4\left\{1-\cosh\gamma z\cos\delta z + \tfrac{1}{2}\left(\frac{\delta C^2}{\gamma}-\frac{\gamma D^2}{\delta}\right)\sinh\gamma z\sin\delta z\right\}. \quad (26)$$

It will be convenient to denote the left-hand side of this equation by X, the cz term on the right-hand side by Y, the dz^3 term on the right-hand side by Z, and the cdz^4 term on the right-hand side by Z′. These terms will next be simplified, using the values of the powers of C, D, γ, and δ derived from the definitions of these quantities; the products of the trigonometrical and hyperbolic functions will then be expanded in series, and finally X, Y, Z, and Z′ will be expressed as terms involving z^0, z^4, and z^8. As in the cases treated in D.1, D.2, and D.3, sufficient accuracy for all practical purposes is obtained by considering these terms and rejecting higher powers of z.

Considering first the value of X, it follows from the definitions of γ, δ, C, and D, that

$$C^2+D^2=2+\beta^4z^4(1-\epsilon)^2\,;\quad \gamma^2-\delta^2=-\beta^2z^2(1+\epsilon).$$

Thus

$$X=1+\left[1+\frac{\beta^4z^4}{2}(1-\epsilon)^2\right]\cosh\gamma z\cos\delta z - \frac{\beta^2z^2(1+\epsilon)}{2\gamma\delta}\sinh\gamma z\sin\delta z. \quad (27)$$

Expanding the products of the trigonometrical and hyperbolic functions in series, it is found that

$$\cosh\gamma z\cos\delta z=1+\frac{z^2}{2}(\gamma^2-\delta^2)+\frac{z^4}{24}(\gamma^4+\delta^4-6\gamma^2\delta^2) + \frac{z^6}{760}[\gamma^6-\delta^6-15\gamma^2\delta^2(\gamma^2-\delta^2)] + \frac{z^8}{40320}[\gamma^8+\delta^8-28\gamma^2\delta^2(\gamma^4+\delta^4)+70\gamma^4\delta^4]$$

$$\sinh\gamma z\sin\delta z=\gamma\delta z^2\left\{1+\frac{z^2}{6}(\gamma^2-\delta^2) + \frac{z^4}{120}(\gamma^4+\delta^4-\frac{10}{3}\gamma^2\delta^2)\right\}. \quad (28)$$

The various functions of γ and δ are given by the following equations if terms involving z^{12} and higher powers in the final result are neglected :—

$$\gamma^2\delta^2=1-\epsilon\beta^4z^4\,;\ \gamma^4+\delta^4=2+\beta^4z^4(1+\epsilon^2)\,;$$

$$\gamma^6-\delta^6=-3\beta^2z^2(1+\epsilon)\,;\ \gamma^8+\delta^8=2. \quad . \quad . \quad . \quad (29)$$

Finally, X reduces to the form

$$X=\frac{A_0z^8}{2520}-\frac{B_0z^4}{6}+2, \quad . \quad . \quad . \quad . \quad (30)$$

where

$$A_0=1+56\beta^2(1+\epsilon)+105\beta^4(1+14\epsilon+\epsilon^2)$$
$$-630\beta^6(1-\epsilon^2)(1+\epsilon),$$
$$B_0=1+6\beta^2(1+\epsilon)-3\beta^4(1-\epsilon)^2. \quad . \quad . \quad . \quad . \quad . \quad . \quad . \quad (31)$$

It should be noted that if X is equated to zero the frequency equation for an *unloaded* bar is obtained; in this case the coefficients A_0 and B_0 given in the above equation reduce to the values given in D.3 equation (20) if the effect of shear is negligibly small.

Considering next the term Y on the right-hand side of equation (26), this becomes

$$Y=\tfrac{1}{2}cz(\gamma^2+\delta^2)\gamma^2\delta^2\left(\frac{1}{\delta}\cosh\gamma z\sin\delta z-\frac{1}{\gamma}\sinh\gamma z\cos\delta z\right)$$
$$+\tfrac{1}{2}\epsilon cz^3\beta^2(\gamma^2+\delta^2)(\delta\cosh\gamma z\sin\delta z+\gamma\sinh\gamma z\cos\delta z.$$
$$. \quad . \quad . \quad (32)$$

Now

$$\cosh\gamma z\sin\delta z=\delta z\left\{1+\frac{z^2}{6}(3\gamma^2-\delta^2)+\frac{z^4}{120}(5\gamma^4-10\gamma^2\delta^2+\delta^4)\right.$$
$$\left.+\frac{z^6}{5040}(7\gamma^6-35\gamma^4\delta^2+21\gamma^2\delta^4-\delta^6)\right\},$$

$$\sinh\gamma z\cos\delta z=\gamma z\left\{1+\frac{z^2}{6}(\gamma^2-3\delta^2)+\frac{z^4}{120}(\gamma^4-10\gamma^2\delta^2+5\delta^4)\right.$$
$$\left.+\frac{z^6}{5040}(\gamma^6-21\gamma^4\delta^2+35\gamma^2\delta^4-7\delta^6)\right\}.$$
$$. \quad . \quad . \quad (33)$$

Hence

$$Y=\frac{cz^4}{6}[4(1+3\epsilon\beta^2)]$$
$$-\frac{cz^8}{2520}[8+168\beta^2(1+2\epsilon)-420\beta^4(1-8\epsilon-\epsilon^2)$$
$$-1260\beta^6\epsilon(1-\epsilon)^2]. \quad . \quad . \quad (34)$$

Taking next the term Z on the right-hand side of equation (26), we find that

$$Z=\tfrac{1}{2}dz^3(\gamma^2+\delta^2)(\delta\cosh\gamma z\sin\delta z+\gamma\sinh\gamma z\cos\delta z)$$
$$-\frac{\epsilon dz^5\beta^2}{2}(\gamma^2+\delta^2)\left(\frac{1}{\delta}\cosh\gamma z\sin\delta z-\frac{1}{\gamma}\sinh\gamma z\cos\delta z\right).$$
$$. \quad . \quad . \quad (35)$$

Using the expressions given in equation (33), this reduces to

$$Z_1=\frac{dz^4}{6}.12-\frac{dz^8}{2520}[168+840\beta^2(1+3\epsilon)-1260\beta^4(1-\epsilon)^2].$$
$$. \quad . \quad . \quad (36)$$

Taking finally the term Z′ on the right-hand side of equation (26), it is found that

$$\frac{\delta^2C^2-\gamma^2D^2}{\gamma\delta}=-\beta^2z^2(1-3\epsilon),$$

and thus

$$Z'=cdz^4[\cosh\gamma z\cos\delta z-1+\tfrac{1}{2}\beta^2z^2(1-3\epsilon)\sinh\gamma z\sin\delta z].$$
$$. \quad . \quad . \quad (37)$$

Using the expansions given in equation (28) we obtain

$$Z'=-\frac{cdz^8}{2520}(420+5040\beta^2\epsilon). \quad . \quad . \quad . \quad (38)$$

Collecting terms, it is found that equation (26) can be written in the form

$$\frac{\alpha^2A}{2520}-\frac{\alpha B}{6}+2=0, \quad . \quad . \quad . \quad . \quad . \quad (39)$$

where $\alpha=z^4$ and

$$\left.\begin{aligned}A=1&+8c+168d+420cd\\&+56\beta^2[(1+\epsilon)+3c(1+2\epsilon)+15d(1+3\epsilon)+90\epsilon cd]\\&+105\beta^4[(1+14\epsilon+\epsilon^2)-4c(1-8\epsilon-\epsilon^2)-12d(1-\epsilon^2)]\\&-630\beta^6[(1-\epsilon^2)(1+\epsilon)+2c\epsilon(1-\epsilon)^2]\end{aligned}\right\}$$
$$. \quad (40)$$

$$B=1+4c+12d+6\beta^2[(1+\epsilon)+2\epsilon c]-3\beta^4(1-\epsilon)^2.$$

If the effect of shear is negligibly small equations (39) and (40) reduce to equations (17) and (18) of D.3.

As in the cases examined in D.1, D.2, and D.3, the larger root of equation (39), regarded as a quadratic equation in α, corresponds to the first overtone, whilst the smaller root corresponds to the fundamental mode of vibration. In the case of the first overtone the value of z^4 is comparatively large, and will not be given to any high degree of accuracy by the present method. On the other hand, the error in z^4 for the fundamental is unlikely to exceed 0·1 per cent. for cases which are likely to occur in practice, and considering only the fundamental it is found that

$$\alpha=z^4=\frac{210}{A}[B-\sqrt{B^2-4A/35}]. \quad . \quad . \quad . \quad (41)$$

Equation (41), together with equation (40), gives the value of z^4 in terms of c, d, β, and ϵ.

In discussing these results it will be convenient to consider first the case of an *unloaded bar*. In this case A and B reduce to the values A_0 and B_0 already given in equation (31). In many practical cases the value of β is sufficiently small to allow terms involving β^4 and β^6 to be neglected; under these conditions

$$A_0=1+56\beta^2(1+\epsilon)\,;\ B_0=1+6\beta^2(1+\epsilon).$$

These values of A_0 and B_0 give

$$\alpha=z^4=12{\cdot}364\{1-4{\cdot}624\beta^2(1+\epsilon)\}, \quad . \quad . \quad (42)$$

which reduces to equation (21) of D.3 when ϵ vanishes.

It is clear from equation (42) that the effect of shear in this case is to multiply the correction term for the rotatory inertia of the bar by the factor $(1+\epsilon)$; since ϵ is approximately 3 the correction for shear is about four times as large as the correction for rotatory inertia. It is interesting to compare this result with the results obtained by Timoshenko [6], [7] and by Goens [8] for small values of ϵ and for vibration in the fundamental mode. In the case of a bar with hinged ends investigated by Timoshenko the effect of shear is given by multiplying the correction term for rotatory inertia by the same factor $(1+\epsilon)$, whilst in the case of a free-free bar investigated by Goens the multiplying factor is $(1+0{\cdot}2485\epsilon)$.

The variation of z with β is shown graphically in fig. 2, in which z is plotted as ordinate and β as abscissa. In

this diagram, curve A shows the variation of z with β when the effect of shear is neglected; curve B shows the variation of z with β when the effect of shear is taken into account, the value of ϵ being assumed to be 3. For small values of β the value of z derived from the approximate equation (42) gives excellent agreement with the

Fig. 2.

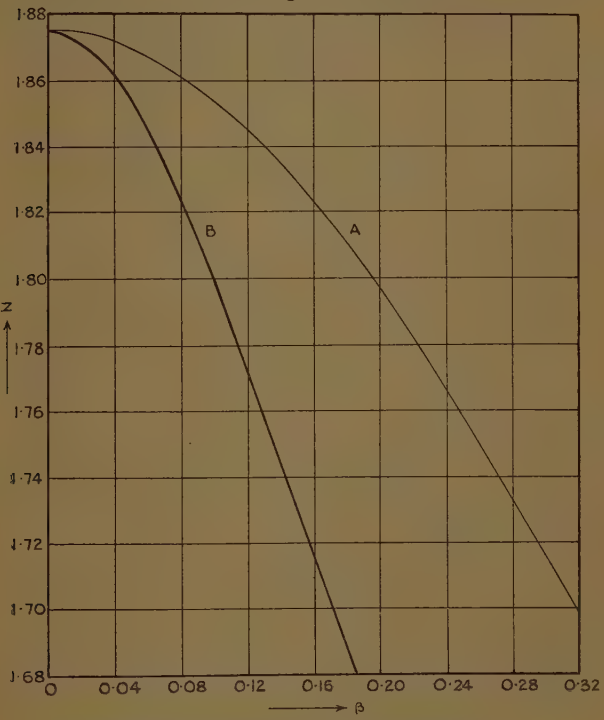

The relation between z and β for unloaded bars.

Curve [A] :—$\epsilon = 0$.

Curve [B] :—$\epsilon = 3$.

more accurate values deduced from equations (31) and (41); calculation shows that the difference between the approximate and accurate values of z amounts to about 0·1 per cent. when β becomes 0·05. It should be noted that $\beta = 0{\cdot}05$ corresponds to a bar whose thickness

is 0·1732 times its length when the cross-section of the bar is rectangular, and to a bar whose radius is 0·1 times its length when the bar is of circular cross-section.

The discussion of the case of a *loaded* bar is greatly simplified by finding the effect of d, β, and $\epsilon\beta^2$ on the value of z; in this connexion, it should be noted that the value of z is determined mainly by the value of c and that, in most practical cases (*cf.* D.2 and D.3), the effects of d, β, and $\epsilon\beta^2$ may be regarded as small correction terms. Let A′ and B′ be the values of A and B when $d=\beta=\epsilon=0$. Thus

$$A'=1+8c\ ;\ B'=1+4c.$$

Let z' be the value of z obtained from equation (41) when $A=A'$ and $B=B'$; z' is thus the value of z corresponding to a point-load, the effects of rotation and shear of the bar being neglected.

$$\text{Let}\quad z'^4=f(A', B')=\frac{210}{A'}\left[B'-\sqrt{B'^2-\frac{4A'}{35}}\right]. \quad (43)$$

If d, β, and ϵ are not zero we may write that A and B of equation (40) are of the form

$$A=A'+a\ ;\ B=B'+b. \quad . \quad . \quad . \quad . \quad (44)$$

In most practical cases terms in β^4 and β^6 may be neglected, and thus

$$\left.\begin{aligned} a&=168d(1+2{\cdot}5c)+56\beta^2(1+3c+15d)\\ &\quad +56\epsilon\beta^2(1+6c+45d+90cd),\\ b&=12d+6\beta^2+6\epsilon\beta^2(1+2c). \end{aligned}\right\} \quad . \quad . \quad (45)$$

Equation (41) may be written

$$f(A, B)=z^4=\frac{210}{A}[B-\sqrt{B^2-4A/35}], \quad . \quad (46)$$

and, if $D=z^4-z'^4=f(A, B)-f(A', B')$, then, by Taylor's Theorem,

$$D=a\frac{\partial f}{\partial A'}+b\frac{\partial f}{\partial B'}, \quad . \quad . \quad . \quad . \quad . \quad (47)$$

since $a^2\dfrac{\partial^2 f}{\partial A'^2}$ and $b^2\dfrac{\partial^2 f}{\partial B'^2}$ are small in most practical cases.

Differentiating equation (43), it is found that

$$\frac{\partial f}{\partial A'}=-\frac{210}{A'^2}\left[B'-\left(B'^2-\frac{2A'}{35}\right)\left(B'^2-\frac{4A'}{35}\right)^{-\frac{1}{2}}\right],$$

$$\frac{\partial f}{\partial B'}=\frac{210}{A'}\left[1-B'\left(B'^2-\frac{4A'}{35}\right)^{-\frac{1}{2}}\right].$$

Substituting these values of the derivatives in equation (47), it is found that

$$D=[-12a-z'^4(A'b-B'a)]/[A'.\sqrt{B'^2-4A'/35}], \quad . \quad (48)$$

which gives the correction D to be added to z'^4 in terms of d, β, and ϵ. By making $\beta=\epsilon=0$ we obtain the value of D appropriate to the case treated in D.2—that in which the effects of the rotatory inertia and shear of the bar are negligible, whilst if $\epsilon=0$ we obtain the value of D for cases in which the shear effect is negligible (D.3). The calculation of z^4 from equations (43) and (48) is much less laborious than direct calculation from equations (40) and (41). The value of D for the particular case of an unloaded bar may be obtained by putting

$$A'=B'=1\ ;\ a=56\beta^2(1+\epsilon)\ ;\ b=6\beta^2(1+\epsilon)\ ;$$

the value of z'^4 is that appropriate to an unloaded bar in which the effects of rotatory inertia and shear are negligible, *i. e.*, $z'^4=12{\cdot}364$. From equation (48) it is found that $D=-12{\cdot}364\times4{\cdot}624\beta^2(1+\epsilon)$, in agreement with equation (42).

As regards the effect of shear in the experiments of Davies and James and Davies and Thomas, we may consider the cases quoted in D.2 and D.3 for the purpose of illustration. In order to estimate the error due to neglect of shear it is necessary to make some assumption as to the numerical value of ϵ; the bars in question were nickel bars, and from the data given by Grüneisen [12] for nickel it is found that E/G is 2·618, giving $\epsilon=3{\cdot}142$ for a bar of rectangular cross-section. In the following tables D denotes the value obtained from equation (48) in the general case, *i. e.*, the value of the correction when the effects of the rotatory inertia of the load and bar and shear in the bar are taken into account; D′ denotes the value of the correction when ϵ is zero, and, finally, D″ denotes the value of the correction when $\beta=\epsilon=0$. Bar no. I. is the first case quoted in D.2 and D.3, and this corresponds to a small value of c; for this bar $c=0{\cdot}03663$, $d=1{\cdot}157\times10^{-4}$, and $\beta^2=7{\cdot}399\times10^{-5}$. Bar. no. II. is an example of a case in which c and d are comparatively large; for this bar $c=0{\cdot}1153$, $d=4{\cdot}458\times10^{-4}$, and $\beta^2=8{\cdot}175\times10^{-5}$. As pointed out in D.2 and D.3 the value of d for Bar no. II. is considerably greater than the values used in the experiments quoted; a closer approximation to practical conditions is given by bar no. III.,

for which $d=1\cdot605\times10^{-4}$, c and β^2 having values identical with those for bar no. II.

Table I. gives the values of D, D′, and D″ for bars nos. I., II., and III. when $\epsilon=3\cdot142$.

In the experimental results given in the papers of Davies and James [4], and Davies and Thomas [5], it was assumed in the calculation of z^4 that the load was a point mass and that the effects of the rotatory inertia and shear of the bar were negligibly small, *i. e.*, the value of z^4 used in the calculation of Young's Modulus from the experimental results was the value z'^4 given by equation (43) above. Since the value of Young's Modulus is inversely proportional to z^4 the error in the final results given in these papers for Young's Modulus, due to the simplifying assumptions made in the calculation of z^4, may be estimated from the figures given in the first

TABLE I.

$\epsilon=3\cdot142$.

Bar no.	z'^4.	D.	D′.	D″.
I.	10·779	−0·0226	−0·0117	−0·0085
II.	8·4355	−0·0319	−0·0230	−0·0209
III.	8·4355	−0·0185	−0·0098	−0·0076

column of Table I. In the case of bar no. I. it is seen that the error amounts to about 0·21 per cent., in the case of bar no. II. it is about 0·4 per cent., whilst in the case of bar no. III. the error is approximately 0·23 per cent.

Bar no. II. represents an extreme case and may be left out of consideration for the present purpose. Bars nos. I. and III. are, however, typical of the bars and loads actually used, and from the results given for these two bars it is clear that the final values of Young's Modulus given in these papers will be subject to an uncertainty of about 0·2 to 0·25 per cent.

It is interesting to compare the magnitudes of D−D″ and D′−D″ ; the former is the correction for the rotatory inertia of the bar together with shear, whilst the latter represents the correction for the rotatory inertia of the bar alone. In the case of bar no. I. it is found that D−D″ = −0·0141 and D′−D″ = −0·0032, whilst for bar no. III. D−D″ = −0·0110 and D′−D″ = −0·0023. These figures emphasize the importance of the shear

correction as compared with the correction for rotatory inertia.

Another point of interest is the effect of the value of ϵ on the value of D; this may be illustrated by taking the extreme values of 2·1 and 3·5 given for the ratio E/G by Goens; these figures correspond to extreme values of 2·52 and 4·20 for ϵ in the case of a bar of rectangular cross-section. The values of D for various values of ϵ in the case of bars no. I. and III. are given in Table II.

TABLE II.

Bar no. I. $z'^4=10{\cdot}779\ldots$	(i.) $\epsilon=3{\cdot}142$,	$D=-0{\cdot}0226$.
	(ii.) $\epsilon=2{\cdot}52$,	$D=-0{\cdot}0204$.
	(iii.) $\epsilon=4{\cdot}20$,	$D=-0{\cdot}0261$.
Bar no. III. $z'^4=8{\cdot}4355\ldots$	(i.) $\epsilon=3{\cdot}142$,	$D=-0{\cdot}0185$.
	(ii.) $\epsilon=2{\cdot}52$,	$D=-0{\cdot}0171$.
	(iii.) $\epsilon=4{\cdot}20$,	$D=-0{\cdot}0220$.

It is clear from this table that the variation of ϵ between the two extreme limits has little effect on the value of D. The difference in the value of z^4 obtained by assuming the two extreme values of ϵ amounts only to 0·06 per cent. Since the experimental error in the dynamical method of measuring Young's Modulus is greater than this figure it is thus perfectly justifiable to assume a mean value for ϵ, say $\epsilon=3$, for the purpose of calculating D.

In conclusion, the author desires to record his sincere thanks to Vice-Principal Gwilym Owen for his constant encouragement and interest, and to Mr. Thomas Lewis, Head of the Applied Mathematics Department, for discussing and checking the results.

References.

(1) Davies, Phil. Mag. xxii. p. 892 (1936).
(2) Davies, Phil. Mag. xxiii. p. 464 (1937).
(3) Davies, Phil. Mag. xxiii. p. 563 (1937).
(4) Davies and James, Phil. Mag. xviii. p. 1023 (1934); James and Davies, Phil. Mag. xviii. p. 1053 (1934).
(5) Davies and Thomas, Phil. Mag. xxiii. p. 361 (1937).
(6) Timoshenko, Phil. Mag. xli. p. 744 (1921).
(7) Timoshenko, 'Vibration Problems in Engineering,' pp. 227 & 231 (New York, 1928).
(8) Goens, *Ann. der Phys.* xi. p. 649 (1931).
(9) Prescott, 'Applied Elasticity' (London, 1924).
(10) Southwell, 'Theory of Elasticity' (Oxford, 1936).
(11) Föppl, 'Vorlesungen über Technische Mechanik,' p. 152 (Leipzig, 1900).
(12) Grüneisen, *Ann. der Phys.* xxv. p. 829 (1908).

January 1937.

CVI. *An Approximate Solution of the Boundary Layer Equations for a Flat Plate. By* W. G. L. Sutton, *M.A.**

THIS paper deals with the approximate solution of Prandtl's † boundary layer equations for steady laminar flow past a thin flat plate placed edgewise in a fluid stream of small viscosity. The exact solution of these equations was given by Blasius ‡ in 1908, and has been verified experimentally by several observers §. The difficulty of obtaining an exact solution in this and other cases has led several writers to develop approximate methods more amenable to calculation. The method to be described is based upon that of von Kármán ‖ and Pohlhausen ¶, and yields a value for the frictional drag which is practically identical with that given by Blasius. Moreover, it gives a velocity distribution in the boundary layer agreeing within about 1 per cent. everywhere with that calculated from Blasius's solution. Such close agreement must be regarded as being to some extent accidental, but the method is of some interest on its own account.

The Approximate Equations.

We take rectangular coordinates x, y, with Ox along the plate in the direction of flow and the origin at the leading edge. Let u, v be the component fluid velocities at any point (x, y) in the boundary layer. At the surface of the plate the fluid is at rest and the variable thickness $\delta(x)$ of the boundary layer is defined by the condition that at the outer edge of the layer, $u=\mathrm{U}$, the velocity that would occur at the corresponding point of the plate in the absence of viscosity. In this case, therefore, U is a constant, and if ν is the kinematic viscosity of the

* Communicated by the Author.

† See, *e. g.*, Prandtl-Tietjens, 'Applied Hydro- and Aero-Mechanics,' ch. iv. (McGraw-Hill, 1934).

‡ *Z. f. Math. u. Phys.* lvi. p. 13 (1908).

§ See, *e. g.*, Hansen, *Z. angew. Math. u. Mech.* viii. p. 185 (1928); also Fage, 'Frictional Drag of Flat Plates below the Critical Reynolds Number' (Air Ministry R. & M. no. 1580), 1933.

‖ *Z. angew. Math. u. Mech.* i. p. 233 (1921).

¶ *Ibid.* p. 252.

fluid Prandtl's assumptions lead to the equation of motion in the layer

$$u\frac{\partial u}{\partial x}+v\frac{\partial u}{\partial y}=\nu\frac{\partial^2 u}{\partial y^2}, \quad \ldots\ldots \quad (1)$$

with the boundary conditions

$$\left.\begin{aligned} &u=0,\ v=0 \text{ for } y=0,\\ &u=\mathrm{U},\ \frac{\partial u}{\partial y}=0 \text{ for } y=\delta \end{aligned}\right\} \quad \ldots\ldots \quad (2)$$

We have also the equation of continuity

$$\frac{\partial u}{\partial x}+\frac{\partial v}{\partial y}=0. \quad \ldots\ldots \quad (3)$$

In what follows the range of integration $0\leqslant y\leqslant\delta$ is to be understood, and an accent will denote differentiation with respect to x along the plate.

From (2) and (3) we get *

$$\begin{aligned} v(x,\delta) &= -\int\frac{\partial u}{\partial x}dy \\ &= \mathrm{U}\delta'-\frac{d}{dx}\int u\,dy. \end{aligned}$$

Hence, with $n>0$, integrating by parts we get

$$\begin{aligned} \int vu^{n-1}\frac{\partial u}{\partial y}.dy &= \frac{1}{n}\Big[vu^n\Big]_0^\delta-\frac{1}{n}\int u^n\frac{\partial v}{\partial y}dy \\ &= \frac{1}{n}\left(\mathrm{U}^{n+1}\delta'-\mathrm{U}^n\frac{d}{dx}\int u\,dy+\int u^n\frac{\partial u}{\partial x}dy\right) \quad (4) \end{aligned}$$

We now multiply (1) by u^{n-1}, integrate with respect to y from 0 to δ, and use (4), thus getting

$$n\left[(n+1)\int u^n\frac{\partial u}{\partial x}dy+\mathrm{U}^{n+1}\delta'\right]-\frac{\mathrm{U}^n}{n}\frac{d}{dx}\int u\,dy=\nu\int u^{n-1}\frac{\partial^2 u}{\partial y^2}dy,$$

that is *

$$\frac{1}{n}\frac{d}{dx}\int u^{n+1}dy-\frac{\mathrm{U}^n}{n}\frac{d}{dx}\int u\,dy=\nu\int u^{n-1}\frac{\partial^2 u}{\partial y^2}dy.$$

* Using the formula

$$\frac{d}{dx}\int_{a(x)}^{b(x)}f(x,y)\,dy=f(x,b)\frac{db}{dx}-f(x,a)\frac{da}{dx}+\int_a^b\frac{\partial f}{\partial x}dy$$

If in this we write

$$u(x, y) = \mathrm{U}w(x, y), \quad \int_0^\delta w^m \, dy = \mathrm{I}_m(x),$$

we obtain on division by U^n/n

$$\mathrm{U}(\mathrm{I}'_{n+1} - \mathrm{I}_1') = n\nu \int w^{n-1} \frac{\partial^2 w}{\partial y^2} dy. \quad . \quad . \quad . \quad (5)$$

In the present case we take as the approximate equivalent of (1) the pair of equations obtained from (5) by putting $n=1$ and $n=2$. We use the boundary conditions (2) to simplify the right-hand side, and get

$$\mathrm{U}(\mathrm{I}_1' - \mathrm{I}_2') = \nu \left(\frac{\partial w}{\partial y} \right)_{y=0}, \quad . \quad . \quad . \quad . \quad (6)$$

$$\mathrm{U}(\mathrm{I}_1' - \mathrm{I}_3') = 2\nu \int_0^\delta \left(\frac{\partial w}{\partial y} \right)^2 dy. \quad . \quad . \quad . \quad (7)$$

Of these (6) is von Kármán's momentum equation.

The Velocity Profile.

Following von Kármán and Pohlhausen we now assume for w a polynomial in y which contains one arbitrary function of x, for all values of which the boundary conditions

$$w = 0, \quad (y = 0)$$

$$w = 1, \quad \frac{\partial w}{\partial y} = 0, \quad \frac{\partial^2 w}{\partial y^2} = 0, \quad (y = \delta)$$

are satisfied. It is convenient to write

$$s = 1 - y/\delta,$$

so that the boundary layer is obtained by making s go from 1 at the surface of the plate to 0 at the outer edge of the layer. In virtue of the conditions just stated we assume for w a polynomial in s of degree 4 and easily obtain

$$w = 1 - s^3 - \lambda(s^3 - s^4), \quad . \quad . \quad . \quad . \quad . \quad (8)$$

where λ is a function of x alone. It should be noted that for profiles of the type required we must have

$$\frac{\partial w}{\partial s} < 0, \quad (0 < s < 1).$$

This yields the condition *

$$-1 \leqslant \lambda \leqslant 3. \quad \ldots\ldots \quad (9)$$

With the assumption (8) we obtain

$$I_1 - I_2 = \delta\left(\frac{3}{28} + \frac{1}{70}\lambda - \frac{1}{252}\lambda^2\right)$$
$$= \delta . \phi(\lambda), \text{ say,}$$

$$I_1 - I_3 = \delta\left(\frac{6}{35} + \frac{31}{1540}\lambda - \frac{17}{2310}\lambda^2 + \frac{1}{2860}\lambda^3\right)$$
$$= \delta . f(\lambda), \text{ say,}$$

$$\int\left(\frac{\partial w}{\partial y}\right)^2 dy = \frac{1}{\delta}\left(\frac{9}{5} - \frac{2}{5}\lambda + \frac{3}{35}\lambda^2\right)$$

$$\left(\frac{\partial w}{\partial y}\right)_{y=0} = \frac{3-\lambda}{\delta}.$$

If we make these substitutions and write

$$z = \delta^2/\nu$$

equations (6) and (7) become respectively

$$U\left(z' + 2\frac{\lambda'}{\phi(\lambda)}\frac{d\phi}{d\lambda} . z\right) = \frac{2(3-\lambda)}{\phi(\lambda)}, \quad \ldots\ldots \quad (10)$$

$$U\left(z' + 2\frac{\lambda'}{f(\lambda)}\frac{df}{d\lambda} . z\right) = \frac{4(9-2\lambda+\frac{3}{7}\lambda^2)}{5f(\lambda)} . \quad \ldots \quad (11)$$

To these we must add the condition

$$z = 0 \quad \text{for} \quad x = 0. \quad \ldots\ldots \quad (12)$$

(10), (11), and (12) form the required approximate system for the determination of z and λ as functions of x.

It is clear that equations (10) and (11) will be identical if λ is chosen to be a constant satisfying the equation

$$\frac{2(3-\lambda)}{\phi(\lambda)} = \frac{4(9-2\lambda+\frac{3}{7}\lambda^2)}{5f(\lambda)}.$$

This equation is

$$49{\cdot}5 - 29{\cdot}55\,\lambda - 13{\cdot}42143\,\lambda^2 + 1{\cdot}0721\,\lambda^3 + 0{\cdot}12729\,\lambda^4 = 0,$$

and it is not difficult to show that there is just one root

* $\lambda < -1$ would make $u > U$ at some point of the boundary layer, and $\lambda > 3$ makes $\frac{\partial w}{\partial s} > 0$ at the surface of the plate, which would imply "back flow."

satisfying condition (9), namely, $\lambda = 1{\cdot}14315$. With this value for λ, (10) and (11) give on integration

$$\delta = 5{\cdot}603\sqrt{\frac{\nu x}{U}} \quad . \quad . \quad . \quad . \quad . \quad . \quad (13)$$

In the table given below the velocity distribution

$$w = 1 - s^3 - 1{\cdot}14315(s^3 - s^4)$$

is compared with that of Blasius calculated by Töpfer *. Töpfer's results are given in terms of the variable $\eta = y\Big/\sqrt{\frac{\nu x}{U}}$, which by (13) is connected with s by the relation

$$s = 1 - 0{\cdot}17847\,\eta.$$

It is seen that the divergence is less than 1 per cent. over almost the whole range.

TABLE I.

η.	w.	w (Töpfer).	η.	w.	w (Töpfer).
0·2	0·0667	0·0664	3·0	0·8383	0·8461
0·4	·1338	·1328	3·2	·8696	·8761
0·6	·2009	·1990	3·4	·8970	·9018
0·8	·2672	·2647	3·6	·9207	·9233
1·0	·3325	·3298	3·8	·9408	·9411
1·2	·3959	·3938	4·0	·9575	·9555
1·4	·4573	·4563	4·2	·9712	·9670
1·6	·5163	·5168	4·4	·9812	·9759
1·8	·5726	·5778	4·6	·9889	·9827
2·0	·6256	·6298	4·8	·9942	·9878
2·2	·6753	·6813	5·0	·9975	·9916
2·4	·7217	·7290	5·2	·9992	·9943
2·6	·7643	·7725	5·4	·9999	·9962
2·8	·8032	·8115	5·6	1·0	·9975

The Frictional Drag.

If l is the length of the plate then the frictional drag D per unit breadth of both surfaces is given by

$$D = 2\mu \int \left(\frac{\partial u}{\partial y}\right)_{y=0} dx$$

$$= 2\mu U \int_0 \frac{3-\lambda}{\delta}\, dx,$$

* *Z. f. Math. u. Phys.* lx. p. 397 (1912). The results are quoted in 'Aerodynamic Theory' (Guggenheim Trust pub.) vol. iii. sect. G 14, p. 88.

where $\mu=\nu\rho$ is the coefficient of viscosity and ρ is the fluid density. On substituting for λ and δ, and performing the integration, we get

$$D=1{\cdot}326\sqrt{(\mu\rho U^3 l)},$$

whence the drag coefficient $k_D=D/\rho l U^2$ is

$$k_D=1{\cdot}326\ R^{-\frac{1}{2}},$$

where $R=Ul/\nu$ is the Reynolds number. This value for k_D compares very favourably with Blasius's result $k_D=1{\cdot}328\,R^{-\frac{1}{2}}$, and, so far as I am aware, is better than has been previously obtained by an approximate method.

The Uniqueness of Solution.

The value of λ obtained was derived from the condition that equations (10) and (11) should be identical, whereas all that is necessary is that these equations should possess a common solution z satisfying (12). If, however, we restrict λ and z to be analytic near $x=0$, it can be shown that the solution just obtained is unique. In fact, if we eliminate in turn z and z' from (10) and (11) we obtain two equations of the form

$$z'=g(\lambda), \quad . \quad . \quad . \quad . \quad . \quad . \quad . \quad . \quad (14)$$

$$z\lambda'=h(\lambda). \quad . \quad . \quad . \quad . \quad . \quad . \quad . \quad . \quad (15)$$

We use a zero suffix to denote the value of any quantity for $x=0$, and get from (15) and (12)

$$h(\lambda_0)=0,$$

which gives the value for λ_0 already obtained. We now differentiate (15) n times with respect to x, and get

$$z\lambda^{(n+1)}+nz'\lambda^{(n)}+\ \ldots\ =\frac{dh}{d\lambda}\lambda^{(n)}+\ldots, \quad . \quad (16)$$

where the omitted terms all contain as factors lower derivates of λ, down to λ'. Hence, if we assume that $\lambda_0'=\lambda_0''=\ \ldots\ =\lambda_0^{(n-1)}=0$, we get, by putting $x=0$ in (16) and using (14),

$$\lambda_0^{(n)}\left(ng(\lambda_0)-\left(\frac{dh}{d\lambda}\right)_0\right)=0, \quad (n=1,\ 2,\ldots). \quad (17)$$

It may be verified that $g(\lambda_0)$ is positive and $\left(\frac{dh}{d\lambda}\right)_0$ is negative, so that the coefficient of $\lambda_0^{(n)}$ cannot vanish.

Hence, step by step, we prove that all the derivates of λ must vanish for $x=0$, so that λ itself must be a constant.

The College of Technology,
Cookridge Street, Leeds, 2

CVII. *Notices respecting New Books.*

Reports on Progress in Physics.—Vol. III. General Editor, Dr. Allan Ferguson. Published by the Physical Society of London. Price to non-Fellows, 20*s.* net.

THIS series of annual reports has now entered its third year. It differs from the abstracts of a Society's publications inasmuch as each subject is dealt with by a special editor, who writes with authority and discrimination concerning it.

Perhaps many readers will turn in the first instance to the very full description by C. E. Wynn-Williams of the new high-speed electrical counting methods which have been developed to replace the scintillation screen, which is now seldom used. A good deal of tedious routine observational work may be avoided by means of these new devices, and statistical results can be rapidly collected.

The classified table of contents exhibits the wide range of the articles. In General Physics are included Surface Tension (R. C. Brown), Elasticity (H. L. Cox and D. G. Sopwith), and Viscosity (G. Barr). Dr. A. Fage deals with Fluid motion, Prof. S. Chapman with the upper atmosphere. Under the heading Atomic Physics Dr. N. Feather is concerned with (2) Isotopic constitution, (3) Exact masses and spin moments of nuclei, (4) Nuclear transformation by fast particles, (5) Slow neutron effects and the nuclear model of Bohr; while Dr. Nunn May is concerned with the conservation of energy and momentum in elementary processes. Dr. E. G. Richardson writes a masterly essay on original work in Sound in continuation of his previous articles, and Dr. G. W. C. Kaye writes on the undesirable properties of Noise. Prof. L. F. Bates writes on Magnetism, Dr. R. W. Powell on Heat, L. C. Martin on Optics, while the Staff of the Physics Department, National Physical Laboratory, writes mainly on X-rays, Radium, and Crystal Structure. Dr. W. Jevons edits four articles on Spectroscopy written by M. F. Crawford (of Toronto) A. Hunter, R. W. B. Pearce, and W. H. J. Childs.

It is impossible to deal further with this wealth of material in our columns.

[*The Editors do not hold themselves responsible for the views expressed by their correspondents.*]

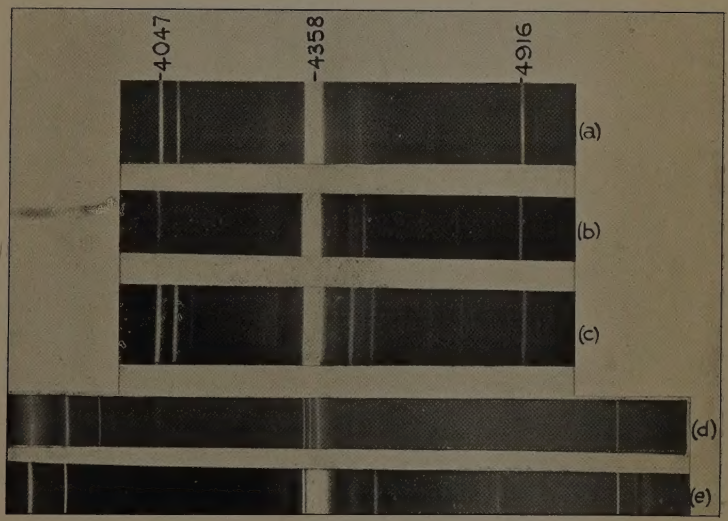

(*a*) α-Chlor-butyryl chloride.
(*b*) Oxalyl chloride.
(*c*) Succinyl chloride.
(*d*) α-Chlor-propionyl chloride.
(*e*) Caproyl chloride.

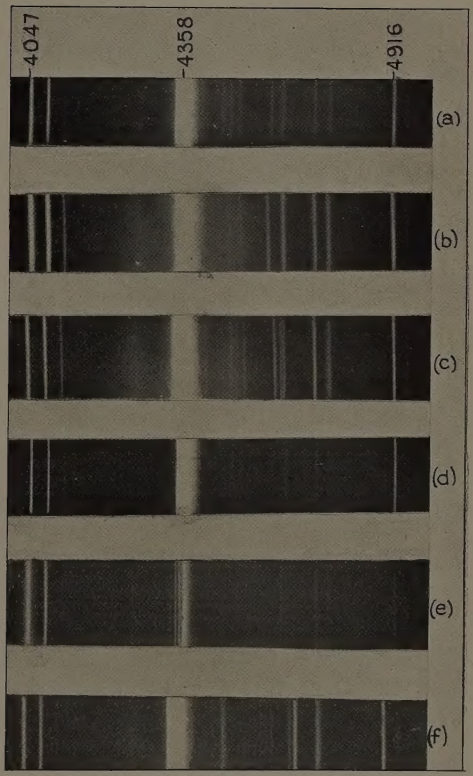

(*a*) Ortho-chlor-benzoyl chloride.
(*b*) Meta-chlor-benzoyl chloride.
(*c*) Para-chlor-benzoyl chloride
(*d*) Phthalyl chloride.
(*e*) Anisoyl chloride.
(*f*) α-Furoyl chloride.